Chapter 5

PRODUCTION

Conveners: G.T. Bodwin, E. Braaten, M. Krämer, A.B. Meyer, V. Papadimitriou

Authors: G.T. Bodwin, E. Braaten, C.-H. Chang, M. Krämer, J. Lee, A.B. Meyer, V. Papadimitriou, R. Vogt

1 FORMALISM FOR INCLUSIVE QUARKONIUM PRODUCTION

1.1 NRQCD factorization method

In both heavy-quarkonium annihilation decays and hard-scattering production, large energy–momentum scales appear. The heavy-quark mass m is much larger than $\Lambda_{\rm QCD}$, and, in the case of production, the transverse momentum p_T can be much larger than $\Lambda_{\rm QCD}$ as well. This implies that the associated values of the QCD running coupling constant are much less than one. ($\alpha_s(m_c) \approx 0.25$ and $\alpha_s(m_b) \approx 0.18$.) Therefore, one might hope that it would be possible to calculate the rates for heavy quarkonium decay and production accurately in perturbation theory. However, there are clearly low-momentum, nonperturbative effects associated with the dynamics of the quarkonium bound state that invalidate the direct application of perturbation theory.

In order to make use of perturbative methods, one must first separate the short-distance/high-momentum, perturbative effects from the long-distance/low-momentum, nonperturbative effects — a process which is known as "factorization." One convenient way to carry out this separation is through the use of the effective field theory Nonrelativistic QCD (NRQCD) [1–3]. NRQCD reproduces full QCD accurately at momentum scales of order mv and smaller, where v is the typical heavy-quark velocity in the bound state in the CM frame. ($v^2 \approx 0.3$ for charmonium, and $v^2 \approx 0.1$ for bottomonium.) Virtual processes involving momentum scales of order m and larger can affect the lower-momentum processes, and their effects are taken into account through the short-distance coefficients of the operators that appear in the NRQCD action.

Because $Q\bar{Q}$ production occurs at momentum scales of order m or larger, it manifests itself in NRQCD through contact interactions. As a result, the inclusive cross-section for the direct production of the quarkonium H at large transverse momentum (p_T of order m or larger) in hadron or *ep* colliders or at large momentum in the CM frame (p^* of order m or larger) in e^+e^- colliders can be written as a sum of products of NRQCD matrix elements and short-distance coefficients:

$$\sigma[H] = \sum_n \sigma_n(\Lambda) \langle \mathcal{O}_n^H(\Lambda) \rangle. \tag{5.1}$$

Here, Λ is the ultraviolet cutoff of the effective theory, the σ_n are short-distance coefficients, and the $\langle \mathcal{O}_n^H \rangle$ are vacuum-expectation values of four-fermion operators in NRQCD. There is a formula analogous to Eq. (5.1) for inclusive quarkonium annihilation rates, except that the vacuum-to-vacuum matrix elements are replaced by quarkonium-to-quarkonium matrix elements [3].

The short-distance coefficients $\sigma_n(\Lambda)$ in (5.1) are essentially the process-dependent partonic cross-sections to make a $Q\bar{Q}$ pair, convolved with parton distributions if there are hadrons in the initial state. The $Q\bar{Q}$ pair can be produced in a colour-singlet state or in a colour-octet state. Its spin state can be singlet or triplet, and it also can have orbital angular momentum. The short-distance coefficients are determined by matching the square of the production amplitude in NRQCD to full QCD. Because the scale of the $Q\bar{Q}$ production is of order m or greater, this matching can be carried out in perturbation theory.

The four-fermion operators in Eq. (5.1) create a $Q\bar{Q}$ pair in the NRQCD vacuum, project it onto a state that in the asymptotic future consists of a heavy quarkonium plus anything, and then annihilate the $Q\bar{Q}$ pair. The vacuum matrix element of such an operator is the probability for a $Q\bar{Q}$ pair to form a quarkonium plus anything. These matrix elements are somewhat analogous to parton fragmentation functions. They contain all of the nonperturbative physics associated with evolution of the $Q\bar{Q}$ pair into a quarkonium state. An important property of the matrix elements, which greatly increases the predictive power of NRQCD, is the fact that they are universal, i.e., process independent.

The colour-singlet and colour-octet four-fermion operators that appear in Eq. (5.1) correspond to the evolution into a colour-singlet quarkonium of a $Q\bar{Q}$ pair created at short distance in a colour-singlet state or a colour-octet state, respectively. In the case of decay, the colour-octet matrix elements have the interpretation of the probability to find the quarkonium in a Fock state consisting of a $Q\bar{Q}$ pair plus some number of gluons. It is a common misconception that colour-octet production proceeds through the production of a higher Fock state of the quarkonium. However, in the leading colour-octet production mechanisms, the gluons that neutralize the colour are not present at the time of the creation of the colour-octet $Q\bar{Q}$ pair, but are emitted during the subsequent hadronization process. The production of the quarkonium through a higher Fock state requires the production of gluons that are nearly collinear to the $Q\bar{Q}$ pair, and it is suppressed by additional powers of v.

NRQCD power-counting rules allow one to organize the sum over operators in Eq. (5.1) as an expansion in powers of v. Through a given order in v, only a finite set of matrix elements contributes. Furthermore, there are simplifying relations between matrix elements, such as the heavy-quark spin symmetry and the vacuum-saturation approximation, that reduce the number of independent matrix elements [3]. Some examples of relations between colour-singlet matrix elements that follow from heavy-quark spin symmetry are

$$\langle \mathcal{O}_1^{J/\psi}({}^3S_1)\rangle = 3\,\langle \mathcal{O}_1^{\eta_c}({}^1S_0)\rangle, \tag{5.2}$$

$$\langle \mathcal{O}_1^{\chi_{cJ}}({}^3P_J)\rangle = \tfrac{1}{3}(2J+1)\langle \mathcal{O}_1^{h_c}({}^1P_1)\rangle. \tag{5.3}$$

These relations hold up to corrections of order v^2. The prefactors on the right side of Eqs. (5.2)–(5.3) are just ratios of the numbers of spin states. Since the operators in Eqs. (5.2) and (5.3) have the same angular momentum quantum numbers as the $Q\bar{Q}$ pair in the dominant Fock state of the quarkonium, the vacuum-saturation approximation can be used to express the matrix elements in terms of the squares of wave functions or their derivatives at the origin, up to corrections of order v^4. heavy-quark spin symmetry also gives relations between colour-octet matrix elements, such as

$$\langle \mathcal{O}_8^{J/\psi}({}^3S_1)\rangle = 3\,\langle \mathcal{O}_8^{\eta_c}({}^1S_0)\rangle, \tag{5.4}$$

$$\langle \mathcal{O}_8^{J/\psi}({}^1S_0)\rangle = \langle \mathcal{O}_8^{\eta_c}({}^3S_1)\rangle, \tag{5.5}$$

$$\langle \mathcal{O}_8^{J/\psi}({}^3P_J)\rangle = \tfrac{1}{3}(2J+1)\langle \mathcal{O}_8^{\eta_c}({}^1P_1)\rangle, \tag{5.6}$$

$$\langle \mathcal{O}_8^{\chi_{cJ}}({}^3S_1)\rangle = \tfrac{1}{3}(2J+1)\langle \mathcal{O}_8^{h_c}({}^1S_0)\rangle. \tag{5.7}$$

These relations hold up to corrections of order v^2. The prefactors on the right side of Eqs. (5.4)–(5.7) are again just ratios of the numbers of spin states. The vacuum-saturation approximation is not applicable to colour-octet matrix elements.

The relative importance of the terms in the factorization formula in Eq. (5.1) is determined not only by the sizes of the matrix elements but also by the sizes of the coefficients σ_n in Eq. (5.1). The size of the coefficient depends on its order in α_s, colour factors, and dimensionless kinematic factors, such as m^2/p_T^2.

The NRQCD factorization approach is sometimes erroneously called the "colour-octet model," because colour-octet terms are expected to dominate in some situations, such as J/ψ production at large p_T in hadron colliders. However, there are also situations in which colour-singlet terms are expected

to dominate, such as J/ψ production in continuum e^+e^- annihilation at the B factories. Moreover, NRQCD factorization is not a model, but a rigorous consequence of QCD in the limit $\Lambda_{\rm QCD}/m \to 0$.

A specific truncation of the NRQCD expansion in Eq. (5.1) could be called a model, although, unlike most models, it is in principle systematically improvable. In truncating at a given order in v, one can reduce the number of independent matrix elements by making use of approximate relations, such as Eqs. (5.2)–(5.3) and Eqs. (5.4)–(5.7). The simplest truncation of the NRQCD expansion in Eq. (5.1) that is both phenomenologically viable and corresponds to a consistent truncation in v includes four independent NRQCD matrix elements for each S-wave multiplet (one colour-singlet and three colour-octet) and two independent NRQCD matrix elements for each P-wave multiplet (one colour-singlet and one colour-octet). We will refer to this truncation as the standard truncation in v. For the S-wave charmonium multiplet consisting of J/ψ and η_c, one can take the four independent matrix elements to be $\langle \mathcal{O}_1^{J/\psi}(^3S_1)\rangle$, $\langle \mathcal{O}_8^{J/\psi}(^1S_0)\rangle$, $\langle \mathcal{O}_8^{J/\psi}(^3S_1)\rangle$, and $\langle \mathcal{O}_8^{J/\psi}(^3P_0)\rangle$. Their relative orders in v are v^0, v^3, v^4, and v^4, respectively. It is convenient to define the linear combination

$$M_k^H = \langle \mathcal{O}_8^H(^1S_0)\rangle + \frac{k}{m_c^2}\langle \mathcal{O}_8^H(^3P_0)\rangle\,, \tag{5.8}$$

because many observables are sensitive only to the linear combination of these two colour-octet matrix elements corresponding to a specific value of k. These four independent matrix elements can be used to calculate the cross-sections for the η_c and each of the 3 spin states of the J/ψ. Thus, this truncation of NRQCD gives unambiguous predictions for the polarization of the J/ψ. For the P-wave charmonium multiplet consisting of χ_{c0}, χ_{c1}, χ_{c2}, and h_c, we can take the two independent matrix elements to be $\langle \mathcal{O}_1^{\chi_{c0}}(^3P_0)\rangle$ and $\langle \mathcal{O}_8^{\chi_{c0}}(^3S_1)\rangle$. Their orders in v relative to $\langle \mathcal{O}_1^{J/\psi}(^3S_1)\rangle$ are both v^2. These two independent matrix elements can be used to calculate the cross-sections for each of the 12 spin states in the P-wave multiplet. Thus, this truncation of NRQCD gives unambiguous predictions for the polarizations of the χ_{c1}, χ_{c2}, and h_c.

The NRQCD *decay matrix* elements can be calculated in lattice simulations [4–8] or determined from phenomenology. However, it is not yet known how to formulate the calculation of production matrix elements in lattice simulations, and, so, the production matrix elements must be obtained phenomenologically. In general, the production matrix elements are different from the decay matrix elements. The exceptions are the colour-singlet production matrix elements in which the $Q\bar{Q}$ pair has the same quantum numbers as the quarkonium state, such as those in Eqs. (5.2) and (5.3). They can be related to the corresponding decay matrix elements through the vacuum-saturation approximation, up to corrections of relative order v^4 [3]. Phenomenological determinations of the production matrix elements for charmonium states are given in Section 2.1.

The proof of the factorization formula in Eq. (5.1) relies both on NRQCD and on the all-orders perturbative machinery for proving hard-scattering factorization. A detailed proof does not yet exist, but work is in progress [9]. At a large transverse momentum (p_T of order m or larger), corrections to hard-scattering factorization are thought to be of order $(mv)^2/p_T^2$ (not m^2/p_T^2) in the unpolarized case and of order mv/p_T (not m/p_T) in the polarized case. At a small transverse momentum, p_T of order mv or smaller, the presence of soft gluons in the quarkonium binding process makes the application of the standard factorization techniques problematic. It is not known if there is a factorization formula for $d\sigma/dp_T^2$ at small p_T or for $d\sigma/dp_T^2$ integrated over p_T.

In practical calculations of the rates of quarkonium decay and production, a number of significant uncertainties arise. In many instances, the series in α_s and v in the factorization formula in Eq. (5.1) converge slowly, and the uncertainties from their truncation are large — sometimes 100% or larger. In addition, the matrix elements are often poorly determined, either from phenomenology or lattice measurements, and the important linear combinations of matrix elements vary from process to process, making tests of universality difficult. There are also large uncertainties in the heavy-quark masses (approximately

8% for m_c and approximately 2.4% for m_b) that can be very significant for quarkonium rates that are proportional to a large power of the mass.

Many of the largest uncertainties in the theoretical predictions, as well as some of the experimental uncertainties, cancel in the ratios of cross-sections. Examples in charmonium production are the ratio R_ψ of the inclusive cross-sections for $\psi(2S)$ and J/ψ production and the ratio R_{χ_c} of the inclusive cross-sections for χ_{c1} and χ_{c2} production. These ratios are defined by

$$R_\psi = \frac{\sigma[\psi(2S)]}{\sigma[J/\psi]}, \tag{5.9}$$

$$R_{\chi_c} = \frac{\sigma[\chi_{c1}]}{\sigma[\chi_{c2}]}. \tag{5.10}$$

Other useful ratios are the fractions F_H of J/ψ's that come from decays of higher quarkonium states H. The fractions that come from decays of $\psi(2S)$ and from $\chi_c(1P)$ are defined by

$$F_{\psi(2S)} = \mathrm{Br}[\psi(2S) \to J/\psi + X] \, \frac{\sigma[\psi(2S)]}{\sigma[J/\psi]}, \tag{5.11}$$

$$F_{\chi_c} = \sum_{J=0}^{2} \mathrm{Br}[\chi_{cJ}(1P) \to J/\psi + X] \, \frac{\sigma[\chi_{cJ}(1P)]}{\sigma[J/\psi]}. \tag{5.12}$$

The $J = 0$ term in (5.12) is usually negligible, because the branching fraction $\mathrm{Br}[\chi_{c0} \to \mathrm{J}/\psi\,\mathrm{X}]$ is so small. The fraction of J/ψ's that are produced directly can be denoted by $F_{J/\psi}$.

Another set of observables in which many of the uncertainties cancel out consists of polarization variables, which can be defined as ratios of cross-sections for the production of different spin states of the same quarkonium. The angular distribution of the decay products of the quarkonium depends on the spin state of the quarkonium. The polarization of a 1^{--} state, such as the J/ψ, can be measured from the angular distribution of its decays into lepton pairs. Let θ be the angle in the J/ψ rest frame between the positive lepton momentum and the chosen polarization axis. The most convenient choice of polarization axis depends on the process. The differential cross-section has the form

$$\frac{d\sigma}{d(\cos\theta)} \propto 1 + \alpha \cos^2\theta, \tag{5.13}$$

which defines a polarization variable α whose range is $-1 \le \alpha \le +1$. We can define longitudinally and transversely polarized J/ψ's to be ones whose spin components along the polarization axis are 0 and ± 1, respectively. The polarization variable α can then be expressed as $(1 - 3\xi)/(1 + \xi)$, where ξ is the fraction of the J/ψ's that are longitudinally polarized. The value $\alpha = 1$ corresponds to J/ψ with 100% transverse polarization, while $\alpha = -1$ corresponds to J/ψ with 100% longitudinal polarization.

One short-coming of the NRQCD factorization approach is that, at leading order in v, some of the kinematics of production are treated inaccurately. Specifically, the mass of the light hadronic state that forms during the evolution of the $Q\bar{Q}$ pair into the quarkonium state is neglected, and no distinction is made between $2m$ and the quarkonium mass. While the corrections to these approximations are formally of higher order in v, they can be important numerically in the cases of rapidly varying quarkonium-production distributions, such as p_T distributions at the Tevatron and z distributions at the B factories and HERA near the kinematic limit $z = 1$. These effects can be taken into account through the resummation of certain operator matrix elements of higher order in v [10]. The resummation results in universal nonperturbative shape functions that give the probability distributions for a $Q\,\bar{Q}$ pair with a given set of quantum numbers to evolve into a quarkonium with a given fraction of the pair's momentum. The shape functions could, in principle, be extracted from the data for one process and applied to another process. Effects from resummation of logarithms of $1 - z$ and model shape functions have been calculated for the

process $e^+e^- \to J/\psi + X$ [11]. For shape functions that satisfy the velocity-scaling rules, these effects are comparable in size. It may be possible to use this resummed theoretical prediction to extract the dominant shape function from the Belle and BaBar data for $e^+e^- \to J/\psi + X$ and then use it to make predictions for J/ψ photoproduction near $z = 1$ [12].

1.2 Colour-singlet model

The colour-singlet model (CSM) was first proposed shortly after the discovery of the J/ψ. The initial applications were to η_c and χ_c production through two-gluon fusion [13–16]. Somewhat later, the CSM was applied to the production of J/ψ and η_c in B-meson decays [17–19] and to the production of J/ψ plus a gluon [20–25] through two-gluon fusion and photon–gluon fusion. The CSM was taken seriously until around 1995, when experiments at the Tevatron showed that it under-predicts the cross-section for prompt charmonium production in $p\bar{p}$ collisions by more than an order of magnitude. An extensive review of the colour-singlet model can be found in Ref. [26].

The colour-singlet model can be obtained from the NRQCD factorization formula in Eq. (5.1) by dropping all of the colour-octet terms and all but one of the colour-singlet terms. The term that is retained is the one in which the quantum numbers of the $Q\bar{Q}$ pair are the same as those of the quarkonium. The CSM production matrix elements are related to the corresponding decay matrix elements by the vacuum-saturation approximation, and, so, they can be determined from annihilation decay rates. Thus, the CSM gives absolutely normalized predictions for production cross-sections. The heavy-quark spin symmetry relates the CSM matrix elements of the $4(2L + 1)$ states within an orbital-angular-momentum multiplet with quantum number L. Thus, the CSM also gives nontrivial predictions for polarization.

In the case of an S-wave state, the CSM term in Eq. (5.1) is the one whose matrix element is of leading order in v. However, owing to kinematic factors or factors of α_s in the short-distance coefficients, the CSM term may not be dominant. In the case of a P-wave state or a state of higher orbital angular momentum, the CSM term is only one of the terms whose matrix element is of leading order in v. For these states, the CSM leads to infrared divergences that cancel only when one includes colour-octet terms whose matrix elements are also of leading order in v. Thus, the CSM is theoretically inconsistent for quarkonium states with nonzero orbital angular momentum.

1.3 Colour-evaporation model

The colour evaporation model (CEM) was first proposed in 1977 [27–30] and has enjoyed considerable phenomenological success. In the CEM, the cross-section for a quarkonium state H is some fraction F_H of the cross-section for producing $Q\bar{Q}$ pairs with invariant mass below the $M\bar{M}$ threshold, where M is the lowest mass meson containing the heavy quark Q. (The CEM parameter F_H should not be confused with the fraction of J/ψ's that come from decay of H.) This cross-section has an upper limit on the $Q\bar{Q}$ pair mass but no constraints on the colour or spin of the final state. The $Q\bar{Q}$ pair is assumed to neutralize its colour by interaction with the collision-induced colour field, that is, by "colour evaporation." The Q and the $\bar{Q}$ either combine with light quarks to produce heavy-flavoured hadrons or bind with each other to form quarkonium. If the $Q\bar{Q}$ invariant mass is less than the heavy-meson threshold $2m_M$, then the additional energy that is needed to produce heavy-flavoured hadrons can be obtained from the nonperturbative colour field. Thus, the sum of the fractions F_H over all quarkonium states H can be less than unity. The fractions F_H are assumed to be universal so that, once they are determined by data, they can be used to predict the cross-sections in other processes and in other kinematic regions.

In the CEM at leading order in α_s, the production cross-section for the quarkonium state H in collisions of the light hadrons h_A and h_B is

$$\sigma_{\rm CEM}^{\rm (LO)}[h_A h_B \to H + X] = F_H \sum_{i,j} \int_{4m^2}^{4m_M^2} d\hat{s} \int dx_1 dx_2 \; f_i^{h_A}(x_1,\mu) \; f_j^{h_B}(x_2,\mu) \; \hat{\sigma}_{ij}(\hat{s}) \; \delta(\hat{s} - x_1 x_2 s) \,, \tag{5.14}$$

where $ij = q\bar{q}$ or gg, $\hat{s}$ is the square of the partonic centre-of-mass energy, and $\hat{\sigma}_{ij}(\hat{s})$ is the $ij \to Q\bar{Q}$ subprocess cross-section. The leading-order calculation cannot describe the quarkonium p_T distribution, since the p_T of the $Q\bar{Q}$ pair is zero at LO. At NLO in α_s, the subprocesses $ij \to kQ\bar{Q}$, where i, j, and k are light quarks, antiquarks, and gluons, produce $Q\bar{Q}$ pairs with nonzero p_T. Complete NLO calculations of quarkonium production in hadronic collisions using the CEM have been carried out in Refs. [31, 32], using the exclusive $Q\bar{Q}$ production code of Ref. [33] to obtain the $Q\bar{Q}$ pair distributions. The resulting values of the parameters F_H are given in Section 3.3. There are also calculations in the CEM beyond LO that use only a subset of the NLO diagrams [34] and calculations that describe the soft colour interaction within the framework of a Monte Carlo event generator [35]. Calculations beyond LO in the CEM have also been carried out for γp, $\gamma\gamma$ and neutrino–nucleon collisions and for Z^0 decays [36–40]. Apparently, the colour-evaporation model has not been applied to quarkonium production in e^+e^- annihilation.

The most basic prediction of the CEM is that the ratio of the cross-sections for any two quarkonium states should be constant, independent of the process and the kinematic region. Some variations in these ratios have been observed. For example, the ratio of the cross-sections for χ_c and J/ψ are rather different in photoproduction and hadroproduction. Such variations present a serious challenge to the status of the CEM as a quantitative phenomenological model for quarkonium production.

In some papers on the Colour Evaporation Model [34], the collision-induced colour field that neutralizes the colour of the $Q\bar{Q}$ pair is also assumed to randomize its spin. This leads to the prediction that the quarkonium production rate is independent of the quarkonium spin. This prediction is contradicted by measurements of nonzero polarization of the J/ψ, the $\psi(2S)$, and the $\Upsilon(nS)$ in several experiments. The assumption of the randomization of the $Q\bar{Q}$ spin also implies simple spin-counting ratios for the cross-sections for the direct production of quarkonium states in the same orbital-angular-momentum multiplet. For example, the CEM with spin randomization predicts that the direct-production cross-sections for charmonium satisfy $\sigma_{\rm dir}[\eta_c] : \sigma_{\rm dir}[J/\psi] = 1 : 3$ and $\sigma_{\rm dir}[\chi_{c0}] : \sigma_{\rm dir}[\chi_{c1}] : \sigma_{\rm dir}[\chi_{c2}] = 1 : 3 : 5$. The inclusive cross-sections need not satisfy these spin-counting relations if there is significant feeddown from decay of higher quarkonium states, as is the case for J/ψ. Deviations from the predicted spin-counting ratio for χ_{c1} to χ_{c2} have been observed. One might conclude that the CEM is ruled out by the observations of nonzero polarization and of deviations from the spin-counting relations. On the other hand, the assumption of the randomization of the $Q\bar{Q}$ spin is really independent of the assumption of colour evaporation. Some proponents of the CEM omit the assumption of spin randomization. Alternatively, since the CEM is just a model, one can simply declare it to apply only to spin-averaged cross-sections. In the remainder of this chapter, when we mention the predictions of the CEM for the relative production rates of quarkonium states that differ only in their spin or total-angular-momentum quantum numbers, we are referring to the version of the CEM that includes the assumption of spin randomization.

There is a simple correspondence between the CEM and the NRQCD factorization approach. The CEM amounts to the assumption that an NRQCD production matrix element $\langle \mathcal{O}_n^H(\Lambda) \rangle$ is proportional to the expectation value of the operator that is obtained by replacing the projector onto the hadronic state H with a projector onto the set of $Q\bar{Q}$ states with invariant mass less than $2m_M$. In addition to an integral over the $Q\bar{Q}$ phase space, the projector contains sums over the $Q\bar{Q}$ spins and colours. The only dependence on the quarkonium H is through a common factor F_H in the proportionality constant for each NRQCD matrix element. Since, in this picture, the probability of forming a specific quarkonium state H is independent of the colour and spin state of the $Q\bar{Q}$ pair, NRQCD matrix elements that differ only by colour and spin quantum numbers are equal up to simple group theory factors. This picture also implies a hierarchy of NRQCD matrix elements according to their orbital-angular-momentum quantum number L. In the integration over the $Q\bar{Q}$ phase space of an NRQCD operator with orbital-angular-momentum quantum number L, the leading term scales as k^{2L+1}, where k is the Q or $\bar{Q}$ momentum in the $Q\bar{Q}$ rest frame. The difference $s_{\rm max} - 4m^2$ is proportional to k^2. Hence, there is an orbital-angular-momentum suppression factor $[(s_{\rm max} - 4m^2)/4m^2]^L \sim v^{2L}$ in the matrix elements.[1] That is, the CEM

[1] From the perspective of NRQCD, the upper limit $s_{\rm max} = 4m_M^2$ on the $Q\bar{Q}$ invariant mass that traditionally has been used in the CEM is quite arbitrary. Any choice that satisfies $s_{\rm max} - 4m_Q^2 \sim 4m_Q^2 v^2$ leads to the same velocity-scaling rules.

implies that S-wave NRQCD matrix elements dominate and that those with orbital-angular-momentum quantum number $L \geq 1$ are suppressed as v^{2L}. One way to test the assumptions of the CEM is to extract the NRQCD matrix elements from data and compare them with the predictions of the CEM.

The qualifier NLO in "the CEM at NLO" is somewhat misleading. As is described in Section 1.4, the NLO cross-section for $Q\bar{Q}$ production that is used in computing the CEM predictions is accurate through order α_s^3, which is next-to-leading order at zero p_T, but leading order at nonzero p_T. This is the same accuracy in α_s as the existing predictions in the NRQCD factorization approach. The NLO $Q\bar{Q}$ p_T distribution is singular at $p_T = 0$, but integrable. The existing NLO calculations in the CEM obtain a smooth p_T distribution at small p_T by using a smearing prescription to mimic the effects of multiple gluon emission. The smearing has a significant effect on the shape of the p_T distribution, except at very large p_T.

1.4 Multiple gluon emission

Multiple gluon emission can be very important for transverse momentum distributions, distributions near kinematic limits, and in situations in which production near threshold is important. For example, a fixed-order perturbative calculation typically gives a transverse momentum distribution $d\sigma/dp_T^2$ for quarkonium that includes terms proportional to $\delta(p_T^2)$ and $1/p_T^2$ that are singular as $p_T \to 0$. (However, the distribution has a well-behaved integral over p_T.) This singular distribution becomes a smooth one when the effects of multiple gluon emission are taken into account to all orders in perturbation theory. Several methods, which we now describe, have been developed to take into account some of these effects.

Resummation methods sum, to all orders in α_s, certain logarithmically enhanced terms that are associated with soft- and collinear-gluon emission. The resummations can be carried out at various levels of precision in the logarithmic enhancements, that is, in leading logarithmic (LL) order, in next-to-leading logarithmic (NLL) order, etc. Resummation can, in principle, be extended to arbitrarily high precision in the logarithmic enhancements. However, in practice, it is seldom carried out beyond LL or NLL accuracy. Generally, logarithms of p_T^2/M^2 have the largest effect on p_T distributions [42], although logarithms of the available partonic energy above threshold (threshold logarithms) and logarithms of s/p_T^2 (small-x logarithms) can also be important for particular processes and kinematic regions[2]. Because arbitrarily soft or collinear gluon emissions are resummed, the resummed expressions depend on nonperturbative functions. This dependence lessens as the mass and transverse momentum scales of the process increase, and it may be insignificant at large masses and/or transverse momenta. Some practical disadvantages of the resummation method are that it has to be reformulated, to some extent, for every process and that it usually does not yield results that are fully differential in all of the kinematic variables. Since resummation calculations retain only soft and collinear logarithmically enhanced terms, they generally do not describe accurately processes in which hard gluons are emitted at large angles — so called "Mercedes events." This situation can be remedied to some extent by combining resummation with exact next-to-leading order (NLO) calculations, which retain all contributions associated with gluon emission at NLO, not just logarithmically enhanced contributions [44].

Parton-shower Monte Carlos share with resummation methods the approach of modeling multiple gluon emission by retaining certain logarithmically enhanced terms in the cross-section. The Monte Carlos take into account a finite, but arbitrarily large, number of gluon emissions. The original implementations of shower Monte Carlo methods, such as ISAJET [45,46], generally treat only the leading collinear logarithmic enhancements correctly, while more recent implementations, such as PYTHIA [47, 48] and HERWIG [49,50] treat both the leading collinear and soft logarithmic enhancements correctly. Generally, the showering processes are cut off so that they do not become so soft or collinear as to be nonperturbative in nature. The showering may then be supplemented with nonperturbative models that describe the hadronization of the partons. A practical advantage of the shower Monte Carlo approach is that it is

[2]For a general discussion of resummation techniques for logarithms of p_T^2/M^2 and threshold logarithms, see Ref. [43].

generally applied easily to any Born-level production process. Furthermore, it produces results that are differential in all of the kinematic variables that are associated with the final-state particles. Hence, it lends itself to the application of experimental cuts. As is the case with resummation methods, the shower Monte Carlo approach does not yield an accurate modeling of processes in which hard gluons are emitted at large angles. A partial remedy for this problem is to use shower Monte Carlos in conjunction with exact NLO calculations, rather than LO calculations. Recently, important progress has been made in this direction [51–56]. In contrast with resummation methods, some shower Monte Carlos do not take into account virtual gluon emission. Such shower Monte Carlos do not yield reliable estimates of the total cross-section.

The *k_T-factorization* method is an attempt to take into account initial-state radiation through parton distributions that depend the parton's transverse momentum k_T, as well as on the parton's longitudinal momentum fraction x. It generally gives answers that are very different from those of collinear factorization. The k_T-dependent parton distributions are not very well known phenomenologically, and there are possibly unresolved theoretical issues, such as the universality of the k_T-dependent parton distributions.

The *k_T-smearing* method is a phenomenological model for multiple initial-state radiation. As in the k_T-factorization method, the k_T smearing method makes use of k_T-dependent parton distributions. It is assumed that the distribution factors into the x-dependent PDF's that are defined by collinear factorization and a Gaussian distribution in the transverse momentum k_T. The width $\langle k_T^2 \rangle$ of the Gaussian can be treated as a process-dependent phenomenological parameter. One advantage of this model is that it is easy to implement. On the other hand, while this model may capture some of the crude features of soft- and collinear-gluon emission, it is probably incorrect in detail: resummation methods and shower Monte Carlos yield transverse-momentum distributions that have longer tails than those of a Gaussian distribution. The impact of a parton shower on the quarkonium transverse momentum distribution is, in general, larger than for the Gaussian k_T smearing, and it extends out to larger values of p_T.

1.5 Production in nuclear matter

The existing factorization "theorems" for quarkonium production in hadronic collisions are for cold hadronic matter. These theorems predict that nuclear matter is "transparent" for J/ψ production at large p_T. That is, at large p_T, all of the nuclear effects are contained in the nuclear parton distributions. The corrections to this transparency are of order $(mv)^2/p_T^2$ for unpolarized cross-sections and of order mv/p_T for polarized cross-sections.

The effects of transverse-momentum kicks from multiple elastic collisions between active partons and spectators in the nucleons are among those effects that are suppressed by $(mv)^2/p_T^2$. Nevertheless, these multiple-scattering effects can be important because the production cross-section falls steeply with p_T and because the number of scatterings grows linearly with the length of the path through the nuclear matter. Such elastic interactions can be expressed in terms of eikonal interactions [57] or higher-twist matrix elements [58].

Inelastic scattering of the quarkonium by the nuclear matter is also an effect of higher order in $(mv)^2/p_T^2$. However, it can become dominant when the amount of nuclear matter that is traversed by the quarkonium is sufficiently large. Factorization breaks down when the length L of the quarkonium path in the nucleus satisfies

$$L \gtrsim \frac{\mathrm{Min}(z_Q, z_{\bar{Q}}) P_{\mathrm{onium}}^2}{M_A (k_T^{\mathrm{tot}})^2}, \tag{5.15}$$

where M_A is the mass of the nucleus, z is the parton longitudinal momentum fraction, P_{onium} is the momentum of the quarkonium in the parton CM frame, and k_T^{tot} is the accumulated transverse-momentum "kick" from passage through the nuclear matter. This condition for the break-down of factorization is similar to "target-length condition" in Drell–Yan production [59, 60]. Such a breakdown of factorization

is observed in the Cronin effect at low p_T and in Drell–Yan production at low Q^2, where the cross-section is proportional to the nucleon number raised to a power less than unity.

It is possible that multiple-scattering effects may be larger for colour-octet production than for colour-singlet production. In the case of colour-octet production, the pre-quarkonium $Q\bar{Q}$ system carries a nonzero colour charge and, therefore, has a larger amplitude to exchange soft gluons with spectator partons.

At present, there is no complete, rigorous theory to account for all of the effects of multiple scattering, and we must resort to "QCD-inspired" models. A reasonable requirement for models is that they be constructed so that they are compatible with the factorization result in the large-p_T limit. Many models treat interactions of the pre-quarkonium with the nucleus as on-shell scattering (Glauber scattering). This assumption should be examined carefully, as on-shell scattering is known, from the factorization proofs, not to be a valid approximation in leading order in $(mv)^2/p_T^2$.

2 QUARKONIUM PRODUCTION AT THE TEVATRON

Charmonium and bottomonium are produced copiously in high energy hadron colliders. The present and future hadron colliders include

- the Tevatron, a $p\bar{p}$ collider operating at Fermilab with centre-of-mass energy of 1.8 TeV in Run I and 1.96 TeV in Run II,
- RHIC, a heavy-ion or pp collider operating at Brookhaven with centre-of-mass energy of up to 200 GeV per nucleon–nucleon collision,
- the LHC at CERN, a pp collider under construction at CERN with centre-of-mass energy of 17 TeV.

In this section, we focus on the Tevatron, because it has produced the most extensive and precise data on quarkonium production. The photoproduction of quarkonium at high-energy $p\bar{p}$, pp, and heavy ion colliders is discussed in Chapter 7 of this report.

2.1 Charmonium cross-sections

In high energy collisions, charmonium is produced both through direct production mechanisms and through decays of other hadrons. In the case of charmonium production through B-hadron decays, the charmonium is produced at a secondary vertex, and a vertex detector can be used to identify this contribution to the measured production rate. We refer to the inclusive cross-section for production of a charmonium state with the contribution from B decays removed as the *prompt* cross-section. The prompt cross-section includes both the direct production of the charmonium and its production through decays of higher charmonium states.

In Run I of the Tevatron, the CDF collaboration measured the prompt cross-sections for the production of several charmonium states in $p\bar{p}$ collisions at a centre-of-mass energy of 1.8 TeV [61,62]. The CDF data for production of direct J/ψ, prompt $\psi(2S)$, and prompt J/ψ from decay of χ_c are shown in Fig. 5.1. In the CDF analysis, prompt J/ψ's that do not come from decays of $\psi(2S)$ or χ_c were assumed to be produced directly.

At non-vanishing transverse momentum, the leading parton processes for producing charmonium ($ij \to c\bar{c} + k$, where i, j, and k are light quarks, antiquarks, and gluons) occur at order α_s^3. The colour-singlet-model (CSM) predictions are shown as dotted lines in Fig. 5.1. In the top two panels of Fig. 5.1, the more steeply falling dotted lines are the predictions of the CSM at leading order in α_s. The other dotted lines in the top two panels of Fig. 5.1 are contributions of higher order in α_s involving gluon fragmentation. As can be seen in the top panel of Fig. 5.1, the gluon-fragmentation contribution renders the shape of the CSM prediction for direct J/ψ production roughly compatible with the CDF data. However, the normalization is too small by more than an order of magnitude. There is a similar

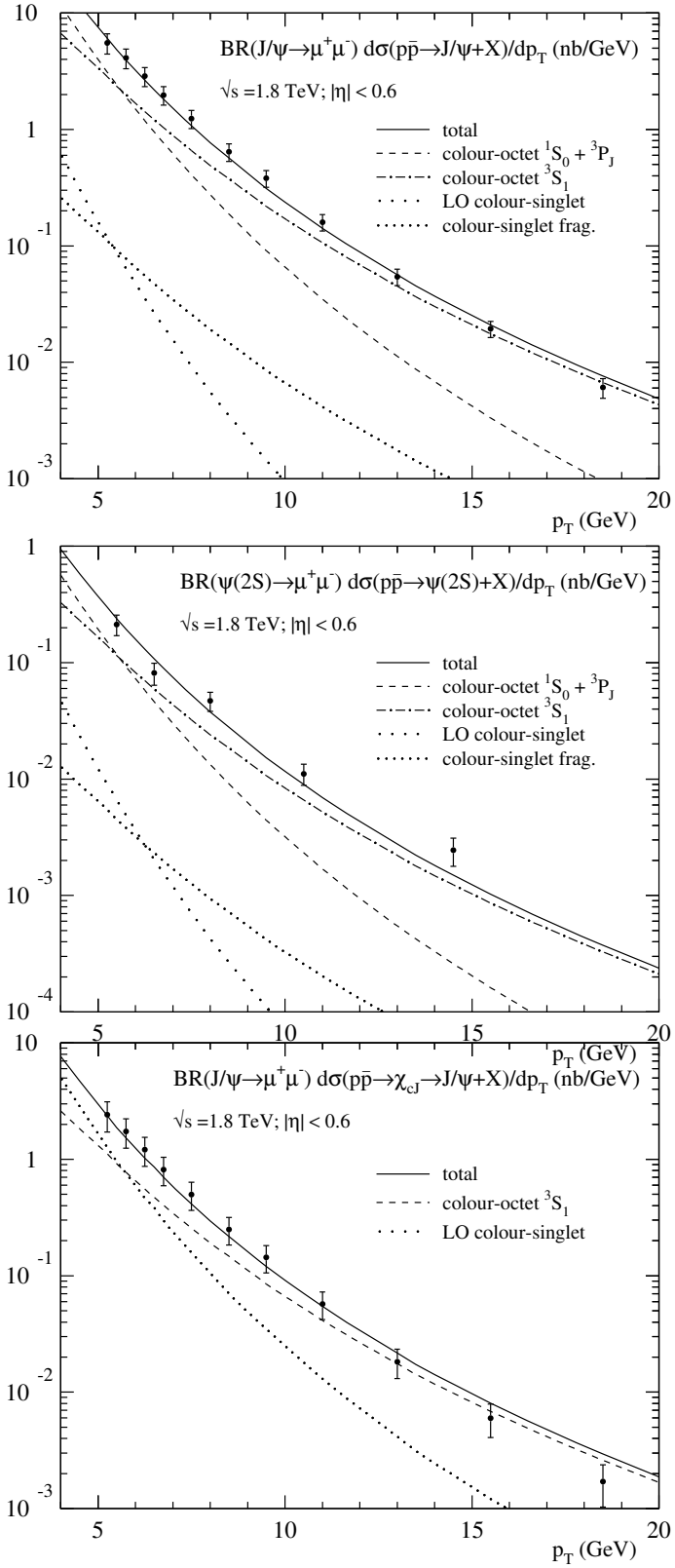

Fig. 5.1: Differential cross-sections for the production of direct J/ψ (top), prompt $\psi(2S)$ (middle), and prompt J/ψ from decay of χ_c (bottom) at the Tevatron as a function of p_T. The data points are CDF measurements from Run I [61, 62]. The dotted curves are the CSM contributions. The solid curves are the NRQCD factorization fits, and the other curves are individual colour-octet contributions to the fits. From Ref. [64].

Table 5.1: NRQCD production matrix elements for charmonium states obtained from the transverse momentum distributions at the Tevatron [64]. The errors quoted are statistical only.

H	$\langle \mathcal{O}_1^H \rangle$	$\langle \mathcal{O}_8^H({}^3S_1) \rangle$	$M_{3.5}^H$
J/ψ	$1.16\ \mathrm{GeV}^3$	$(1.19 \pm 0.14) \times 10^{-2}\ \mathrm{GeV}^3$	$(4.54 \pm 1.11) \times 10^{-2}\ \mathrm{GeV}^3$
$\psi(2S)$	$0.76\ \mathrm{GeV}^3$	$(0.50 \pm 0.06) \times 10^{-2}\ \mathrm{GeV}^3$	$(1.89 \pm 0.46) \times 10^{-2}\ \mathrm{GeV}^3$
χ_{c0}	$0.11\ \mathrm{GeV}^5$	$(0.31 \pm 0.04) \times 10^{-2}\ \mathrm{GeV}^3$	

discrepancy in the normalization for prompt $\psi(2S)$ production, as can be seen in the middle panel of Fig. 5.1. In the case of production of prompt J/ψ from decay of χ_c, which is shown in the bottom panel of Fig. 5.1, the discrepancy is less dramatic, but the cross-section is still under-predicted by the CSM. The large discrepancies between the measurements and the CSM predictions for the production cross-section for S-wave charmonium states rules out the CSM as a credible model for quarkonium production.

According to the NRQCD factorization approach, the charmonium production cross-section contains not only the CSM terms, which are absolutely normalized, but also colour-octet terms, whose normalizations are determined by colour-octet matrix elements. In the case of J/ψ and $\psi(2S)$ production, the most important colour-octet matrix elements are $\langle \mathcal{O}_8^H({}^3S_1) \rangle$, $\langle \mathcal{O}_8^H({}^3P_0) \rangle$, and $\langle \mathcal{O}_8^H({}^1S_0) \rangle$. At large p_T, the J/ψ and $\psi(2S)$ cross-sections are dominated by gluon fragmentation into colour-octet ${}^3S_1$ charm pairs [65], which falls as $d\hat{\sigma}/dp_T^2 \sim 1/p_T^4$. The colour-octet ${}^1S_0$ and ${}^3P_J$ channels are significant in the region $p_T \lesssim 10$ GeV, but fall as $d\hat{\sigma}/dp_T^2 \sim 1/p_T^6$ and become negligible at large p_t. Because the ${}^1S_0^{(8)}$ and ${}^3P_J^{(8)}$ short-distance cross-sections have a similar p_t dependence, the transverse momentum distribution is sensitive only to the linear combination M_k^H defined in (5.8), with $k \approx 3$. As can be seen in the top panel of Fig. 5.1, a good fit to the normalization and shape of the direct J/ψ cross-section can be obtained by adjusting $\langle \mathcal{O}_8^{J/\psi}({}^3S_1) \rangle$ and $M_{3.5}^{J/\psi}$. As is shown in the middle panel of Fig. 5.1, a similarly good fit to the prompt $\psi(2S)$ cross-section can be obtained by adjusting the corresponding parameters for $\psi(2S)$. In the case of production of the χ_{cJ} states, the most important colour-octet matrix element is $\langle \mathcal{O}_8^H({}^3S_1) \rangle$. As can be seen in the bottom panel of Fig. 5.1, the fit to the cross-section for production of prompt J/ψ from decay of χ_c can be improved by adjusting $\langle \mathcal{O}_8^{\chi_{c0}}({}^3S_1) \rangle$. Table 5.1 shows the values of the quarkonium matrix elements that are obtained in the fit of Ref. [64, 66]. The colour-singlet matrix elements are taken from the potential-model calculation of Refs. [67, 68]. The colour-octet matrix elements have been extracted from the CDF data [61, 62]. The CTEQ5L parton distribution functions [69] were used, with renormalization and factorization scales $\mu = (p_T^2 + 4m_c^2)^{1/2}$ and $m_c = 1.5\,\mathrm{GeV}$. The Altarelli–Parisi evolution has been included for the $\langle \mathcal{O}_8^{\chi_{c0}}({}^3S_1) \rangle$ fragmentation contribution. See Ref. [66] for further details. The extraction of the various colour-octet matrix elements relies on the differences in their p_T dependences. Smaller experimental error bars could help to resolve the different p_T dependences with greater precision.

The normalization and the shape of the prompt charmonium cross-section at the Tevatron can also be described reasonably well by the colour-evaporation model (CEM). The CEM parameters can be fixed by fitting to the data from pN collisions and by using the measured branching fractions for charmonium decays. The predictions of the CEM at next-to-leading order in α_s (NLO) can be calculated using the NLO parameter sets that are described in Section 3.3. The normalization of the predicted cross-section for prompt J/ψ production is in reasonable agreement with the CDF data from Run I. The shape can be brought into good agreement by adding k_T smearing, with $\langle k_T^2 \rangle = 2.5\ \mathrm{GeV}^2$. In Fig. 5.2, the resulting

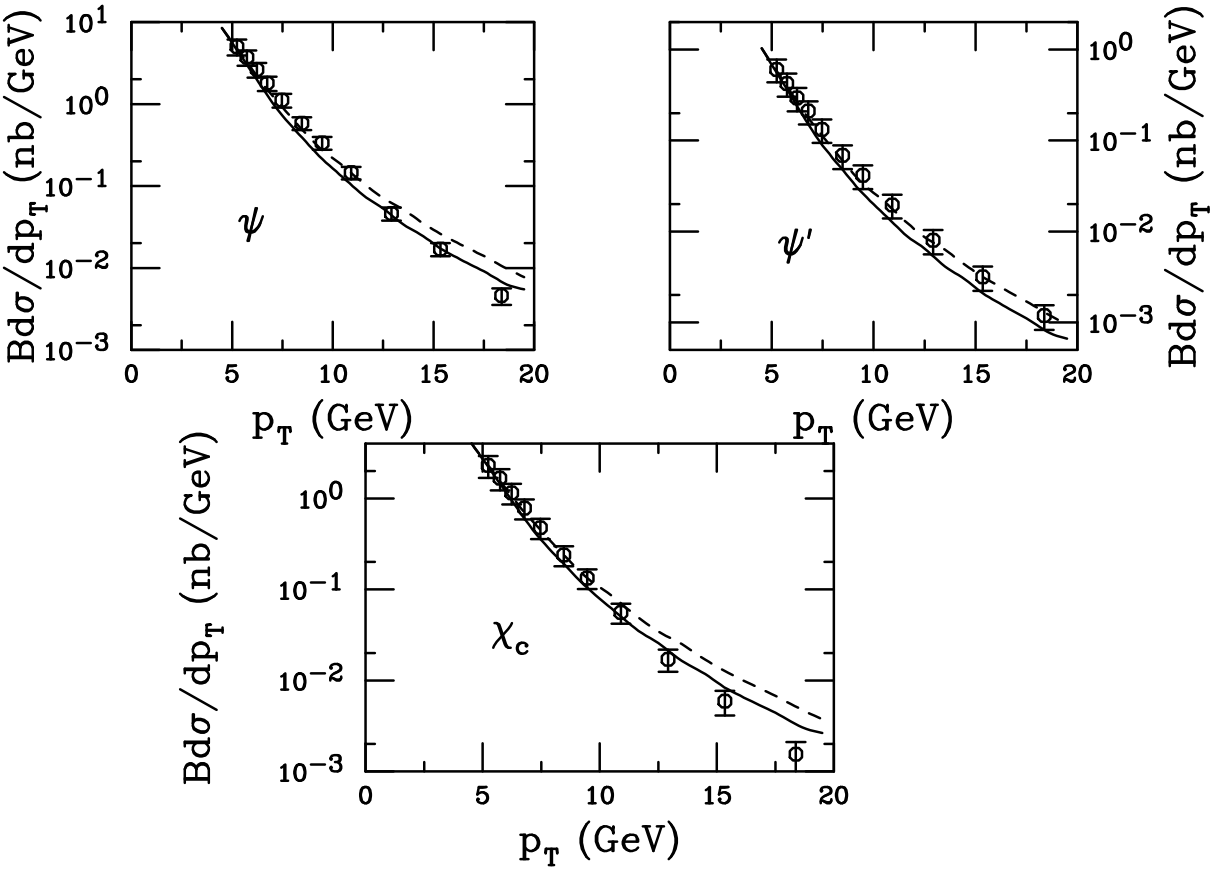

Fig. 5.2: Differential cross-sections for production of direct J/ψ (top left), prompt J/ψ from decays of $\psi(2S)$ (top right), and prompt J/ψ from decays of χ_c (bottom) at the Tevatron as a function of p_T. The data points are the CDF measurements [61, 62]. The dotted and solid curves are the CEM predictions at NLO with $\langle k_T^2 \rangle = 2.5$ GeV^2, using the first and fourth charmonium parameter sets in Table 5.8.

CEM predictions are compared with the CDF charmonium data for production of direct J/ψ, prompt J/ψ from decay of $\psi(2S)$, and prompt J/ψ from decay of χ_c. The predictions are all in good agreement with the CDF data.

In the case of the S-wave production matrix elements, the NRQCD velocity-scaling rules predict that

$$\frac{\langle \mathcal{O}_8 \rangle}{\langle \mathcal{O}_1 \rangle} \sim \frac{v^4}{2N_c}, \tag{5.16}$$

where this estimate includes colour factors that are associated with the expectation values of the NRQCD operators, as advocated by Petrelli *et al.* [70]. As can be seen from Table 5.1, the extracted colour-octet matrix elements are roughly compatible with this estimate [$v^4/(2N_c) \approx 0.015$]. However, a much more stringent test of the theory is to check the universality of the extracted matrix elements in other processes. In the case of the P-wave production matrix elements, the velocity scaling rules yield the estimate

$$\frac{\langle \mathcal{O}_8 \rangle}{\langle \mathcal{O}_1 \rangle / m_c^2} \sim \frac{v^0}{2N_c}. \tag{5.17}$$

The P-wave colour-octet matrix element in Table 5.1 is somewhat smaller than this estimate would suggest. That is also the case for the matrix elements that appear in P-wave quarkonium decays, which have been determined phenomenologically [71] and in lattice calculations [4–8].

In Table 5.2, we show matrix elements for J/ψ production that have been obtained from various other fits to the transverse momentum distribution. We see that there is a large uncertainty that arises from the dependence of the matrix elements on the factorization and renormalization scales, as well as a large dependence on the choice of parton distributions. The extracted values of the colour-octet matrix elements (especially M_k) are very sensitive to the small-p_T behavior of the cross-section and this, in turn, leads to a sensitivity to the behavior of the gluon distribution at small x. Furthermore, the effects of multiple gluon emission are important, and their omission in the fixed-order perturbative calculations leads to overestimates of the sizes of the matrix elements. In Table 5.2, one can see the results of various attempts to estimate the effects of multiple gluon emission. Sanchis–Lozano (S) and Kniehl and Kramer (KK) made use of parton-shower Monte Carlos, while Petrelli (P) and Sridhar, Martin, and Stirling (SMS) employed models containing Gaussian k_T smearing. In addition, Sanchis–Lozano included a resummation of logarithms of p_T^2/m^2. Hägler, Kirschner, Schäfer, Szymanowski, and Teryaev (HKSST) used the k_T-factorization formalism to resum large logarithms in the limit $s \gg 4m_c^2$. (See also the calculations by Yuan and Chao [87, 88].) Similar large dependences on the choices of factorization and renormalization scales, parton distributions, and multiple gluon emission can be seen in the matrix elements that have been extracted from the $\psi(2S)$ and χ_c transverse momentum distributions. See Ref. [64] for details.

Effects of corrections of higher order in α_s are a further uncertainty in the fits to the data in Table 5.2. Such corrections are known to be large in the case of charmonium decays. In the case of charmonium production, a new channel for colour-singlet production, involving t-channel gluon exchange, first appears in order α_s and could yield a large correction. Maltoni and Petrelli [83] have found that real-gluon corrections to colour-singlet $^3S_1$ production give a large contribution. Next-to-leading order (NLO) corrections in α_s for χ_{c0} and χ_{c2} production have been calculated [70], as have NLO corrections for the fragmentation process [89–91]. Large corrections from the resummation of logarithms of p_T^2/m^2 in the fragmentation of partons into quarkonium have also been calculated [80, 92–94].

Similar theoretical uncertainties arise in the extraction of the NRQCD production matrix elements for the $\psi(2S)$ and χ_c states. The statistical uncertainties are larger for $\psi(2S)$ and χ_c production than for J/ψ production. We refer the reader to Ref. [64] for some examples of the NRQCD matrix elements that have been extracted for these states.

The CDF collaboration has measured the fraction of prompt J/ψ's that come from decays of $\psi(2S)$ and $\chi_c(1P)$ states and the fractions that are produced directly [62]. The CDF measurements were made for J/ψ's with transverse momentum $p_T > 4$ GeV and pseudo-rapidity $|\eta| < 0.6$. The fractions, which are defined in Eqs. (5.11) and (5.12), are given in Table 5.3. The fraction of J/ψ's that are directly produced is approximately constant over the range 5 GeV $< p_T <$ 15 GeV. The fraction from decays of $\psi(2S)$ increases from $(7 \pm 2)\%$ at $p_T = 5$ GeV to $(15 \pm 5)\%$ at $p_T = 15$ GeV. The fraction from decays of $\chi_c(1P)$ seems to decrease slowly over this range of p_T. Such variations with p_T are counter to the predictions of the colour-evaporation model.

The CDF collaboration has also measured the ratio of the prompt χ_{c1} and χ_{c2} cross-sections at the Tevatron [95]. The measured value of the ratio R_{χ_c} defined in Eq. (5.10) is

$$R_{\chi_c} = 1.04 \pm 0.29(\text{stat.}) \pm 0.12(\text{sys.}). \tag{5.18}$$

The χ_{c2} and χ_{c1} were observed through their radiative decays into a J/ψ and a photon, which were required to have transverse momenta exceeding 4 GeV and 1 GeV, respectively. The colour-evaporation model predicts that this ratio should be close to the spin-counting ratio $3/5$, since the feeddown from the $\psi(2S)$ is small. The NRQCD factorization fit to the prompt χ_c cross-section in the region $p_T > 5$ GeV implies a ratio of 0.9 ± 0.2 [96]. The CDF result slightly favors the NRQCD factorization prediction.

Charmonium production data from Tevatron Run II have recently become available. Using a 39.7 pb^{-1} data sample from Run II, the CDF Collaboration has measured the inclusive cross-section for J/ψ production and subsequent decay into $\mu^+\mu^-$ [97]. The inclusive cross-section includes both prompt J/ψ's and J/ψ's from decays of b-hadrons. The inclusive differential cross-section as a function of p_T

Table 5.2: J/ψ production matrix elements in units of 10^{-2} GeV^3 [64]. The first error bar is statistical; the second error bar (where present) is obtained by varying the factorization and renormalization scales.

Reference	PDF	$\langle \mathcal{O}_8^{J/\psi}(^3S_1)\rangle$	$M_k^{J/\psi}$	k
LO collinear factorization				
CL [73]	MRS(D0) [74]	0.66 ± 0.21	6.6 ± 1.5	3
BK [66]	CTEQ4L [75]	$1.06 \pm 0.14^{+1.05}_{-0.59}$	$4.38 \pm 1.15^{+1.52}_{-0.74}$	3.5
	GRV-LO(94) [76]	$1.12 \pm 0.14^{+0.99}_{-0.56}$	$3.90 \pm 1.14^{+1.46}_{-1.07}$	
	MRS(R2) [77]	$1.40 \pm 0.22^{+1.35}_{-0.79}$	$10.9 \pm 2.07^{+2.79}_{-1.26}$	
BKL [78]	MRST-LO(98) [79]	0.44 ± 0.07	8.7 ± 0.9	3.4
	CTEQ5L [69]	0.39 ± 0.07	6.6 ± 0.7	
Parton shower radiation				
S [80]	CTEQ2L [81]	0.96 ± 0.15	1.32 ± 0.21	3
	MRS(D0) [74]	0.68 ± 0.16	1.32 ± 0.21	
	GRV-HO(94) [76]	0.92 ± 0.11	0.45 ± 0.09	
KK [82]	CTEQ4M [75]	0.27 ± 0.05	0.57 ± 0.18	3.5
k_T-smearing				
P [83]	CTEQ4M [75]	$\langle k_T\rangle$[GeV]		3.5
		1	1.5 ± 0.22	8.6 ± 2.1
		1.5	1.7 ± 0.19	4.5 ± 1.5
SMS [84]	MRS(D$'_-$) [74]	0.7	1.35 ± 0.30	8.46 ± 1.41	3
		1	1.5 ± 0.29	7.05 ± 1.17	
k_T-factorization				
HKSST1 [85]	KMS [86]	$\approx 0.04 \pm 0.01$	$\approx 6.5 \pm 0.5$	5

Table 5.3: The fractions F_H of prompt J/ψ mesons that are produced by the decay of higher charmonium states H and the fraction $F_{J/\psi}$ that are produced directly.

H	F_H (in %)
J/ψ	64 ± 6
$\psi(2S)$	7 ± 2 to 15 ± 5
$\chi_c(1P)$	29.7 ± 1.7(stat.) ± 5.7(sys.)

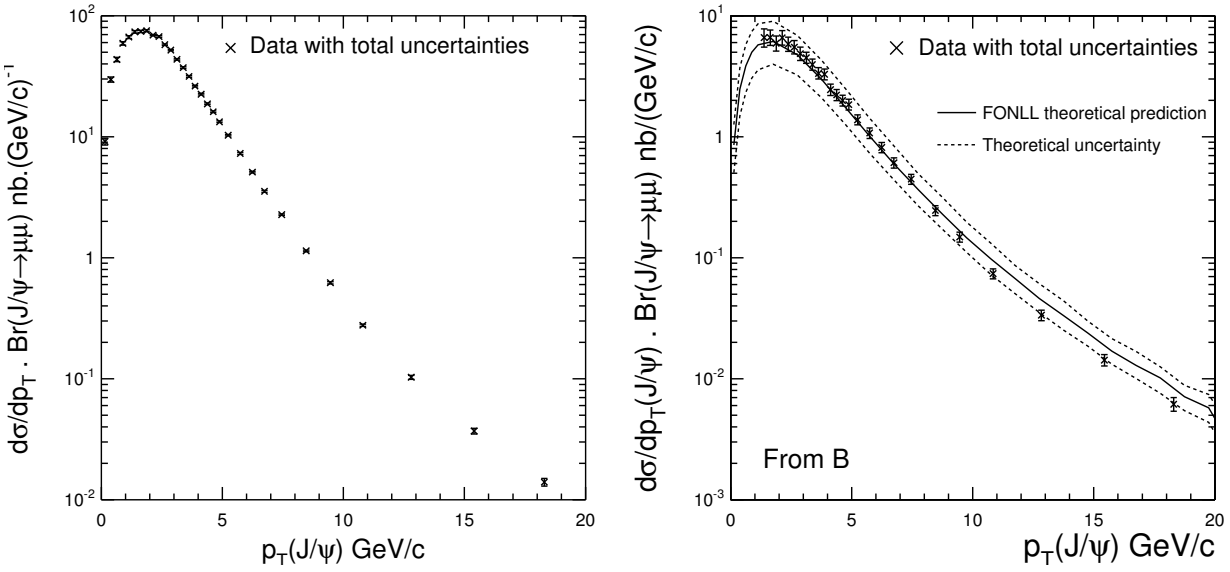

Fig. 5.3: Differential inclusive cross-section for $p\bar{p} \to J/\psi X$ (left). Differential cross-section distribution of J/ψ events from b-hadron decay (right). Both cross-sections are plotted as a function of the transverse momentum p_T of the J/ψ and are integrated over the rapidity range $|y(J/\psi)| < 0.6$.

for rapidity $|y| < 0.6$ has been obtained down to zero transverse momentum and is shown in the left panel of Fig. 5.3. The total integrated cross-section for inclusive J/ψ production in $p\bar{p}$ interactions at $\sqrt{s} = 1.96$ TeV is measured to be

$$\sigma[p\bar{p} \to J/\psi X, |y(J/\psi)| < 0.6] \; = 4.08 \pm 0.02(\mathrm{stat}) \pm 0.36(\mathrm{syst}) \; \mu\mathrm{b}. \tag{5.19}$$

These new measurements await comparison with updated theoretical calculations in the low p_T region.

Using a sample of 4.7 pb^{-1} of Run II data, the D0 collaboration has verified that the J/ψ cross-section is independent of the rapidity of the J/ψ for a rapidity range $0 < |y| < 2$. This analysis has been performed for $p_T(J/\psi) > 5$ GeV and $p_T(J/\psi) > 8$ GeV [98]. The CDF and D0 collaborations have performed studies of forward differential J/ψ production cross-sections in the pseudo-rapidity regions $2.1 < |\eta(J/\psi)| < 2.6$ and $2.5 \leq |\eta(J/\psi)| \leq 3.7$, respectively, using their Run I data [99, 100].

Using 39.7 pb^{-1} of the Run II data, the CDF Collaboration has also measured the differential cross-section as a function of p_T and the cross-section integrated over p_T for the production of b-hadrons that decay in the channel $H_b \to J/\psi X$ [97]. The differential cross-section multiplied by the branching fraction for $J/\psi \to \mu^+\mu^-$ is shown in the right panel of Fig. 5.3. A recent QCD prediction that is based on a fixed order (FO) calculation plus a resummation of next-to-leading order logs (NLL) [101] is overlaid. The cross-section integrated over p_T was found to be

$$\sigma[p\bar{p} \to H_b X, p_T(J/\psi) > 1.25 \text{ GeV}, |y(J/\psi)| < 0.6] \; = 28.4 \pm 0.4(\mathrm{stat})^{+4.0}_{-3.8}(\mathrm{syst}) \; \mu\mathrm{b}. \tag{5.20}$$

This measurement can be used to extract the total inclusive b-hadron cross-section.

2.2 Bottomonium cross-sections

Using Run I data, the CDF Collaboration has reported inclusive production cross-sections for the $\Upsilon(1S)$, $\Upsilon(2S)$ and $\Upsilon(3S)$ states in the region $0 < p_T < 20$ GeV [102]. The rates of inclusive production of the $\Upsilon(1S)$, $\Upsilon(2S)$ and $\Upsilon(3S)$ states for $p_T > 4$ GeV were found to be higher than the rates predicted by CSM calculations by a factor of about five. Inclusion of colour-octet production mechanisms within

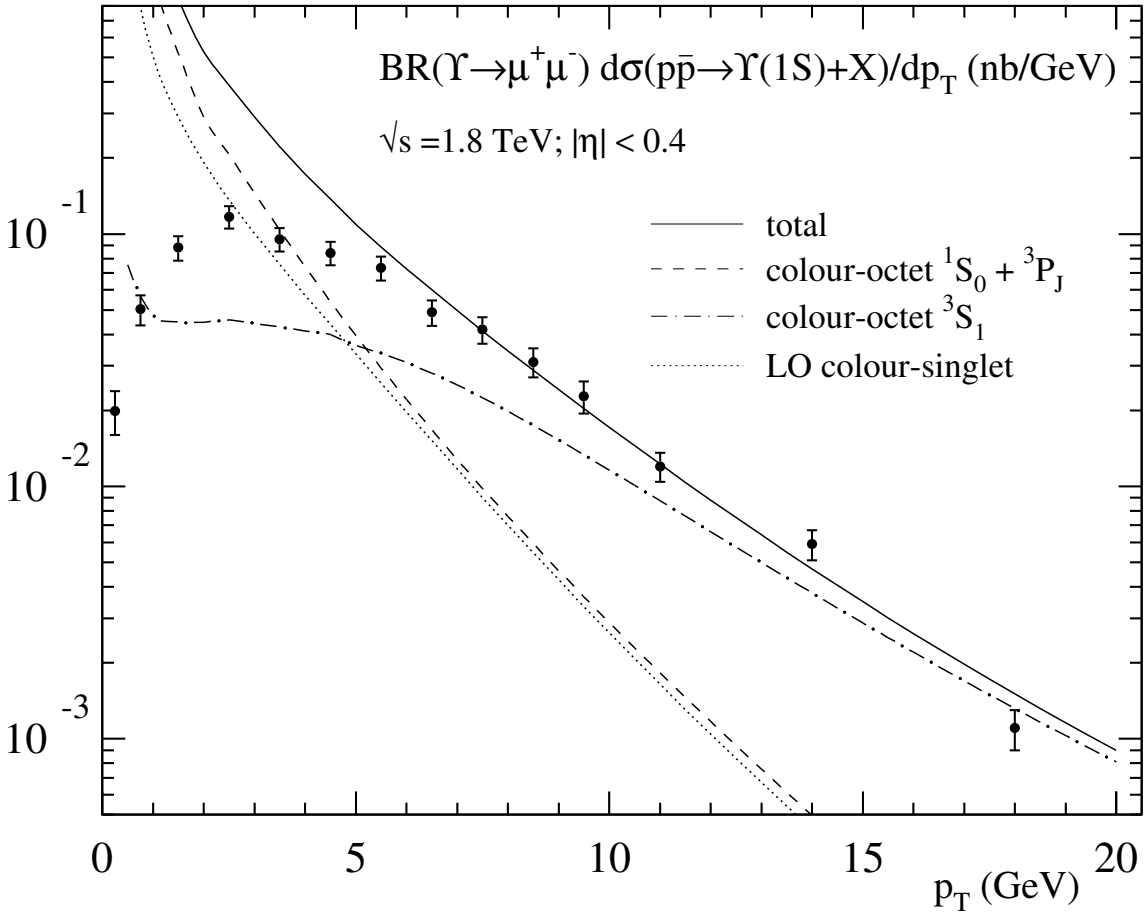

Fig. 5.4: Inclusive $\Upsilon(1S)$ cross-section at the Tevatron as a function of p_T. The data points are the CDF measurements [61]. The solid curve is the NRQCD factorization fit, and the other curves are individual contributions to the NRQCD factorization fit. From Ref. [64, 104].

the NRQCD framework can account for the observed cross-sections for $p_T > 8$ GeV [72, 73, 104, 105], as is shown for $\Upsilon(1S)$ production in Fig. 5.4. An accurate description of the Υ cross-section in the low-p_T region requires NLO corrections and a resummation of multiple gluon radiation. A fit to the CDF data using a parton shower Monte Carlo to model the effects of multiple gluon emission has given much smaller values of the colour-octet matrix elements that are compatible with zero [106].

The normalization and the shape of the bottomonium cross-sections at the Tevatron can also be described reasonably well by the colour-evaporation model (CEM). The CEM predictions are compared with the CDF data for $\Upsilon(1S)$, $\Upsilon(2S)$, and $\Upsilon(3S)$ in Fig. 5.5. Most of the relevant parameters can be fixed completely by fitting data from pN collisions and by using measured branching fractions for bottomonium decays. The predictions of the CEM at NLO that are shown in Fig. 5.5 have been calculated using the NLO parameter sets that are described in Section 3.3. The predicted cross-sections for $\Upsilon(1S)$ and $\Upsilon(3S)$ production are a little below the data; the normalizations can be improved by multiplying the cross-sections by a K-factor of 1.4. The shapes have been brought into good agreement with the data by including k_T smearing, with $\langle k_T^2 \rangle = 3.0$ GeV^2. This value of $\langle k_T^2 \rangle$ is a little larger than the value $\langle k_T^2 \rangle = 2.5$ GeV^2 that gives the best fit to the charmonium cross-sections.

A recent calculation of the production cross-sections for the $\Upsilon(1S)$, $\Upsilon(2S)$, and $\Upsilon(3S)$ at the Tevatron combines a resummation of logarithms of M_Υ^2/p_T^2 with a calculation at leading order in α_s in what is, in essence, the colour-evaporation model [41]. The resummation of the effects of multiple gluon

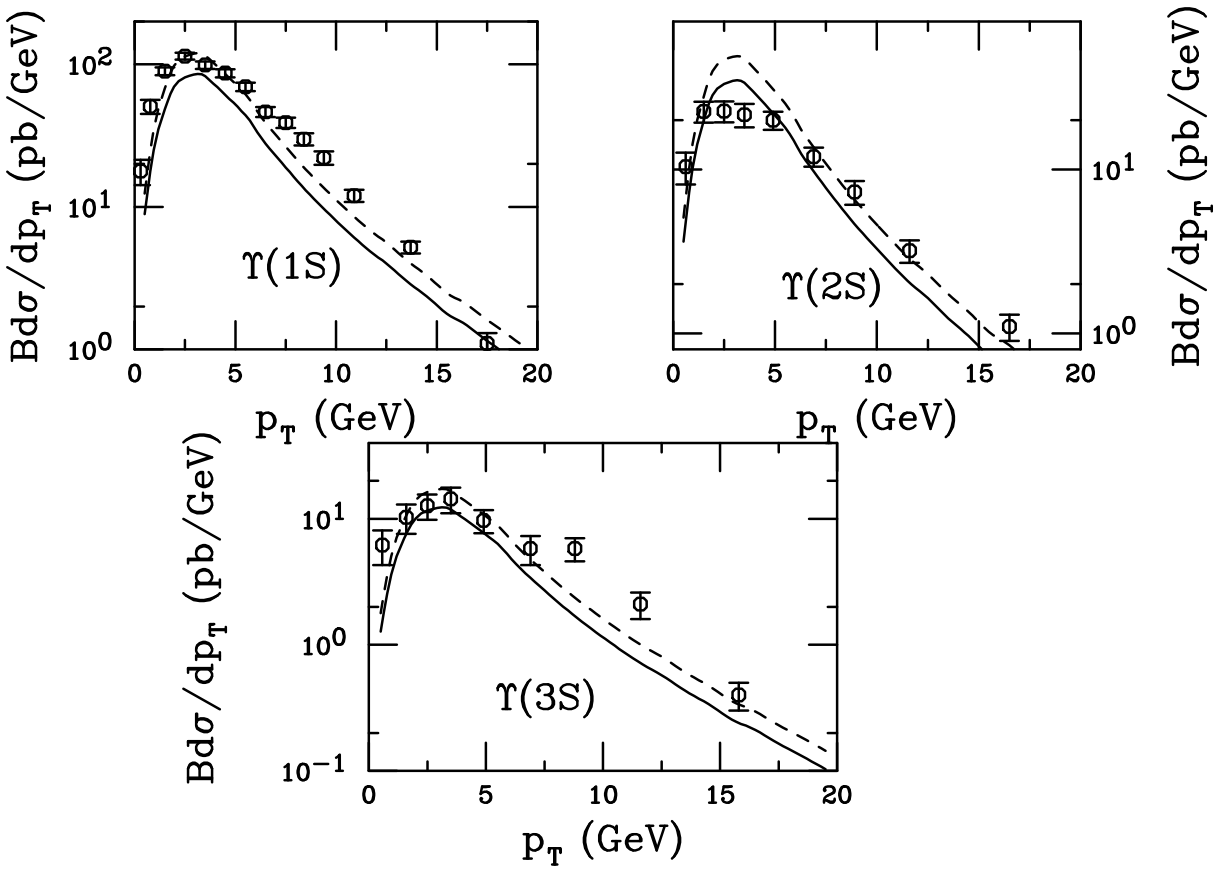

Fig. 5.5: Differential cross-sections for $\Upsilon(1S)$ (top left), $\Upsilon(2S)$ (top right), and $\Upsilon(3S)$ (bottom) at the Tevatron as a function of p_T. The data points are the CDF measurements [102]. The solid curves are the CEM predictions at NLO with $\langle k_T^2 \rangle = 3.0$ GeV^2, using the first bottomonium parameter set in Tables 5.8. The dashed curves are multiplied by a K-factor of 1.4.

emission in the CEM has some simplifications that do not occur in the NRQCD factorization approach. The results of the calculation of Ref. [41] are shown, along with CDF data, in Fig. 5.6. The resummation of logarithms of M_Υ^2/p_T^2 allows the calculation to reproduce the shape of the data at small p_T. The normalizations have been adjusted to obtain the best fit to the data. the best fit to the data.

The CDF Collaboration has also reported the fractions of $\Upsilon(1S)$ mesons, for $p_T > 8$ GeV, that come from decays of $\chi_b(1P)$, $\chi_b(2P)$, $\chi_b(3P)$, $\Upsilon(2S)$, and $\Upsilon(3S)$ and the fraction that originate from direct production [103]. The fractions from decays of $\Upsilon(nS)$ and for $\chi_b(nP)$ are defined by

$$F_{\Upsilon(nS)} = \mathrm{Br}[\Upsilon(nS) \to \Upsilon(1S) + X] \, \frac{\sigma[\Upsilon(nS)]}{\sigma[\Upsilon(1S)]}, \tag{5.21}$$

$$F_{\chi_b(nP)} = \sum_{J=0}^{3} \mathrm{Br}[\chi_{bJ}(nP) \to \Upsilon(1S) + X] \, \frac{\sigma[\chi_{bJ}(nP)]}{\sigma[\Upsilon(1S)]}. \tag{5.22}$$

The fraction of $\Upsilon(1S)$'s that are produced directly can be denoted by $F_{\Upsilon(1S)}$. The fractions are given in Table 5.4.

2.3 Polarization

The polarization of the quarkonium contains important information about the production mechanism. The polarization variable α for a 1^{--} state, such as J/ψ, $\psi(2S)$, or $\Upsilon(1S)$, is defined by Eq. (5.13),

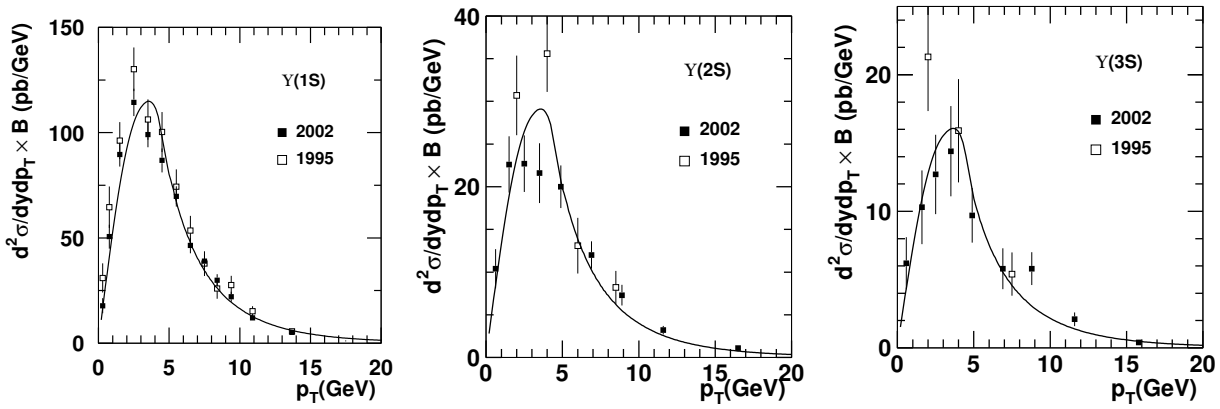

Fig. 5.6: Calculated differential cross-sections times leptonic branching fractions B, evaluated at $y = 0$, as functions of transverse momentum for hadronic production of (a) $\Upsilon(1S)$, (b) $\Upsilon(2S)$, and (c) $\Upsilon(3S)$ [41], along with CDF data [102, 107] at $\sqrt{S} = 1.8$ TeV. The solid lines show the result of the full calculation. The 1995 CDF cross-sections are multiplied a factor 0.88.

Table 5.4: The fractions F_H of $\Upsilon(1S)$ mesons that are produced by the decay of a higher bottomonium state H and the fraction $F_{\Upsilon(1S)}$ that are produced directly.

H	F_H (in %)
$\Upsilon(1S)$	$50.9 \pm 8.2(\text{stat.}) \pm 9.0(\text{sys.})$
$\Upsilon(2S)$	$10.7^{+7.7}_{-4.8}$
$\Upsilon(3S)$	$0.8^{+0.6}_{-0.4}$
$\chi_b(1P)$	$27.1 \pm 6.9(\text{stat.}) \pm 4.4(\text{sys.})$
$\chi_b(2P)$	$10.5 \pm 4.4(\text{stat.}) \pm 1.4(\text{sys.})$
$\chi_b(3P)$	< 6

where the angle θ is measured with respect to some polarization axis. At a hadron collider, a convenient choice of the polarization axis is the direction of the boost vector from the quarkonium rest frame to the centre-of-momentum frame of the colliding hadrons.

The NRQCD factorization approach gives a simple prediction for the polarization variable α at very large transverse momentum. The production of a quarkonium with p_T that is much larger than the quarkonium mass is dominated by gluon fragmentation — a process in which the quarkonium is formed in the hadronization of a gluon that is created with even larger transverse momentum. The NRQCD factorization approach predicts that the dominant gluon-fragmentation process is gluon fragmentation into a $Q\bar{Q}$ pair in a colour-octet ${}^3S_1$ state. The fragmentation probability for this process is of order α_s, while the fragmentation probabilities for all other processes are of order α_s^2 or higher. The NRQCD matrix element for this fragmentation process is $\langle \mathcal{O}_8^H({}^3S_1) \rangle$. At large p_T, the fragmenting gluon is nearly on its mass shell, and, so, is transversely polarized. Furthermore, the velocity-scaling rules predict that the colour-octet $Q\bar{Q}$ state retains the transverse polarization as it evolves into an S-wave quarkonium state [108], up to corrections of relative order v^2. Radiative corrections and colour-singlet production dilute the quarkonium polarization somewhat [66, 89]. In the case of J/ψ production, feeddown from higher quarkonium states is also important [78]. Feeddown from χ_c states is about 30% of the J/ψ sample and dilutes the polarization. Feeddown from the $\psi(2S)$ is about 10% of the J/ψ sample and is largely transversely polarized. Despite these various diluting effects, a substantial polarization is

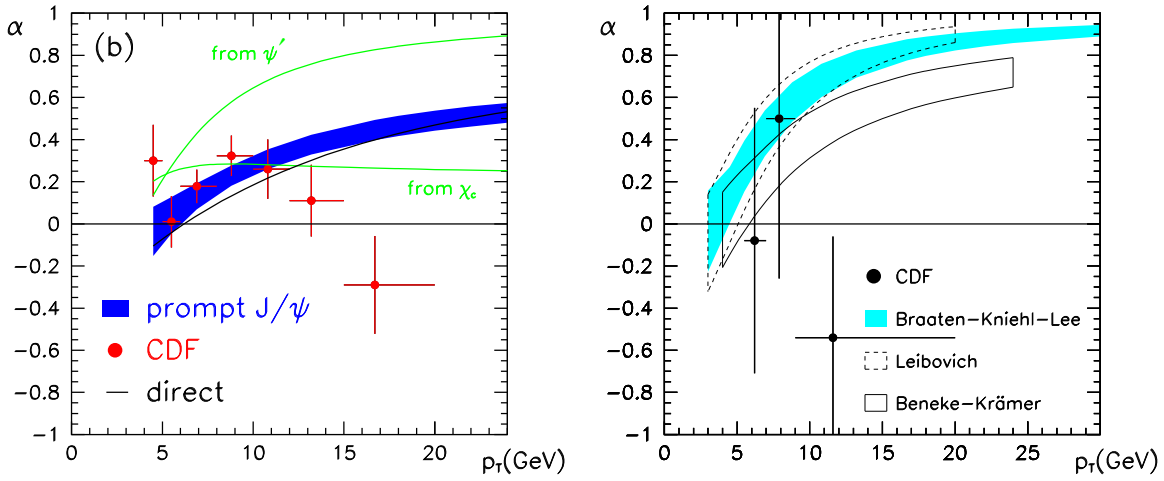

Fig. 5.7: Polarization variable α for prompt J/ψ (left) and for prompt $\psi(2S)$ (right) at the Tevatron as a function of p_T. The data points are the CDF measurements from Run I [103]. In the left panel (prompt J/ψ), the band is the NRQCD factorization prediction of Ref. [78], and the other curves are the values of α for individual components of the prompt J/ψ signal. In the right panel (prompt $\psi(2S)$), the bands are various NRQCD factorization predictions [66, 78, 109].

expected at large p_T, and its detection would be a "smoking gun" for the presence of the colour-octet production mechanism. In contrast, the colour-evaporation model predicts zero quarkonium polarization.

The CDF measurement of the J/ψ polarization as a function of p_T [103] is shown in the left panel of Fig. 5.7, along with the NRQCD factorization prediction [78]. The observed J/ψ polarization is in agreement with the prediction, except for the highest p_T bin. However, the prediction of increasing polarization with increasing p_T is not in evidence. The CDF data [103] and the NRQCD factorization prediction [66, 78, 109] for $\psi(2S)$ polarization are shown in the right panel of Fig. 5.7. The theoretical analysis of $\psi(2S)$ polarization is simpler than for the J/ψ, since feeddown does not play a rôle. However, the experimental statistics are not as good for the $\psi(2S)$ as for J/ψ. Again, the expectation of increasing polarization with increasing p_T is not confirmed.

Because the polarization depends on ratios of matrix elements, some of the theoretical uncertainties are reduced compared with those in the production cross-section. The polarization is probably not strongly affected by multiple gluon emission or K-factors. Uncertainties from contributions of higher-order in α_s could conceivably change the rates for the various spin states by a factor of two. Therefore, it is important to carry out the NLO calculation, but that calculation is very difficult technically and is computing intensive. order-v^2 corrections to parton fragmentation to quarkonium can be quite large. Bodwin and Lee [110] have found that the v^2 corrections to gluon fragmentation to J/ψ are about $+70\%$ for the colour-singlet channel and -50% for the colour-octet channel. The colour-singlet correction shifts α down by about 10% at the largest p_T. Since the colour-octet matrix element is fit to Tevatron data, the v^2 correction merely changes the size of the matrix element and has no immediate effect on the theoretical prediction. An additional theoretical uncertainty comes from the presence of order-v^2 spin-flip processes in the evolution of the $Q\bar{Q}$ pair into the quarkonium. It could turn out that spin-flip contributions are large, either because their velocity-scaling power laws happen to have large coefficients or because, as has been suggested in Refs. [111–115], the velocity scaling rules themselves need to be modified. Then spin-flip contributions could significantly dilute the J/ψ polarization. Nevertheless, it is is difficult to see how there could not be substantial polarization in J/ψ or $\psi(2S)$ production for $p_T > 4m_c$.[3]

[3]It has been argued that re-scattering interactions between the intermediate charm-quark pair and a co-moving colour field could yield unpolarized quarkonium [116, 117]. The theoretical analysis of these effects, however, relies on several simplifying

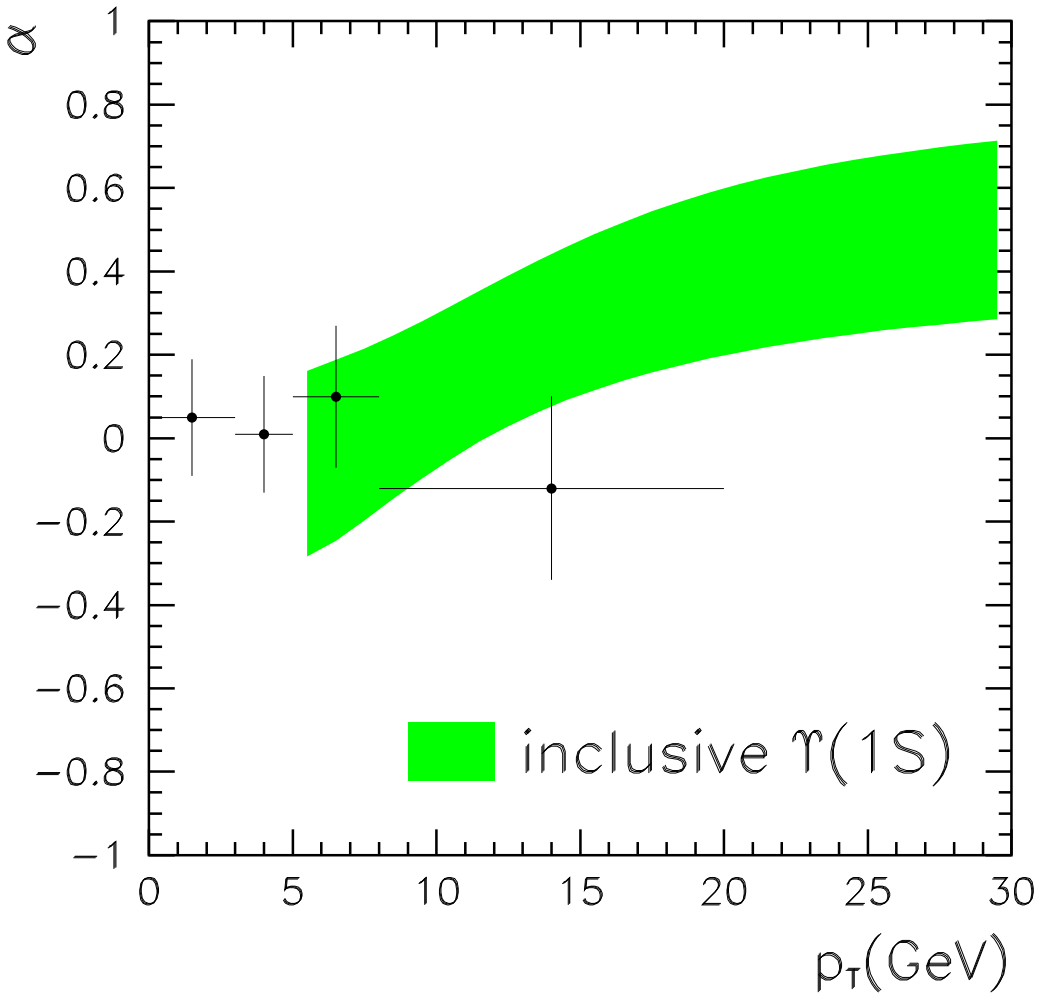

Fig. 5.8: Polarization variable α for inclusive $\Upsilon(1S)$ production at the Tevatron as a function of p_T. The data points are the CDF measurements from Run I [102]. The theoretical band represents the NRQCD factorization prediction [118].

The CDF data for Υ polarization is shown in Fig. 5.8, along with the NRQCD factorization prediction. Averaging over a range of p_T, the CDF Collaboration finds $\alpha = -0.06 \pm 0.20$ for 1 GeV $< p_T <$ 20 GeV [119, 120], which is consistent with the NRQCD factorization prediction [118]. In comparison with the prediction for J/ψ polarization, the prediction for Υ polarization has smaller v-expansion uncertainties. However, in the case of Υ production, the fragmentation mechanism does not dominate until relatively large values of p_T are reached, and, hence, the transverse polarization is predicted to be small for p_T below about 10 GeV. Unfortunately, the current Tevatron data sets run out of statistics in the high-p_T region.

2.4 Prospects for the Tevatron Run II

Run II at the Tevatron will provide a substantial increase in luminosity and will allow the collider experiments to determine the J/ψ, $\psi(2S)$ and χ_c cross-sections more precisely and at larger values of p_t. An accurate measurement of the J/ψ and $\psi(2S)$ polarization at large transverse momentum will be the most

assumptions, and further work is needed to establish the existence of re-scattering corrections in charmonium hadroproduction at large p_T.

crucial test of NRQCD factorization. In addition, improved data on the J/ψ and $\psi(2S)$ cross-sections will help to reduce some of the ambiguities in extracting the colour-octet matrix elements.

With increased statistics it might be possible to access other charmonium states such as the $\eta_c(nS)$ or the $h_c(nP)$. heavy-quark spin symmetry provides approximate relations between the nonperturbative matrix elements that describe spin-singlet and spin-triplet states. The matrix elements for $\eta_c(nS)$ are related to those for $\psi(nS)$, while the leading matrix elements for $h_c(nP)$ can be obtained from those for $\chi_c(nP)$. [See Eqs. (5.2–5.7).] Within NRQCD, the rates for $\eta(nS)$ and $h(nP)$ production can thus be predicted unambiguously in terms of the nonperturbative matrix elements that describe the J/ψ, $\psi(2S)$ and χ_c production cross-sections. A comparison of the various charmonium production rates would therefore provide a stringent test of NRQCD factorization and the heavy-quark spin symmetry. The cross-sections for producing the η_c and the h_c at Run II of the Tevatron are large [121, 122], but the acceptances and efficiencies for observing the decay modes on which one can trigger are, in general, small, and detailed experimental studies are needed to quantify the prospects. Other charmonium processes that have been studied in the literature include the production of D-wave states [123], J/ψ production in association with photons [124, 125], and double gluon fragmentation to J/ψ pairs [126].

The larger statistics expected at Run II of the Tevatron will also allow the collider experiments to improve the measurements of the bottomonium cross-sections. As yet undiscovered states, such as the $\eta_b(1S)$, could be detected, for example, in the decay $\eta_b \to J/\psi + J/\psi$ [105] or in the decay $\eta_b \to D^* + D^{(*)}$ [127], and the associated production of Υ and electroweak bosons might be accessible [128]. If sufficient statistics can be accumulated, the onset of transverse $\Upsilon(nS)$ polarization may be visible at $p_{T,\Upsilon} \gtrsim 15$ GeV.

3 QUARKONIUM PRODUCTION IN FIXED-TARGET EXPERIMENTS

3.1 Cross-sections

Several collaborations have made predictions for fixed-target quarkonium production within the NRQCD factorization formalism [129–131]. The predictions of Ref. [129] for J/ψ and $\psi(2S)$ production in pN collisions are shown, along with the experimental data, in the left panels of Figs. 5.9 and 5.10. The calculation is at leading-order in α_s and uses the standard truncation in v that is described in Section 1.1. The data are from the compilation in Ref. [26], with additional results from Refs. [132–134]. In the case of pN production of J/ψ, the data clearly require a colour-octet contribution, in addition to a colour-singlet contribution. In the case of $\psi(2S)$ production, it is less clear that a colour-octet contribution is essential. One should keep in mind that the colour-singlet contribution is quite uncertain, owing to uncertainties in the values of m_c and the renormalization scale [111]. One can reduce these uncertainties by considering the ratio of the cross-sections for direct and inclusive J/ψ production, which is predicted to be approximately 0.6 in the NRQCD factorization approach and approximately 0.2 in the colour-singlet model [111]. Clearly, experiment favors the NRQCD factorization prediction. However, the prediction for the ratio depends on our knowledge of feed-down from χ_c states, and, as we shall see, NRQCD factorization predictions for χ_c production in fixed-target experiments are not in good agreement with the data.

In fixed-target production of J/ψ and $\psi(2S)$ at leading order in α_s (LO), the relevant production matrix elements are $\langle \mathcal{O}_8^H(^3S_1)\rangle$, $\langle \mathcal{O}_8^H(^1S_0)\rangle$, and $\langle \mathcal{O}_8^H(^3P_0)\rangle$, but the cross-section is sensitive only to the linear combination M_k^H defined in (5.8) with $k \approx 7$. The fits of the LO predictions for J/ψ and $\psi(2S)$ production in pN collisions [129] yield $M_7^{J/\psi} = 3.0 \times 10^{-2}$ GeV^3 and $M_7^{\psi(2S)} = 5.2 \times 10^{-3}$ GeV^3. The corrections at next-to-leading order in α_s (NLO) give a large K-factor in the colour-octet contributions [70]. A fit to the data using the NLO result for the colour-octet contributions gives $M_{6.4}^{J/\psi} = 1.8 \times 10^{-2}$ GeV^3 and $M_{6.4}^{\psi(2S)} = 2.6 \times 10^{-3}$ GeV^3 [71]. The NLO value of $M_{6.4}^{J/\psi}$ is about a factor 2 smaller than the LO value of $M_7^{J/\psi}$. Note that the NLO fit uses CTEQ4M [75] parton distributions, while the LO fit uses the CTEQ3L [140] parton distributions. The LO result for $M^{J/\psi}$ is somewhat smaller than the

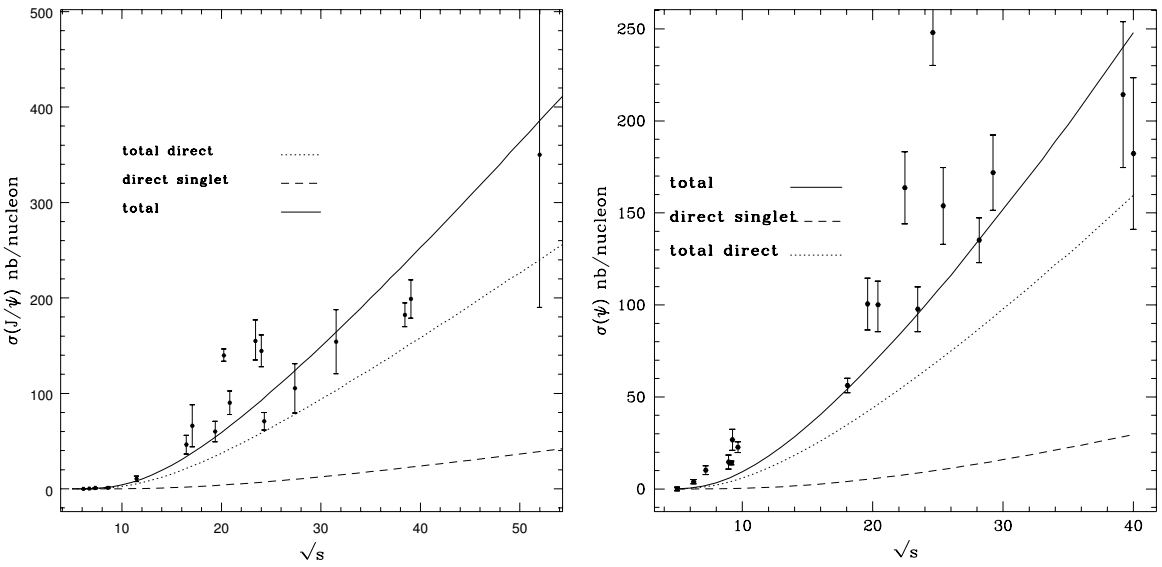

Fig. 5.9: Forward cross-section ($x_F > 0$) for J/ψ production in pN collisions (left) and πN collisions (right). The curves are the CSM predictions for direct J/ψ (dashed lines), the NRQCD factorization predictions for direct J/ψ with $M_7^{J/\psi} = 3.0 \times 10^{-2}$ GeV^3 (dotted lines), and the inclusive cross-sections for J/ψ including radiative feed-down from χ_{cJ} and $\psi(2S)$ (solid lines). From Ref. [129].

LO result from the Tevatron, and the NLO result for $M^{J/\psi}$ is somewhat larger than the parton-shower result from the Tevatron. However, given the large uncertainties in these quantities, the agreement is reasonable. It should also be remembered that the Tevatron cross-sections are sensitive to M_k^H with $k \approx 3$ rather than $k \approx 7$, and, so, comparisons are somewhat uncertain. Attempts to constrain this uncertainty are hampered by the fact that the $\overline{\rm MS}$ matrix elements need not be positive. One can also question whether hard-scattering factorization holds for the total cross-section, which is dominated by small p_T-contributions. Furthermore, kinematic corrections from the difference between $2m$ and the quarkonium mass may be large.

The predictions of Ref. [129] for J/ψ and $\psi(2S)$ production in πN collisions are shown, along with the experimental data, in the right panels of Figs. 5.9 and 5.10. The calculation is at leading-order in α_s and uses the standard truncation in v that is described in Section 1.1. Again, the data are from the compilation in Ref. [26], with additional results from Refs. [132–134]. In the NRQCD predictions in Figs. 5.9 and 5.10, the values of M_7 that are used are the ones that were obtained from the fits to the pN production data. The πN production data clearly show an excess over these predictions that cannot be accounted for by the colour-octet contributions. This discrepancy has been discussed extensively in Ref. [26], and it may reflect our lack of knowledge of the gluon distribution in the pion or the presence of different higher-twist effects in the proton and the pion. Such higher-twist effects are not accounted for in the standard NRQCD factorization formulas, which are based on leading-twist hard-scattering factorization.

Some of the largest uncertainties in the predictions cancel out if we consider ratios of cross-sections. The uncertainties in the NRQCD factorization predictions can still be very large. They arise from uncertainties in the colour-octet matrix elements, uncalculated corrections of higher order in v and α_s, and uncertainties from the choices of renormalization and factorization scales. In addition, one can question whether hard-scattering factorization holds for the cross-section integrated over p_T.

The $\psi(2S)$ to J/ψ ratio R_ψ is defined in Eq. (5.11). The experimental results for R_ψ from fixed-target experiments are compiled in Table 5.5. The result from experiment E673 is obtained by dividing

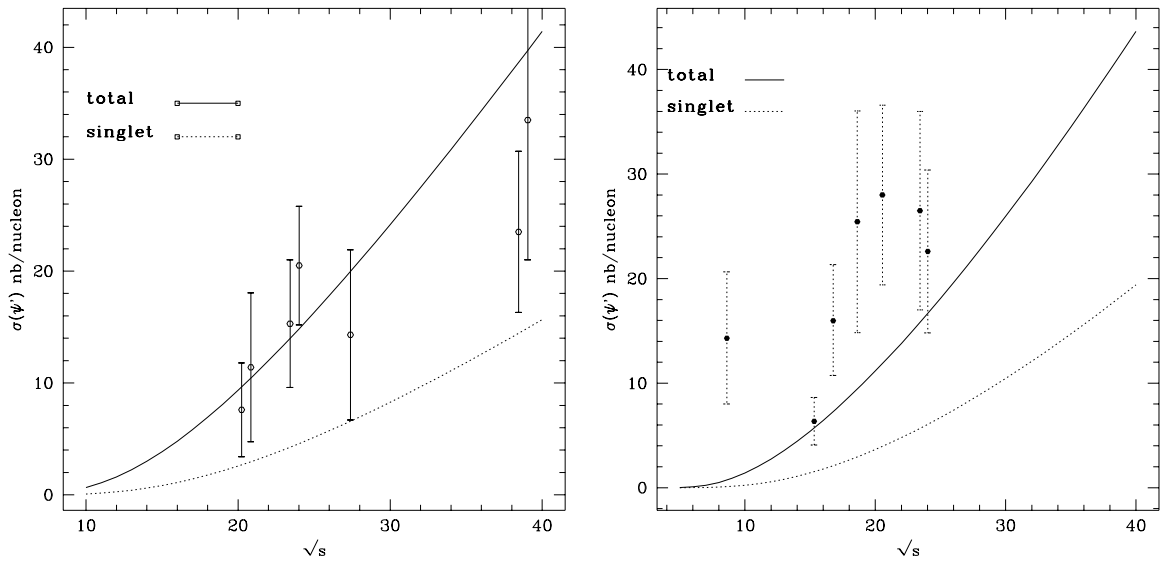

Fig. 5.10: Forward cross-section ($x_F > 0$) for $\psi(2S)$ production in pN collisions (left) and πN collisions (right). The curves are the CSM predictions (dotted lines) and the NRQCD factorization predictions with $M_7^{\psi(2S)} = 5.2 \times 10^{-3}$ GeV^3 (solid lines). From Ref. [129].

the observed fraction of J/ψ's from decays of $\psi(2S)$ by the branching fraction for $\psi(2S) \to J/\psi X$ given by the Particle Data Group [135]. The result from experiment E771 is obtained by dividing the observed ratio of the products of the cross-sections and the branching fractions into $\mu^+\mu^-$ by the ratio of the branching fractions into $\mu^+\mu^-$ given by the Particle Data Group [135]. The NRQCD factorization approach gives the values $R_\psi = 0.16$ for both pN collisions and $\pi^- N$ collisions [129]. The colour-singlet model gives $R_\psi = 0.14$ for pN collisions and $R_\psi = 0.16$ for $\pi^- N$ collisions [129]. In the colour-evaporation model, this ratio is simply an input. Thus the ratio R_ψ is not able to discriminate between any of these approaches.

The fraction F_{χ_c} of J/ψ's that come from χ_c decays is defined in Eq. (5.12). The experimental results for F_{χ_c} from fixed-target experiments are compiled in Table 5.6. The NRQCD factorization approach gives the values $F_{\chi_c} = 0.27$ for pN collisions and $F_{\chi_c} = 0.28$ for $\pi^- N$ collisions [129]. The colour-singlet model gives $F_{\chi_c} = 0.68$ for pN collisions and $F_{\chi_c} = 0.66$ for $\pi^- N$ collisions [129]. In the colour-evaporation model, this ratio is simply an input. Clearly, the experimental results favor the NRQCD factorization approach over the colour-singlet model. The most precise results from pN fixed target experiments are compatible with the Tevatron result in Table 5.3. The most precise results from πN fixed target experiments are somewhat larger.

The χ_{c1} to χ_{c2} ratio R_{χ_c} is defined in Eq. (5.10). There are substantial variations among the NRQCD factorization predictions for R_{χ_c} in fixed-target experiments. Beneke and Rothstein [129] give the values $R_{\chi_c} = 0.07$ for pN collisions and $R_{\chi_c} = 0.05$ for $\pi^- N$ collisions. Their calculation is carried out at leading order in α_s and uses the standard truncation in v that is described in Section 1.1. Beneke and Rothstein [129] suggest that corrections to hard-scattering factorization may be large. Beneke [111] gives the estimate $R_{\chi_c} \approx 0.3$ for both pN and πN collisions. This estimate is based on the assumption that the $^3P_2$ and $^3P_0$ colour-octet matrix elements dominate the χ_{c1} production. It is consistent with the estimate in Ref. [136], once that estimate is modified to take into account the dominant colour-singlet channel in χ_{c2} production [111]. Maltoni [71] gives central values of R_{χ_c} for pN collisions that range from $R_{\chi_c} = 0.04$ to $R_{\chi_c} = 0.1$ as the beam energy ranges from 200 GeV to 800 GeV. Maltoni's calculation takes into account matrix elements at leading order in v, but contains corrections of next-to-leading order in α_s. His calculation displays a very large dependence on the renormalization scale. In

Table 5.5: Experimental results for the ratio R_ψ of the inclusive cross-sections for $\psi(2S)$ and J/ψ production.

Experiment	beam/target	$\sqrt{s}$/GeV	R_ψ
E537 [132]	$\bar{p}$W	15.3	0.185 ± 0.0925
E705 [141]	pLi	23.7	$0.14 \pm 0.02 \pm 0.004 \pm 0.02$
E705 [141]	$\bar{p}$Li	23.7	$0.25 \pm 0.22 \pm 0.007 \pm 0.04$
E771 [134]	pSi	38.8	0.14 ± 0.02
HERA-B [142]	p(C, W)	41.5	0.13 ± 0.02
E537 [132]	π^-W	15.3	0.2405 ± 0.0650
E673 [144]	πBe	20.6	0.20 ± 0.09
E705 [141]	π^+Li	23.7	$0.14 \pm 0.02 \pm 0.004 \pm 0.02$
E705 [141]	π^-Li	23.7	$0.12 \pm 0.03 \pm 0.03 \pm 0.02$
E672/706 [146]	π^-Be	31.1	$0.15 \pm 0.03 \pm 0.02$

summary, the existing predictions for R_χ based on NRQCD factorization are in the range 0.04–0.3 for both pN and πN collisions. The colour-singlet model predicts that $R_{\chi_c} \approx 0.05$–0.07 for both pN and πN collisions [111, 129]. The colour-evaporation model predicts that $R_{\chi_c} \simeq 3/5$ [34, 147].

The experimental results for R_{χ_c} are compiled in Table 5.6. As can be seen, the data are somewhat inconsistent with each other. The results from the most precise experiments are significantly smaller than the Tevatron result in Eq. (5.18). There seems to be a trend toward larger values of R_{χ_c} in πN experiments than in pN experiments. Such a dependence on the beam type is contrary to the predictions of the colour-evaporation model. It also would not be expected in the NRQCD factorization approach, unless there is an unusual enhancement in the $q\bar{q}$ production channel [111]. Both the pN and πN data yield results that are significantly larger than the predictions of the colour-singlet model. The pN experiments seem to favor the NRQCD factorization predictions, while the πN experiments seem to favor the colour-evaporation prediction. However, in light of the large theoretical and experimental uncertainties, no firm conclusions can be drawn.

3.2 Polarization

The polarization variable α for J/ψ production is defined by the angular distribution in Eq. (5.13). In fixed-target experiments, the most convenient choice of the polarization axis is the direction of the boost vector from the J/ψ rest frame to the lab frame. Experimental results for α are shown in Table 5.7. The prediction of the NRQCD factorization approach is $0.31 < \alpha < 0.63$ [129]. Both the theoretical prediction and the data include feeddown from χ_c states. The prediction is largely independent of the target and beam types. It was made specifically for the beam energy 117 GeV. However, the energy dependence of the prediction is quite mild, and the prediction would be expected to hold with little error even at a beam energy of 800 GeV. The colour-singlet model predicts a substantial transverse polarization [151]. The colour-evaporation model predicts that $\alpha = 0$ for all processes. There are also specific predictions for the HERA-B experiment in which the region of small p_T is excluded. The predictions for the range $p_T = 1.5$–4 GeV are $\alpha = 0$–0.1 in the NRQCD factorization approach and $\alpha = 0.2$–0.4 in the colour-singlet model [152]. Experimental results for the polarization variable α in J/ψ production are shown in Table 5.7. The data from the conventional fixed-target experiments are consistent with $\alpha = 0$ and favor the prediction of the colour-evaporation model over the predictions of NRQCD factorization or the colour-singlet model [129]. At the smaller values of p_T, one can question whether resummation

Table 5.6: Experimental results for the fraction of J/ψ's from χ_c decay, F_{χ_c}, and the χ_{c1} to χ_{c2} ratio, R_{χ_c}. In view of the experimental uncertainties, no attempt has been made to rescale older measurements to account for the latest χ_c branching fractions. Modified version of a table from Ref. [111].

Experiment	beam/target	$\sqrt{s}$/GeV	F_{χ_c}	R_{χ_c}
E673 [137]	pBe	19.4/21.7	0.47 ± 0.23	0.24 ± 0.28
E705 [138]	pLi	23.7	—	$0.08^{+0.25}_{-0.15}$
E705 [141]	pLi	23.7	0.30 ± 0.04	—
E771 [139]	pSi	38.8	—	$0.53 \pm 0.20 \pm 0.07$
HERA-B [142]	p(C, W)	41.5	$0.32 \pm 0.06 \pm 0.04$	—
WA11 [143]	πBe	18.6	0.305 ± 0.050	0.68 ± 0.28
E673 [137]	πBe	18.9	0.31 ± 0.10	0.96 ± 0.64
E673 [144]	πBe	20.6	0.37 ± 0.09	0.9 ± 0.4
E705 [138]	πLi	23.7	—	$0.52^{+0.57}_{-0.27}$
E705 [141]	π^+Li	23.7	0.40 ± 0.04	—
E705 [141]	π^-Li	23.7	0.37 ± 0.03	—
E672/706 [145]	π^-Be	31.1	$0.443 \pm 0.041 \pm 0.035$	$0.57 \pm 0.18 \pm 0.06$

of the perturbation series is needed and whether hard-scattering factorization would be expected to hold. The HERA-B data are also consistent with $\alpha = 0$ and favor the predictions of the NRQCD factorization approach and the colour-evaporation model over the prediction of the colour-singlet model.

There is also a measurement of the polarization of $\psi(2S)$ in a fixed-target experiment. The E615 experiment measured α for $\psi(2S)$ mesons produced in πN collisions at 253 GeV [153]. The data yield $-0.12 < \alpha < 0.16$, while the prediction of the NRQCD factorization approach is $0.15 < \alpha < 0.44$ [129].

The E866/NuSea experiment has studied the production of dimuons in the collision of 800 GeV protons with copper [154]. The experiment used the angular distributions of dimuons in the mass range 8.1–15.0 GeV to measure the polarization variable α for Drell–Yan pairs, for $\Upsilon(1S)$ mesons, and for a mixture of $\Upsilon(2S)$ and $\Upsilon(3S)$ mesons. The data cover the kinematic ranges $0.0 < x_F < 0.6$ and $p_T < 4.0$ GeV. The results for the polarization variable α as a function of p_T and x_F are shown in Fig. 5.11. The $\Upsilon(1S)$ data show almost no polarization at small x_F and p_T, but show nonzero transverse polarization at either large p_T or large x_F. A fit at the Υ(1S) mass for a polarization that is independent of x_F and p_T gives α =0.07 $\pm$ 0.04. This observation is substantially smaller than a prediction that is based on the NRQCD factorization approach, which gives α in the range 0.28–0.31 [155,156]. However, it also disagrees with the prediction of the colour-evaporation model that the polarization should be zero [34]. The most remarkable result from this experiment is that the $\Upsilon(2S)$ and $\Upsilon(3S)$ were found to be strongly transversely polarized, with the polarization variable α close to its maximal value $\alpha = +1$ for all x_F and p_T, as in the case of Drell–Yan pairs. This result provides strong motivation for measuring the polarizations of the $\Upsilon(2S)$ and $\Upsilon(3S)$ at the Tevatron to see if these states are also produced with substantial polarizations in $p\bar{p}$ collisions.

It has been proposed that χ_2 production in hadron collisions at zero p_T may serve as a tool to measure the polarized gluon structure function of the proton [157]. This proposal relies on the assumption that χ_2 production at zero p_T is dominated by gluon fusion, and it requires that at least one of the colliding hadrons be polarized, as is the case, for example, in the RHIC polarized program.

Table 5.7: Experimental results for the polarization variable α in J/ψ production. Modified version of a table from Ref. [142].

Experiment	beam/target	Beam Energy/GeV	α
E537 [132]	(π, p)(Be, Cu, W)	125	0.024–0.032
E672/706 [148]	pBe	530	0.01 ± 0.15
E672/706 [148]	pBe	800	-0.11 ± 0.15
E771 [149]	pSi	800	-0.09 ± 0.12
E866 [150]	pCu	800	0.069 ± 0.08
HERA-B [142]	p(C, W)	920	$(-0.5,\ +0.1) \pm 0.1$

Table 5.8: Inclusive CEM parameters $F_{J/\psi}$ and $F_{\Upsilon(1S)}$ from Ref. [158] for various choices of PDF's, quark masses (in GeV), and scales.

PDF	m_c	μ/m_{cT}	$F_{J/\psi}$	PDF	m_b	μ/m_{bT}	$F_{\Upsilon(1S)}$
MRST HO	1.2	2	0.0144	MRST HO	4.75	1	0.0276
MRST HO	1.4	1	0.0248	MRST HO	4.5	2	0.0201
CTEQ 5M	1.2	2	0.0155	MRST HO	5.0	0.5	0.0508
GRV 98 HO	1.3	1	0.0229	GRV 98 HO	4.75	1	0.0225

Table 5.9: Ratios of the direct CEM parameters $F_H^{\rm dir}$ to the inclusive CEM parameter $F_{J/\psi}$ in the case of charmonium states and to the inclusive CEM parameter $F_{\Upsilon(1S)}$ in the case of bottomonium states. From Ref. [159].

H	J/ψ	$\psi(2S)$	χ_{c1}	χ_{c2}	
$F_H^{\rm dir}/F_{J/\psi}$	0.62	0.14	0.60	0.99	
H	$\Upsilon(1S)$	$\Upsilon(2S)$	$\Upsilon(3S)$	$\chi_b(1P)$	$\chi_b(2P)$
$F_H^{\rm dir}/F_{\Upsilon(1S)}$	0.52	0.33	0.20	1.08	0.84

3.3 Colour-evaporation-model parameters

Data from pp and pA collisions have been used to extract the parameters F_H of the colour-evaporation model. (The CEM parameter F_H should not be confused with the fraction of J/ψ's that come from decay of H.) The results of these extractions are given in Tables 5.8 and 5.9. The numerical values of the CEM parameters F_H that are obtained by fitting data depend on the choices of the parton densities (PDF's), the heavy quark mass m_Q, the renormalization/factorization scale μ, and the order in α_s of the calculation. The CEM parameters have been calculated using several sets of parton densities [69,79,160], quark masses, and scales [161,162] that reproduce the measured $Q\bar{Q}$ cross-section. In these calculations, the scale μ was set to a constant times $m_{QT} = (m_Q^2 + p_T^2)^{1/2}$, where p_T is the sum of the transverse momenta of the Q and the $\bar{Q}$.

We first describe the extraction of the CEM parameters F_H for charmonium states. The inclusive cross-section for J/ψ production has been measured in pp and pA collisions up to $\sqrt{s} = 63$ GeV. The data are of two types: the forward cross-section, $\sigma(x_F > 0)$, and the cross-section at zero rapidity, $d\sigma/dy|_{y=0}$. These cross-sections include the feeddown from decays of χ_{cJ} and $\psi(2S)$. The parameters

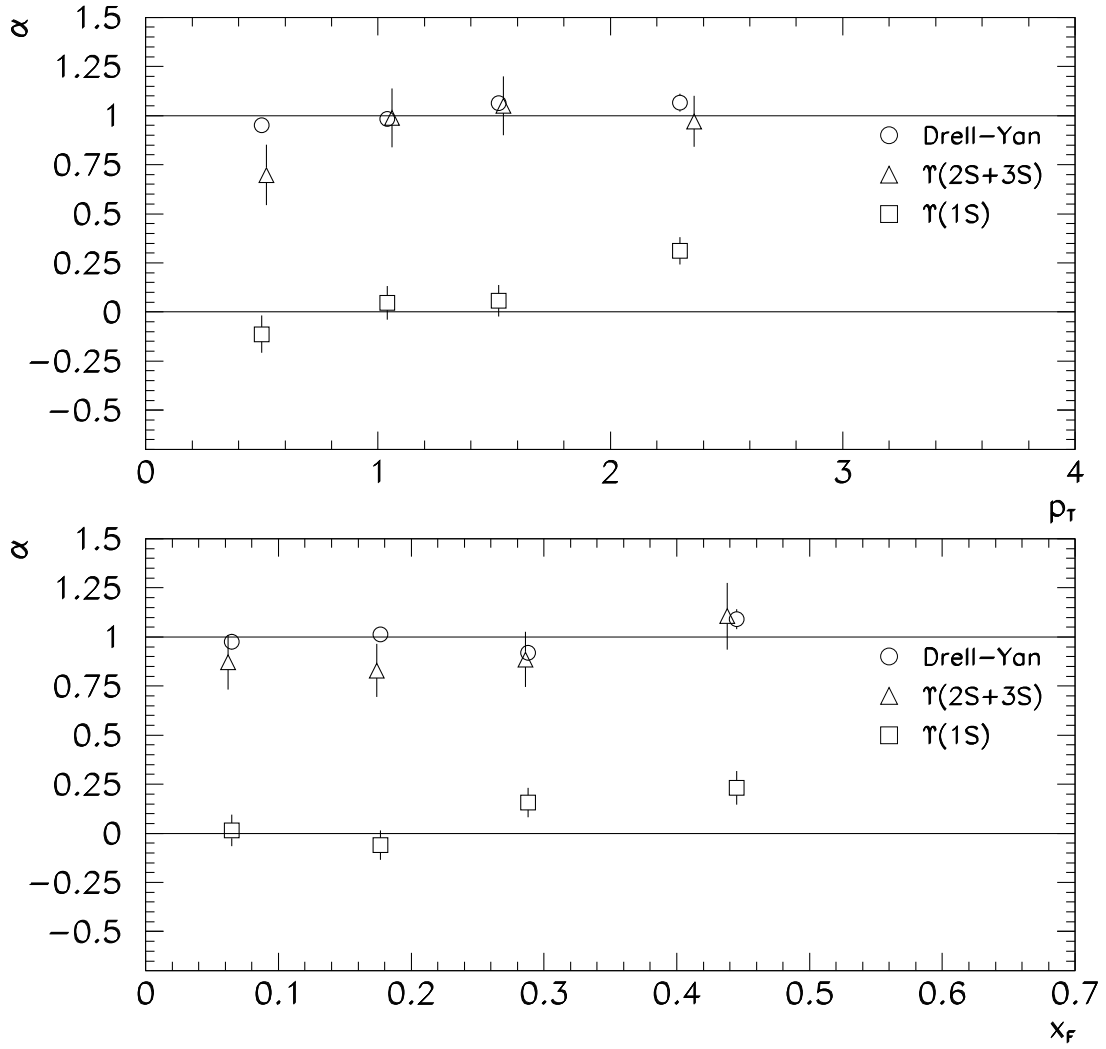

Fig. 5.11: Polarization of Υ mesons and Drell–Yan pairs as a function of p_T and x_F in p–Cu collisions in the E866 experiment. From Ref. [154].

$F_{J/\psi}$ that were obtained by fitting the inclusive J/ψ cross-sections measured in pp and pA collisions are given in Table 5.8 for four sets of PDF's and parameters. The ratio of the parameter $F_H^{\rm dir}$ for the direct production of a charmonium state H to the parameter $F_{J/\psi}$ for the inclusive production of J/ψ can be determined from the measured ratios of the inclusive cross-sections for H and J/ψ using the known branching fractions for the feeddown decays. These ratios are given in Table 5.9 for various charmonium states.

A similar procedure can be used to determine the CEM parameters F_H for bottomonium states. In most data on pp and pA collisions below $\sqrt{s} = 100$ GeV, only the sum of the $\Upsilon(1S)$, $\Upsilon(2S)$, and $\Upsilon(3S)$ cross-sections weighted by their branching fractions to decay into lepton pairs is reported. A fit to the lepton-pair cross-section in the Υ region at zero rapidity therefore gives a linear combination of the inclusive parameters $F_{\Upsilon(nS)}$ weighted by the branching fractions $B[\Upsilon(nS)\to\ell^+\ell^-]$. The inclusive parameters $F_{\Upsilon(1S)}$ given in Table 5.8 were extracted by using the known branching fractions and the measured ratios of the inclusive cross-sections for $\Upsilon(nS)$ in $p\bar{p}$ collisions at the Tevatron [163]. The ratios of the parameters $F_H^{\rm dir}$ for the direct production of a bottomonium state H to the parameter $F_{\Upsilon(1S)}$ for the inclusive production of $\Upsilon(1S)$ that were obtained in Ref. [164] have been updated in Ref. [159] by using recent CDF data on χ_b production and are given in Table 5.9.

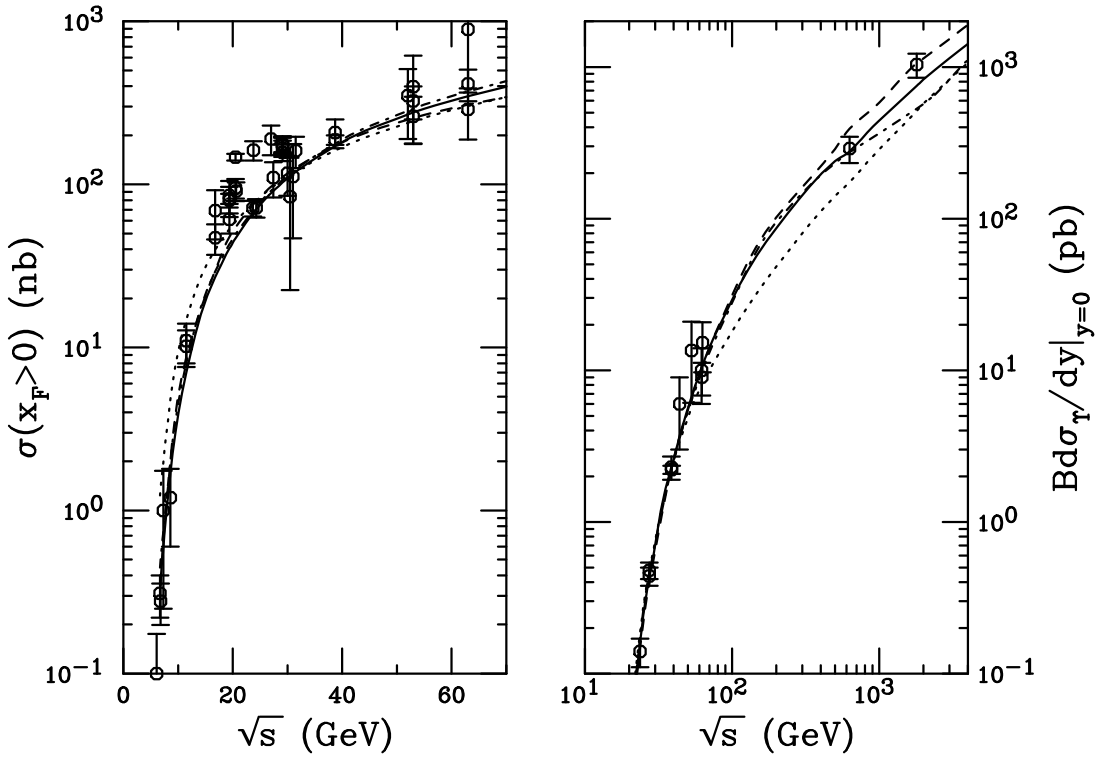

Fig. 5.12: Forward J/ψ production cross-section (left) and weighted average of the $\Upsilon(nS)$ production cross-sections at zero rapidity (right) as a function of the centre-of-mass energy $\sqrt{s}$. The J/ψ data are from pp experiments and from pA experiments with light targets $A \leq 12$. It has been assumed that the cross-sections scale as $A^{0.9}$. The low-energy Υ data are from pp and pA experiments. It has been assumed that the cross-sections are linear in A. The high-energy Υ data are from $p\bar{p}$ experiments. The curves are the cross-sections calculated to NLO in the CEM using the four charmonium parameter sets and the four bottomonium parameter sets in Table 5.8.

The forward cross-section for J/ψ and the weighted cross-section at zero rapidity for $\Upsilon(nS)$ are shown as a function of the centre-of-mass energy in Fig. 5.12. The energy dependence of both cross-sections is well reproduced by the CEM at NLO. All of the CEM parameter sets give good fits to the data for $\sqrt{s} \leq 63$ GeV, but their predictions for $\Upsilon(nS)$ differ by up to a factor of two when extrapolated to 2 TeV. The extrapolation of the forward J/ψ cross-section to 2 TeV cannot be compared with data from Run I of the Tevatron because the lepton-p_T cut excludes a measurement of the cross-section for J/ψ in the region $p_T < 5$ GeV that dominates the integrated cross-section.

4 QUARKONIUM PRODUCTION AT HERA

4.1 Inelastic photoproduction of charmonium

At the ep collider HERA, the inelastic charmonium production process is dominantly virtual-photon-gluon fusion: a photon emitted from the incoming electron or positron interacts with a gluon from the proton to produce a $c\bar{c}$ pair that subsequently forms a charmonium state. In photoproduction, the photon virtuality Q^2 is small and the photon is quasi-real. In this case, the photon can either couple to the c quark directly ("direct" processes, Fig. 5.13a or b) or it can interact via its hadronic component ("resolved" processes, Fig. 5.13c). Many models have been suggested to describe inelastic charmonium production in the framework of perturbative QCD, such as the colour-singlet model (CSM) [21–24] described in Section 1.2, the colour-evaporation model [28, 36] described in Section 1.3, and soft colour interactions [35].

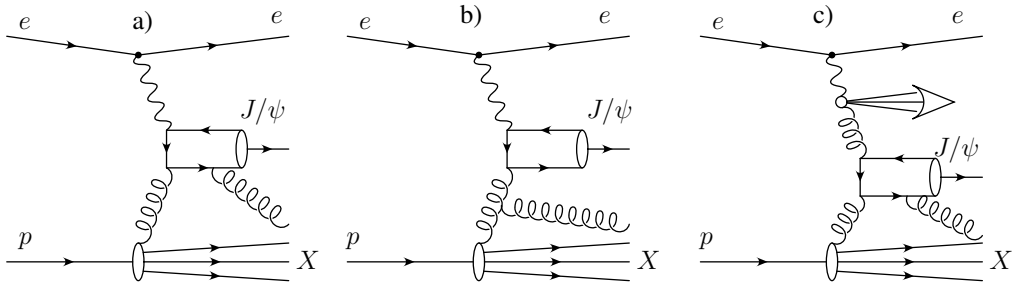

Fig. 5.13: Generic Feynman diagrams for inelastic J/ψ production. a,b) direct-photon processes; c) resolved-photon process. In diagrams a) and c), the $c\bar{c}$ pair leading to the formation of the J/ψ can be in a colour-singlet or a colour-octet state while in b) it can only be in a colour-octet state. Additional soft gluons emitted during the hadronization process are not shown.

For J/ψ and $\psi(2S)$ photoproduction, the CSM calculations are available to next-to-leading order [165, 166]. These are performed using standard hard-scattering factorization in which the gluon density depends only on the momentum fraction x. Alternatively, using the CSM, inelastic J/ψ production can be modeled in the k_T-factorization approach (see Section 1.4) using an unintegrated (k_T-dependent) gluon density in the proton.

Theoretical calculations based on the NRQCD factorization approach [1–3] are available in leading order. For J/ψ and $\psi(2S)$ photoproduction at HERA, these have been performed by Cacciari and Krämer [167], Beneke, Krämer, and Vänttinen [168], Amundson, Fleming, and Maksymyk [169], Ko, Lee, and Song [170], Godbole, Roy, and Sridhar [171], and Kniehl and G. Kramer [172, 173]. The theoretical calculations use the standard truncation in v, in which the independent NRQCD matrix elements are $\langle \mathcal{O}_1^{J/\psi}(^3S_1)\rangle$, $\langle \mathcal{O}_8^{J/\psi}(^1S_0)\rangle$, $\langle \mathcal{O}_8^{J/\psi}(^3S_1)\rangle$, and $\langle \mathcal{O}_8^{J/\psi}(^3P_0)\rangle$. The relative strength of the colour-octet contributions depends crucially on the size of the corresponding NRQCD matrix elements. Unfortunately the values of the matrix elements $\langle \mathcal{O}_8^{J/\psi}(^1S_0)\rangle$ and $\langle \mathcal{O}_8^{J/\psi}(^3P_0)\rangle$, which are most important in J/ψ and $\psi(2S)$ photoproduction at HERA, still show large uncertainties. (See Section 2.1 and Ref. [64].)

The theoretical predictions are sensitive to a number of input parameters, e.g., the parton distributions, the values of α_s, and the charm-quark mass m_c, as well as the choice of the renormalization and factorization scales. In the NRQCD factorization approach, the values of the colour-octet NRQCD matrix elements are additional parameters. The comparison with the data in the NRQCD approach also suffers from the uncertainties associated with LO calculations. Next-to-leading-order corrections might change the results substantially. Although the NLO terms have not been calculated in the NRQCD approach, effects that are similar to those in the CSM may be expected, in which the NLO terms lead to an increase in the cross-section of typically a factor two, with a strong $p_{T,\psi}$ dependence.

Figure 5.14 shows the measurements of the prompt J/ψ cross-section by the H1 collaboration [174] and the ZEUS collaboration [175], compared with the theoretical predictions given in Ref. [64]. The variable z denotes the fraction of the photon energy that is transferred to the J/ψ and is defined as

$$z = \frac{(E - p_z)_{J/\psi}}{(E - p_z)_{\text{hadrons}}}, \tag{5.23}$$

where E and p_z in the numerator are the energy and z-component of the momentum of the J/ψ and E and p_z in the denominator are the sums of the energies and z-components of the momenta of all the hadrons in the final state.

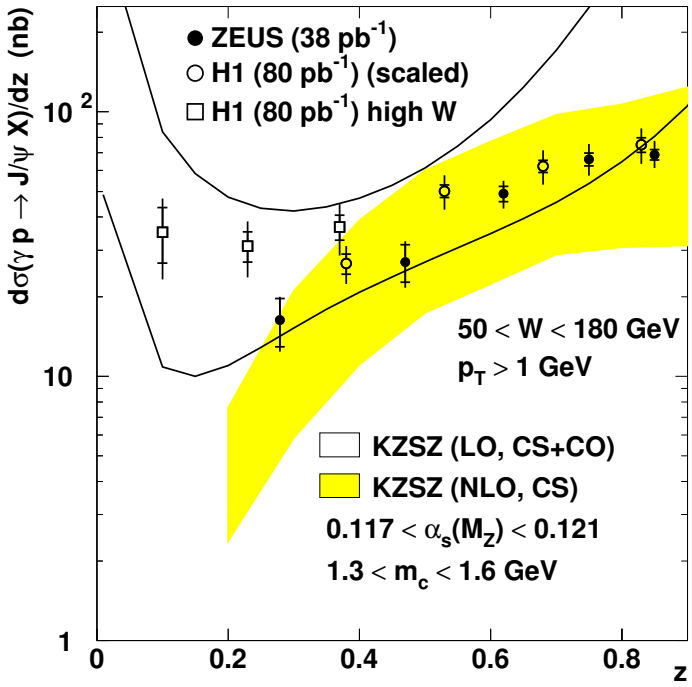

Fig. 5.14: The rate for inelastic J/ψ photoproduction at HERA as a function of z. The open band represents the LO NRQCD factorization prediction [64]. The solid band represents the NLO colour-singlet contribution [64, 166]. The data points are from the H1 [174] and ZEUS [175] measurements.

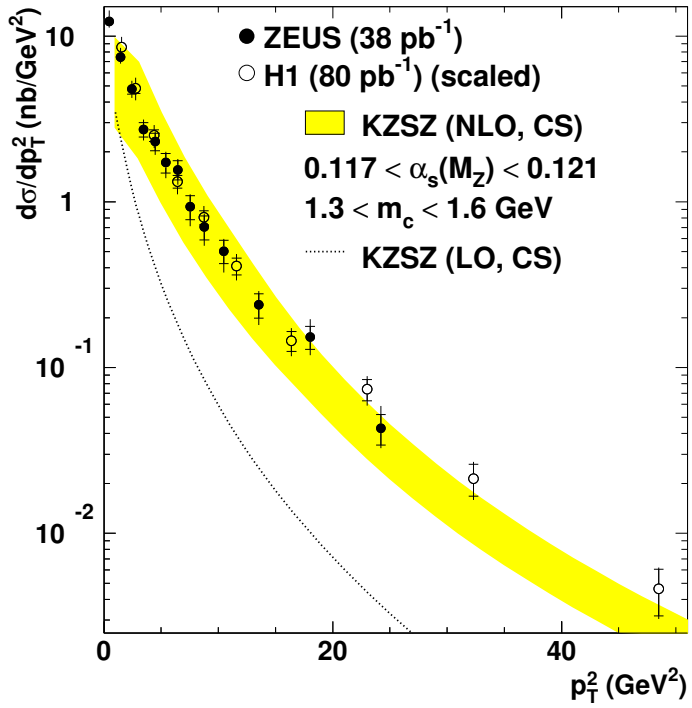

Fig. 5.15: The rate for inelastic J/ψ photoproduction at HERA as a function of $p_{T,\psi}$. The solid band represents the NLO colour-singlet contribution [64, 166]. The dotted line is the LO colour-singlet contribution. The data points are from the H1 [174] and ZEUS [175] measurements.

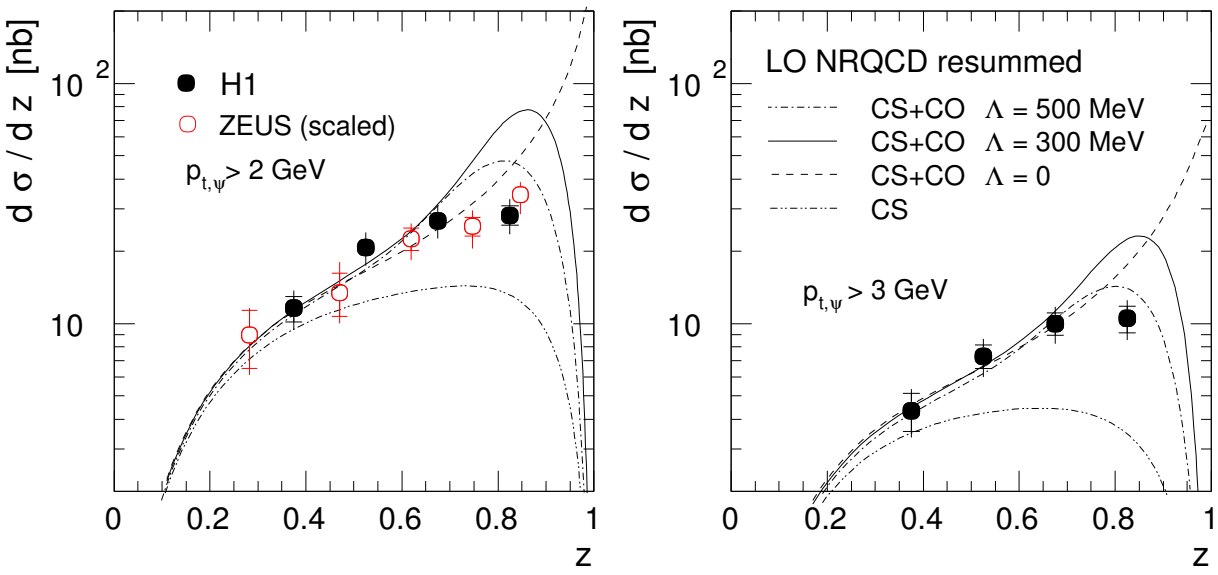

Fig. 5.16: Differential cross-sections $\mathrm{d}\sigma/\mathrm{d}z$ ($60 < W_{\gamma p} < 240\,\mathrm{GeV}$) for $p_{T,\psi} > 2\,\mathrm{GeV}$ (left panel) and $p_{T,\psi} > 3\,\mathrm{GeV}$ (right panel) in comparison with NRQCD calculations that include colour-octet and colour-singlet contributions and resummations of soft contributions at high z [12]. The curves correspond to three values of the parameter Λ: $\Lambda = 0$, i.e., no resummation (dashed line), $\Lambda = 300$ MeV (solid line), and $\Lambda = 500$ MeV (dash–dotted line). The theoretical curves have been scaled with a common factor 2 in the left panel and 3 in the right panel.

The J/ψ data points shown in Fig. 5.14 are not corrected for feeddown processes, such as diffractive and inelastic production of $\psi(2S)$ mesons ($\approx 15\%$), the production of b hadrons with subsequent decays to J/ψ mesons, or feeddown from the production of χ_c states. The latter two contributions are estimated to contribute between 5% at medium z and 30% at the lowest values of z. The open band in Fig. 5.14 represents the sum of the colour-singlet and colour-octet contributions, calculated in leading order in QCD perturbation theory. The uncertainty is due to the uncertainty in the colour-octet NRQCD matrix elements. The NRQCD prediction deviates from the data near $z = 1$, owing to the large colour-octet contribution in that region. The shaded band shows the calculation of the colour-singlet contribution to next-to-leading order in α_s [165, 166]. The NLO corrections increase the colour-singlet contribution by about a factor of two, so that it accounts for the data quite well without the inclusion of a colour-octet contribution.

Uncertainties in m_c could lower the colour-singlet contribution by about a factor of two, leaving more room for colour-octet contributions. In the experimental data, the cut $p_{T,\psi} > 1$ GeV is employed. One can question whether hard-scattering factorization is valid at such small values of $p_{T,\psi}$. However, the data differential in $p_{T,\psi}$ are compatible with colour-singlet production alone at large $p_{T,\psi}$ (Fig. 5.15).

The next-to-leading-order QCD corrections are crucial in describing the shape of the transverse-momentum distribution of the J/ψ. The NLO colour-singlet cross-section includes processes such as $\gamma + g \to (c\bar{c}) + gg$, which are dominated by t-channel gluon exchange and scale as $\alpha_s^3 m_c^2/p_{T,\psi}^6$. At $p_{T,\psi} \gtrsim m_c$ their contribution is enhanced with respect to the leading-order cross-section, which scales as $\sim \alpha_s^2 m_c^4/p_{T,\psi}^8$. The comparison with the experimental data in Fig. 5.15 confirms the importance of the higher-order corrections.

At large z, the emission of soft gluons in the conversion of the $c\bar{c}$ pairs to J/ψ mesons is suppressed, owing to phase-space limitations. Furthermore, the velocity expansion of the NRQCD factorization approach is expected to break down [10]. These effects are not taken into account in the theoretical

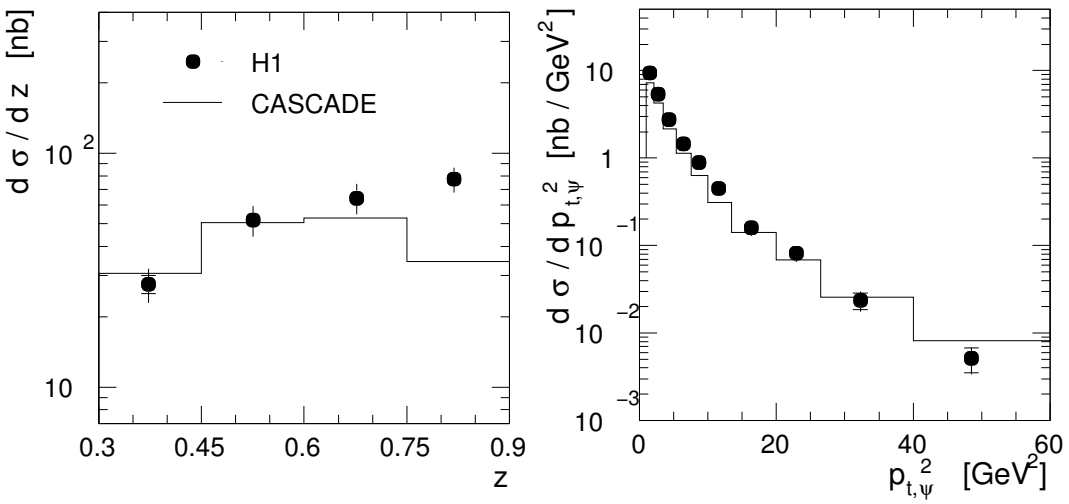

Fig. 5.17: Inelastic J/ψ production in the region $60 < W_{\gamma p} < 240$ GeV, $0.3 < z < 0.9$, and $p^2_{T,\psi} > 1$ GeV^2, in comparison with a k_T-factorization model implemented in the Monte Carlo generator CASCADE [176, 177]. Left panel: differential cross-section $\mathrm{d}\sigma/\mathrm{d}z$; right panel: $d\sigma/dp^2_{T,\psi}$ in the range $0.3 < z < 0.9$.

calculation that is shown in Fig. 5.14. In Ref. [12], a resummation of the nonrelativistic expansion was carried out, leading to a decrease of the predicted cross-section at high z. The resummation involves a parameter Λ that describes the energy in the $c\bar{c}$ rest frame that is lost by the $c\bar{c}$ system in its conversion into the J/ψ meson. In Fig. 5.16, the measured cross-sections $d\sigma/dz$ for $p_{T,\psi} > 2$ GeV and for $p_{T,\psi} > 3$ GeV are compared with the results of these resummed calculations. The calculated curves have been roughly normalized to the data points at low z. The resummed calculation for $\Lambda = 500$ MeV gives an acceptable description of the data at $p_{T,\psi} > 3$ GeV, while the agreement between data and calculation is still poor for $p_{T,\psi} > 2$ GeV or for lower Λ values.

Effects from resummation of logarithms of $1 - z$ and model shape functions have also been calculated for the process $e^+e^- \to J/\psi + X$ [11]. It may be possible to use this resummed theoretical prediction to extract the dominant shape function from the Belle and BaBar data for $e^+e^- \to J/\psi + X$ and then use it to make predictions for J/ψ photoproduction near $z = 1$.

Measurements of the J/ψ production cross-section at large z are available from H1 [204] and from ZEUS [175]. In this region, the contribution from diffractively produced J/ψ mesons is expected to be large, as is discussed below in Section 4.3.

The ZEUS Collaboration has also measured the ψ' to J/ψ cross-section ratio [175] in the range $0.55 < z < 0.9$ and $50 < W < 180$ GeV. It is found to be consistent with being independent of the kinematic variables z, $p_{t,\psi}$ and W, as is expected if the underlying production mechanisms for the J/ψ and the ψ' are the same. An average value $\sigma(\psi')/\sigma(J/\psi) = 0.33 \pm 0.10(\mathrm{stat.})^{+0.01}_{-0.02}(\mathrm{syst.})$ is found which compares well with the prediction from the leading-order colour-singlet model [165].

The k_T-factorization approach (see Section 1.4) has recently been applied successfully to the description of a variety of processes [176–178]. In this approach, the J/ψ production process is factorized into a k_T-dependent gluon density and a matrix element for off-shell partons. A leading-order calculation within this approach is implemented in the Monte Carlo generator CASCADE [176, 177]. Figure 5.17 shows a comparison of the data with the predictions from the k_T-factorization approach. Good agreement is observed between data and predictions for $z \lesssim 0.8$. At high z values, the CASCADE calculation underestimates the cross-section. This may be due to missing higher-order effects, or missing relativistic corrections, which are not available for the off-shell matrix element. It could also indicate a possible missing colour-octet contribution. The CASCADE predictions for the the $p^2_{T,\psi}$ dependence of the cross-

section (Fig. 5.17c) fit the data considerably better than the collinear LO calculations. This improved fit is due to the transverse momentum of the gluons from the proton, which contributes to the transverse momentum of the J/ψ meson. Note, however, that the NLO colour-singlet calculation in collinear factorization [166] also describes the $p^2_{T,\psi}$ distribution.

The polarization of the J/ψ meson is expected to differ in the various theoretical approaches discussed here and could in principle be used to distinguish between them, independently of normalization uncertainties. The general decay angular distribution can be parametrized as

$$\frac{d\Gamma(J/\psi \to l^+l^-)}{d\Omega} \propto 1 + \lambda \cos^2\theta + \mu \sin 2\theta \cos\phi + \frac{\nu}{2}\sin^2\theta \cos 2\phi, \tag{5.24}$$

where θ and ϕ refer to the polar and azimuthal angle of the l^+ three-momentum with respect to a coordinate system that is defined in the J/ψ rest frame. (See, for example, Ref. [168] for details.) The parameters λ, μ, ν can be calculated within NRQCD or the CSM as a function of the kinematic variables, such as z and $p_{T,\psi}$.

In Fig. 5.18, the data are shown, together with the results from two LO calculations: the NRQCD prediction, including colour-octet and colour-singlet contributions [168], and the colour-singlet contribution alone. A calculation that uses a k_T-factorization approach and off-shell gluons is also available [179]. In contrast to the predictions shown in the Fig. 5.18, in which λ is zero or positive, the prediction of the k_T-factorization approach is that λ should become increasingly negative toward larger values of $p_{t,J/\psi}$, reaching $\lambda \sim -0.5$ at $p_{T,\psi} = 6$ GeV. However, at present, the errors in the data preclude any firm conclusions. In this range of $p_{T,\psi}$ none of the calculations predicts a decrease in λ with increasing z. In order to distinguish between full NRQCD and the colour-singlet contribution alone, measurements at larger $p_{T,\psi}$ are required. The measured values of ν, for which no prediction is available from the k_T-factorization approach, favor the full NRQCD prediction.

4.2 Inelastic electroproduction of charmonium

As in photoproduction, inelastic leptoproduction of J/ψ mesons at HERA ($e+p \to e+J/\psi+X$) is dominated by virtual-photon-gluon fusion ($\gamma^* g \to c\bar{c}$). In leptoproduction, or deep inelastic ep-scattering (DIS), the exchanged photon has a nonzero virtuality $Q^2 = -q^2$, where q is the four-momentum of the virtual photon. For events with a photon virtuality of $Q^2 \gtrsim 1$ GeV^2, the electron scattering angle is large enough for the electron to be detected in the central detectors.

The analysis of leptoproduction at finite Q^2 has experimental and theoretical advantages in comparison with the analysis of photoproduction. At high Q^2, theoretical uncertainties in the models decrease and resolved-photon processes are expected to be negligible. Furthermore, the background from diffractive production of charmonia is expected to decrease faster with Q^2 than the inelastic process, and the distinct signature of the scattered lepton makes the inelastic process easier to detect.

A first comparison between data and NRQCD calculations was presented in Ref. [180]. The NRQCD calculations in Ref. [180] were performed by taking into account only "$2 \to 1$" diagrams (see the top left diagram of Fig.5.19) [181], and disagreement between data and theory was observed both in the absolute values of the cross-sections and in their shapes as functions of the variables that were studied.

More recently, the cross-section for J/ψ production in deep-inelastic ep scattering at HERA was calculated in the NRQCD factorization approach at leading order in α_s by Kniehl and Zwirner [182], taking into account diagrams of the type "$2 \to 2$", as are shown in the top right and bottom diagrams of Fig. 5.19. The calculation made use of the matrix elements of Ref. [78] and MRST98LO [79] and CTEQ5L [69] parton distributions.

In Fig. 5.20, the results of this calculation are plotted as a function of Q^2 and $p^2_{T,\psi}$, along with the H1 data [183]. The NRQCD results that are shown in Fig. 5.20 include the contributions from the

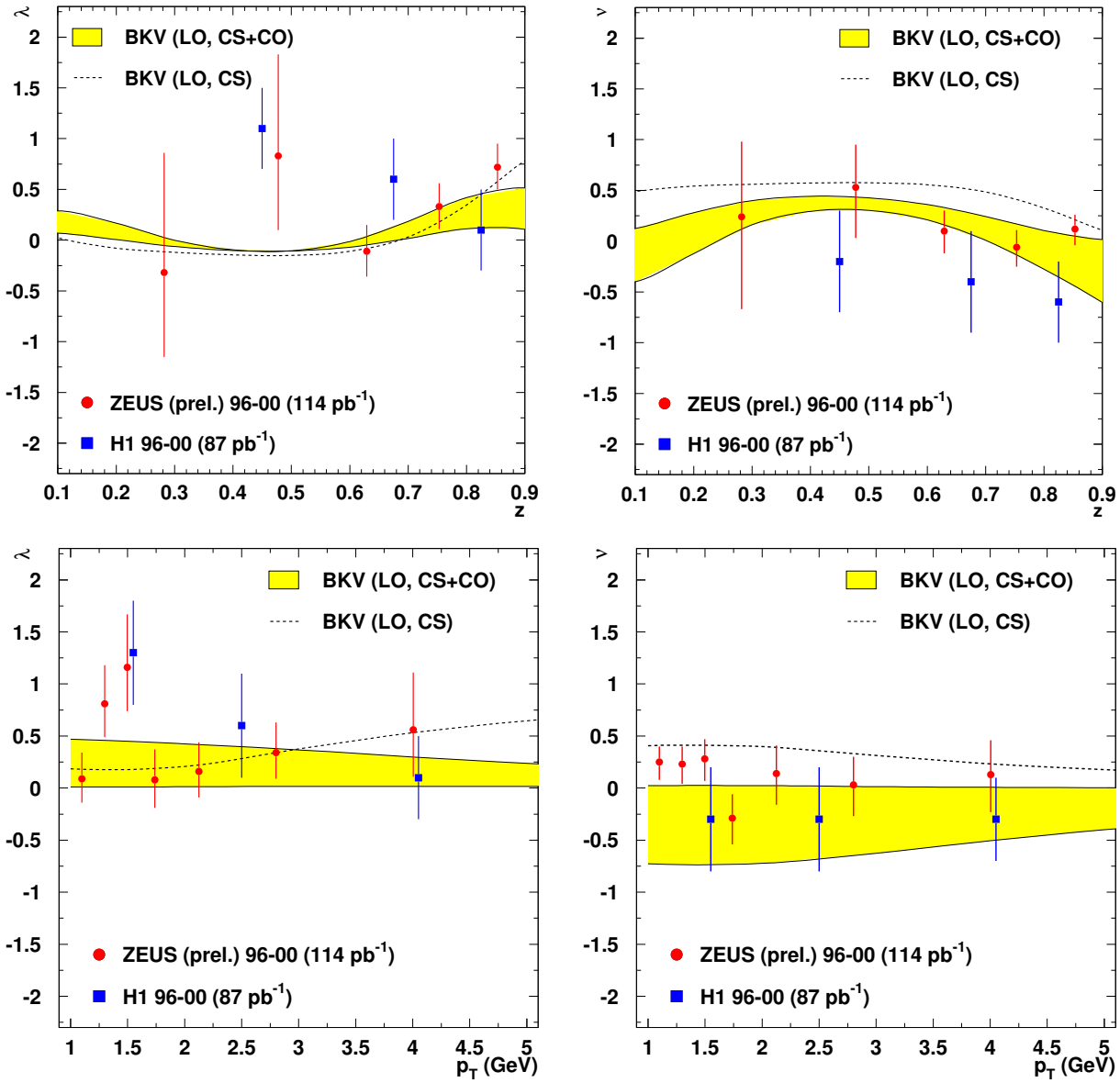

Fig. 5.18: Polarization parameters λ (left panels) and ν (right panels) in the target rest frame as functions of z (top panels) and $p_{T,\psi}$ (bottom panels). The error bars on the data points correspond to the total experimental error. The theoretical calculations shown are from the NRQCD approach [168] (shaded bands) with colour-octet and colour-singlet contributions, while the curves show the result from the colour-singlet contribution separately.

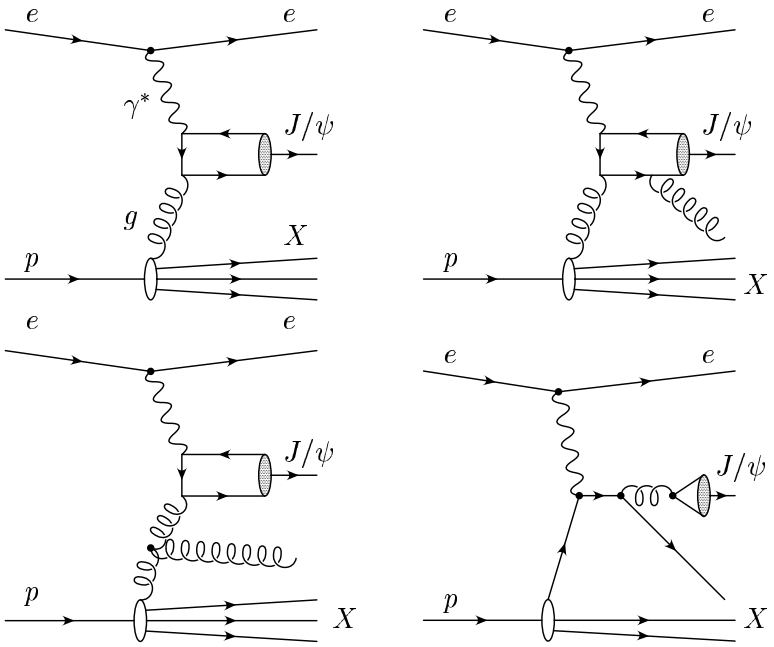

Fig. 5.19: Generic diagrams for charmonium production mechanisms: photon–gluon fusion via a "$2 \to 1$" process (top left diagram) and "$2 \to 2$" processes (remaining diagrams). All the diagrams contribute via colour-octet mechanisms, while the top right diagram can also contribute via the colour-singlet mechanism. Additional soft gluons emitted during the hadronization process are not shown.

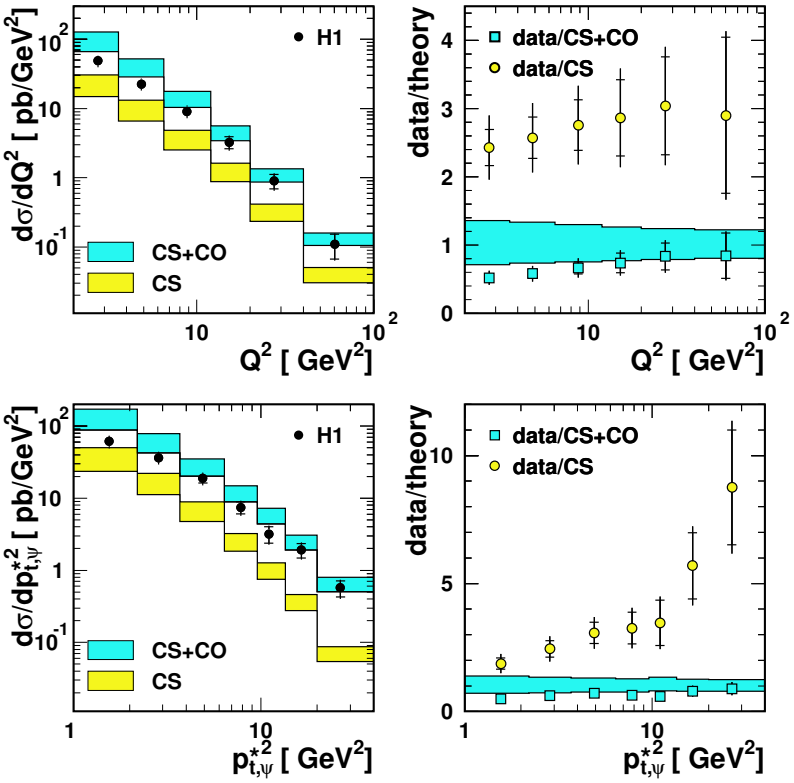

Fig. 5.20: Differential cross-sections $d\sigma/dQ^2$ (top left panel) and $d\sigma/dp^{*2}_{T,\psi}$ (bottom left panel) and the corresponding ratios of data to theory (right panels). The data from H1 [183] are compared with the NRQCD calculation [182] (CO+CS, dark band) and the colour-singlet contribution [182] (CS, light band).

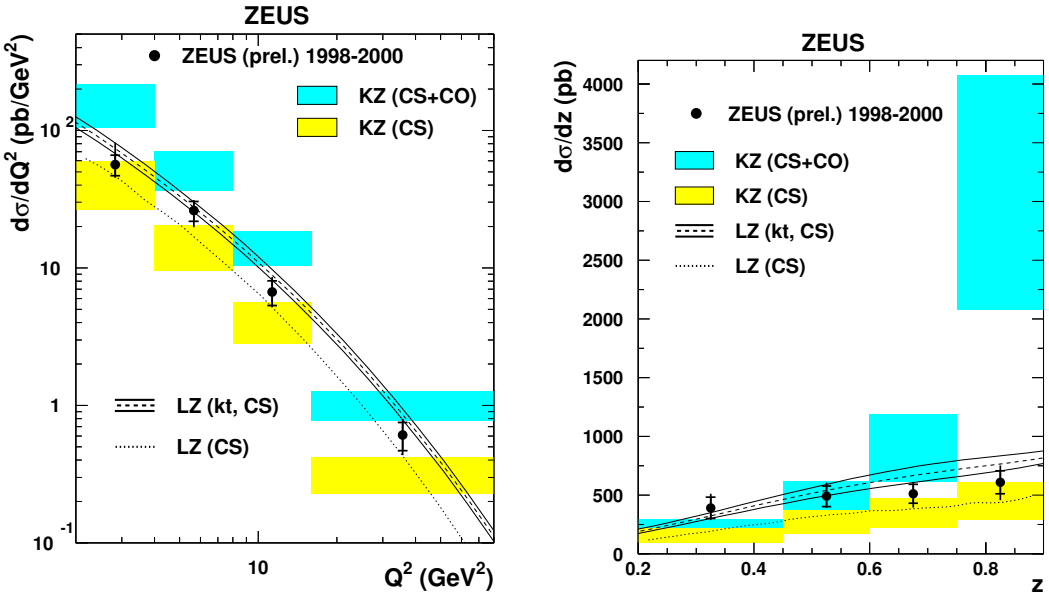

Fig. 5.21: Differential cross-sections $d\sigma/dQ^2$ (left) and $d\sigma/dz$ (right) and theory predictions. The data from ZEUS [184] are compared with the NRQCD calculation [182] (CO+CS, dark band), the colour-singlet contribution (CS, light band), and with the prediction LZ(kt,CS) from the k_T-factorization approach within the CSM [185]. The solid lines delimit the uncertainties, and the dashed line show the central values. The CSM prediction LZ (CS) in the collinear-factorization approach, as given by the authors of Ref. [185], is also shown (dotted line).

colour-octet channels ${}^3S_1$, ${}^3P_{J=0,1,2}$, ${}^1S_0$, as well as from the colour-singlet channel ${}^3S_1$. The contribution of the colour-singlet channel is also shown separately. The values of the NRQCD matrix elements were determined from the distribution of transverse momenta of J/ψ mesons produced in $p\bar{p}$ collisions [78].[4] The bands include theoretical uncertainties, which originate from the uncertainty in the charm-quark mass $m_c = 1.5 \pm 0.1$ GeV, the variation of renormalization and factorization scales by factors 1/2 and 2, and the uncertainties in the NRQCD matrix elements, all of which result mainly in normalization uncertainties that do not affect the shapes of the distributions.

Figure 5.21 shows the differential electroproduction cross-sections for J/ψ mesons as functions of Q^2 and z, as measured by the ZEUS collaboration [184]. The ZEUS data, which are consistent with the H1 results shown in Fig. 5.20, are compared with predictions in the framework of NRQCD (CS+CO) [182] and also with predictions in the k_T-factorization approach in which only the colour-singlet contribution (CS) is included [185]. As in Fig. 5.20, the uncertainties in the NRQCD calculations are indicated in Fig. 5.21 as shaded bands. For the prediction within the k_T-factorization approach (LZ(kt,CS)), only one of the sources of uncertainty is presented, namely the uncertainty in the pomeron intercept Δ, which controls the normalization of the unintegrated gluon density.

In Fig. 5.22, the normalization uncertainties of the theory, which are dominant, are removed by normalizing the differential cross-sections measured by H1 [183] and the theory predictions to the integrated cross-sections in the measured range for each distribution. The comparisons in Figs. 5.20–5.22 indicate that the colour-singlet contribution follows the shape of the data from H1 and ZEUS quite well. In general, the CSM predictions are below the H1 and ZEUS data, but are consistent with the data, given the uncertainties, both in shape and normalization. However, the differential cross-sections as a function of the transverse momentum squared of the J/ψ are too steep compared to the data (lower left plot in

[4] The extracted values for the NRQCD matrix elements depend on the parton distributions. For the set MRST98LO [79], the values are $\langle \mathcal{O}_1^{J/\psi}({}^3S_1)\rangle = 1.3 \pm 0.1\,\text{GeV}^3$, $\langle \mathcal{O}_8^{J/\psi}({}^3S_1)\rangle = (4.4 \pm 0.7) \times 10^{-3}\,\text{GeV}^3$ and $M_{3.4}^{J/\psi} = (8.7 \pm 0.9) \times 10^{-2}\,\text{GeV}^3$, where $M_{3.4}^{J/\psi}$ is the linear combination of two NRQCD matrix elements that is defined in Eq. (5.8).

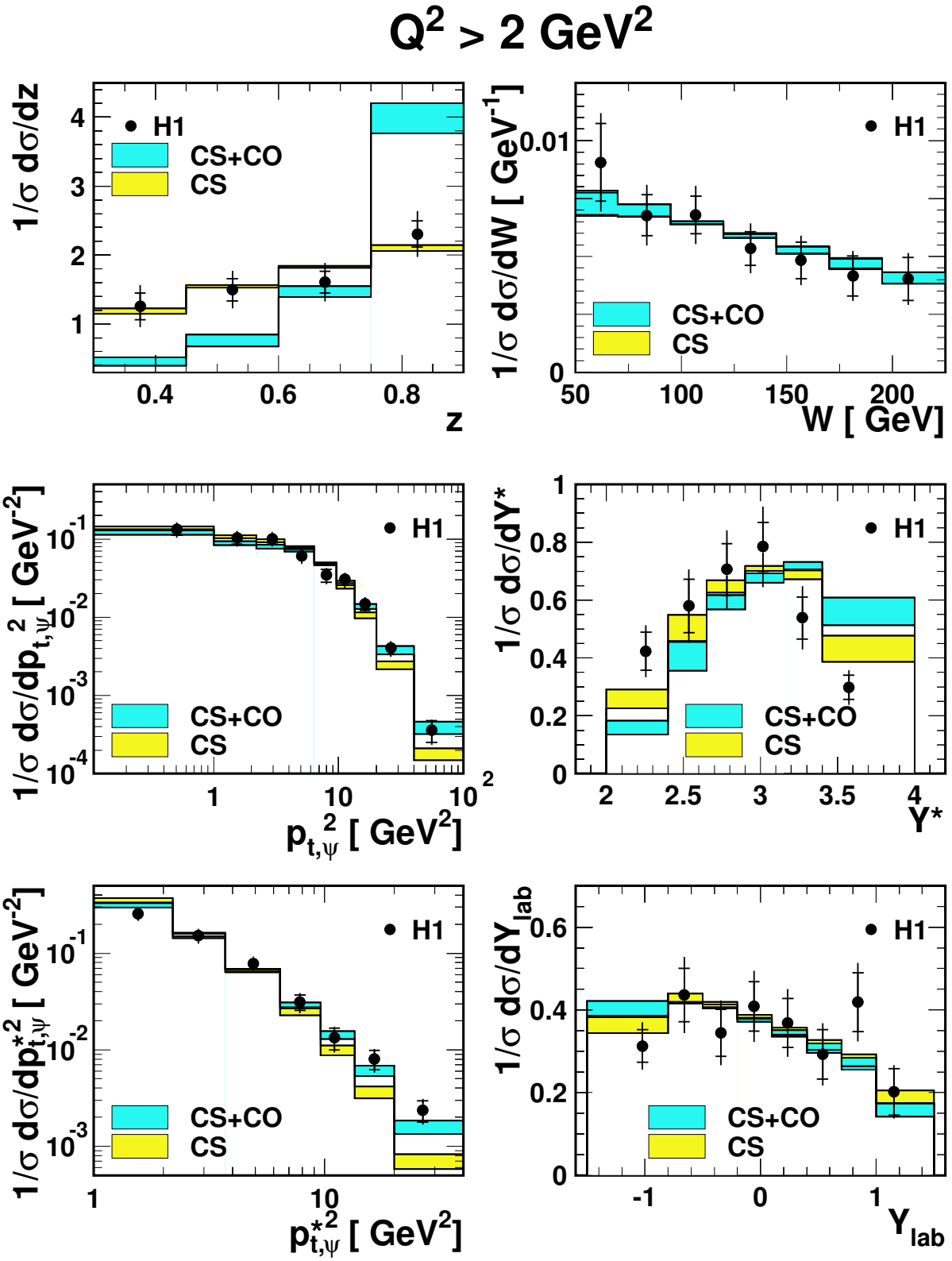

Fig. 5.22: Normalized differential cross-sections. $1/\sigma\, d\sigma/dz$ (top left panel), $1/\sigma\, d\sigma/dW$ (top right panel), $1/\sigma\, d\sigma/dp^2_{T,\psi}$ (middle left panel), $1/\sigma\, d\sigma/dY^*$ (middle right panel), $1/\sigma\, d\sigma/dp^{*2}_{T,\psi}$ (bottom left panel), and $1/\sigma\, d\sigma/dY_{lab}$ (bottom right panel). The histograms show calculations for inelastic J/ψ production within the NRQCD factorization approach [182], which have been normalized to the integrated cross-section. The dark band represents the sum of CS and CO contributions, and the light band represents the CSM contribution alone. These contributions are normalized separately. The error bands reflect the theoretical uncertainties.

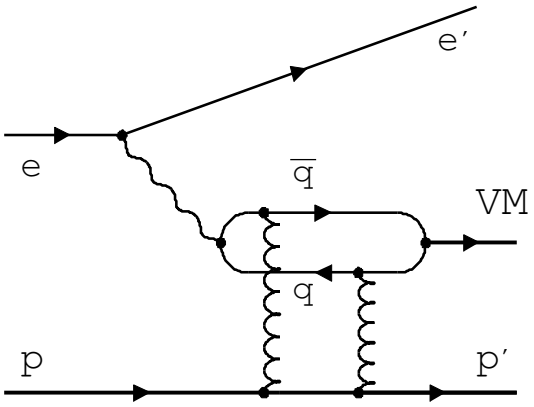

Fig. 5.23: Diagram for diffractive charmonium production via exchange of two gluons in a colour-singlet state.

Fig. 5.20). A similar observation was made for photoproduction (Section 4.1, Fig. 5.15), in which the LO CSM calculation is too steep and the NLO CSM calculation is found to describe the data well. The z distribution (Figs. 5.21 and 5.22) is very poorly described by the full calculation that includes colour-octet contributions, while the colour-singlet contribution alone reproduces the shape of the data rather well. The failure of the colour-octet calculations could be due to the fact that resummations of soft-gluons are not included here. It is worth noting that the calculation of Kniehl and Zwirner disagrees with a number of previous results [186–190], which themselves are not fully consistent.

4.3 Diffractive vector meson production

At HERA, the dominant production channel for quarkonia with quantum numbers of real photons (i.e., $J^{PC} = 1^{--}$) is through diffractive processes. In perturbative QCD, the diffractive production of vector mesons can be modeled in the proton rest frame by a process in which the photon fluctuates into a $q\bar{q}$ pair at a long distance from the proton target. The $q\bar{q}$ subsequently interacts with the proton via a colour-singlet exchange, i.e., in lowest order QCD via the exchange of a pair of gluons with opposite colour (see Fig. 5.23) [191–197]. At small $|t|$, where t is the momentum-transfer-squared at the proton vertex, the elastic process in which the proton stays intact dominates. Toward larger values of $|t|$, the dissociation of the proton into a small-invariant-mass state becomes dominant. Measurements of diffractive vector-meson production cross-sections and helicity structure from the H1 [180, 198–205] and ZEUS [206–211, 213, 214] collaborations are available for ρ^0, ω, ϕ, J/ψ, ψ', and Υ production, spanning the ranges of $0 \simeq Q^2 < 100$ GeV^2, $0 \simeq |t| < 20$ GeV^2, and $20 < W_{\gamma p} < 290$ GeV. ($W_{\gamma p}$ is the γp centre-of-mass energy.) In Fig. 5.24, the elastic photoproduction cross-sections are shown. Perturbative calculations in QCD are available for the kinematic regions in which at least one of the energy scales μ^2 (i.e., Q^2, M_V^2 or $|t|$) is large and the strong-coupling constant $\alpha_s(\mu^2)$ is small [215–221].

In the presence of such a 'hard' scale, QCD predicts a steep rise of the cross-section with $W_{\gamma p}$. At small Q^2, $|t|$ and meson masses M_V, vector-meson production is known to show a non-perturbative "soft" behavior that is described, for example, by Regge-type models [222–226]. Toward larger values of $|t|$, in the leading logarithmic approximation, diffractive J/ψ production can be described by the effective exchange of a gluonic ladder. At sufficiently low values of Bjorken x (i.e., large values of $W_{\gamma p}$), the gluon ladder is expected to include contributions from BFKL evolution [227–231], as well as from DGLAP evolution [232].

Experimentally, diffractive events are generally distinguishable from inelastic events, since, aside from meson-decay products, only a few final-state particles are produced in the central rapidity range in proton dissociation and no particles are produced in the central rapidity range in elastic diffraction. The elasticity variable z defined in Eq. (5.23) is often used to demark the boundary between the elastic

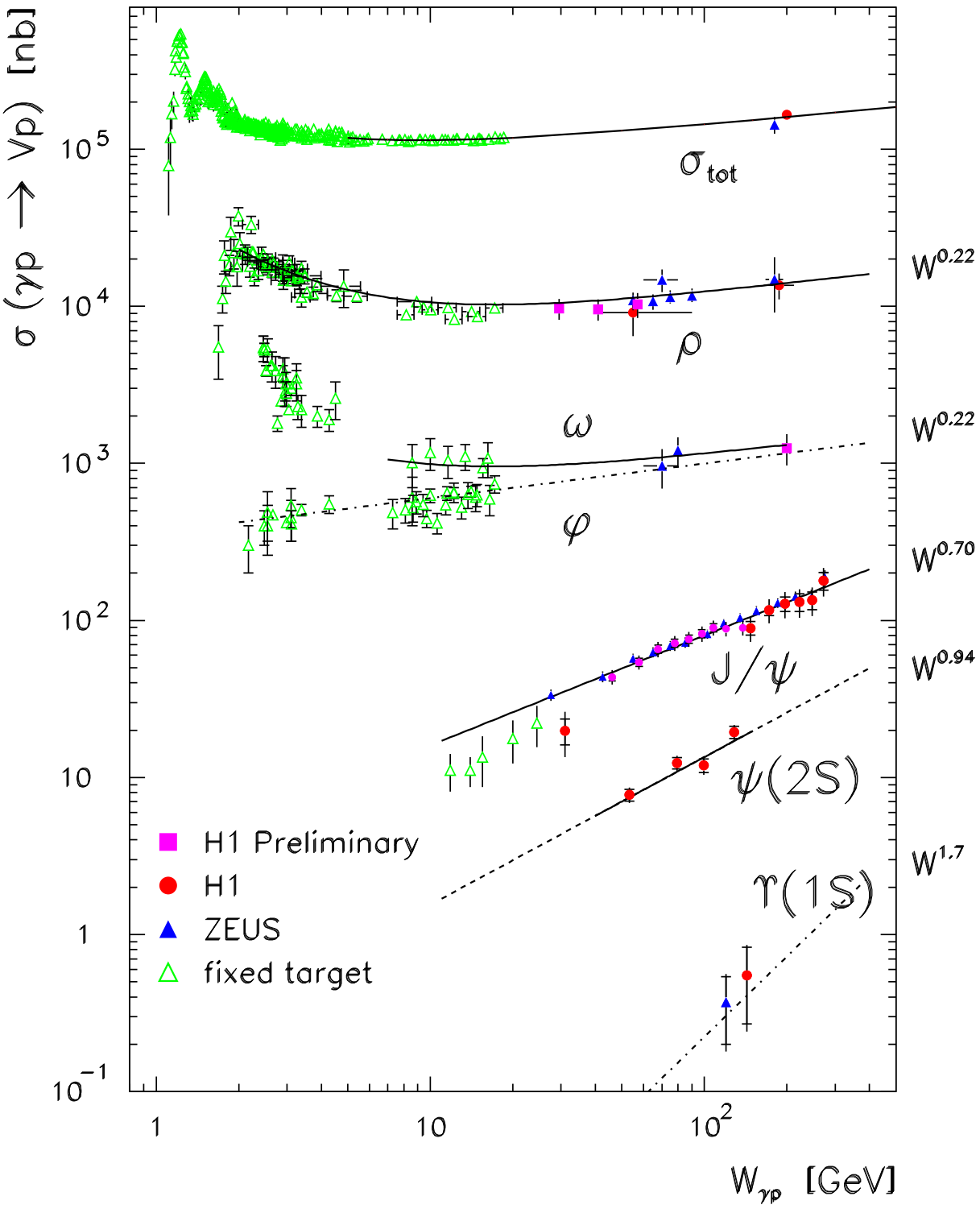

Fig. 5.24: Total cross-section and cross-sections for production of various vector mesons in γp collisions as a function of $W_{\gamma p}$, as measured at HERA and in fixed-target experiments.

and inelastic regions, with a typical demarcation for J/ψ production being $z > 0.95$ for the diffractive region and $z < 0.95$ for the inelastic region. However, at large z, there is actually no clear distinction between inelastic J/ψ production and diffractive J/ψ production in which the proton dissociates into a final state with large invariant mass, owing to the fact that the two processes can produce the same final-state particles. In the region of large z, both inelastic and diffractive processes are expected to contribute to the cross-section. In calculations that are based on the NRQCD factorization approach, the cross-section increases toward large z, owing to large contributions from colour-octet $c\bar{c}$ pairs, as is explained in Section 4.1. These contributions are, however, substantially reduced when one takes into account multiple soft gluon emission, e.g., in resummation calculations [12]. At the same time, calculations in perturbative QCD that assume a diffractive colour-singlet exchange are capable of describing the production cross-sections at large z [204, 211, 212]. A unified description in QCD of the large z region, taking into account both inelastic and diffractive contributions, has yet to be developed.

4.4 Prospects for the upgraded HERA collider

With the HERA luminosity upgrade, a wealth of new quarkonium data will become available. The existing J/ψ and $\psi(2S)$ measurements can be improved and extended into new kinematic regions, and other quarkonium final states may become accessible. The future analyses of quarkonium production at HERA offer unique possibilities to test the theoretical framework of NRQCD factorization. It should be noted here that calculations to next-to-leading order, which are not yet available in the framework of NRQCD factorization, could be an essential ingredient in a full quantitative understanding of charmonium production at HERA, and also at other experiments, such as those at the Tevatron. Some of the most interesting reactions will be discussed briefly below. See Refs. [64, 233] for more details.

The measurement of inelastic χ_c *photoproduction* is a particularly powerful way to discriminate between NRQCD and the colour-evaporation model. The assumption of a single, universal long-distance factor in the colour-evaporation model implies a universal $\sigma[\chi_c]/\sigma[J/\psi]$ ratio. A large χ_c cross-section is predicted for photon–proton collisions. The ratio of χ_c production to J/ψ production is expected to be similar to that at hadron colliders, for which $\sigma[\chi_c]/\sigma[J/\psi] \approx 0.5$ [62]. In NRQCD, on the other hand, the $\sigma[\chi_c]/\sigma[J/\psi]$ ratio is process-dependent and strongly suppressed in photoproduction. Up to corrections of $\mathcal{O}(\alpha_s, v^2)$ one finds that [64]

$$\frac{\sigma[\gamma p \to \chi_{cJ}\, X]}{\sigma[\gamma p \to J/\psi\, X]} \approx \frac{15}{8}\,(2J+1)\,\frac{\langle \mathcal{O}_8^{\chi_{c0}}(^3S_1)\rangle}{\langle \mathcal{O}_1^{J/\psi}(^3S_1)\rangle} \approx (2J+1)\,0.005, \tag{5.25}$$

where the last approximation makes use of the NRQCD matrix elements that are listed in Table 5.1. A search for χ_c production at HERA that results in a cross-section measurement or an upper limit on the cross-section would probe directly the colour-octet matrix element $\langle \mathcal{O}_8^{\chi_J}(^3S_1)\rangle$ and would test the assumption of a single, universal long-distance factor that is implicit in the colour-evaporation model.

The inclusion of colour-octet processes is crucial in describing the photoproduction of the *spin-singlet states* $\eta_c(1S)$, $\eta_c(2S)$, and $h_c(1P)$. With regard to the P-wave state h_c, the colour-octet contribution is required to cancel the infrared divergence that is present in the colour-singlet cross-section [234]. The production of the η_c, on the other hand, is dominated by colour-octet processes, since the colour-singlet cross-section vanishes at leading-order, owing to charge-conjugation invariance [235, 236], as is the case for χ_c photoproduction. The cross-sections for $\eta_c(1S)$, $\eta_c(2S)$, and $h_c(1P)$ photoproduction are sizable [234, 235], but it is not obvious that these particles can be detected experimentally, even with high-statistics data.

The energy spectrum of *J/ψ's produced in association with a photon* via the process $\gamma p \to J/\psi + \gamma\, X$ is a distinctive probe of colour-octet processes [233, 237–239]. In the colour-singlet channel and at leading-order in α_s, $J/\psi + \gamma$ can be produced only through resolved-photon interactions. The corresponding energy distribution is therefore peaked at low values of z. The intermediate-z and large-z regions of the energy spectrum are expected to be dominated by the colour-octet process $\gamma g \to c\bar{c}_8(^3S_1)\,\gamma$.

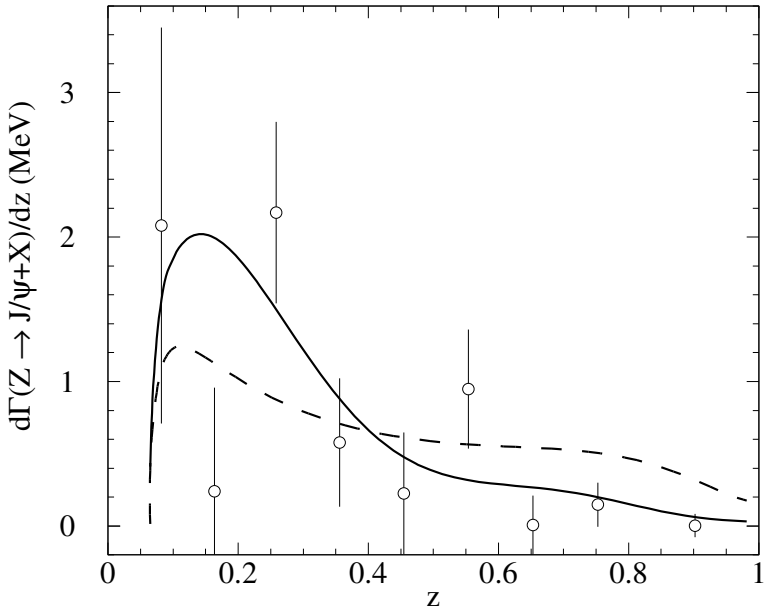

Fig. 5.25: Differential rate $d\Gamma/dz$ for inclusive decay of Z^0 into J/ψ. The data is from the ALEPH collaboration [240]. The dashed line is the sum of the tree-level colour-singlet and colour-octet terms. The solid line is an interpolation between resummed calculations in the small-z and large-z regions. From Ref. [244].

Observation of a substantial fraction of $J/\psi + \gamma$ events at $z \gtrsim 0.5$ would provide clear evidence for the presence of colour-octet processes in quarkonium photoproduction. Experimentally, this measurement is very difficult due to the large background from photons from π^0 decays which are produced in the final state.

With the significant increase in statistics at the upgraded HERA collider, it might be possible to study *inelastic photoproduction of bottomonium states* for the first time. The large value of the b-quark mass makes the perturbative QCD predictions more reliable than for charm production, and the application of NRQCD should be on safer ground for the bottomonium system, in which $v^2 \approx 0.1$. However, the production rates for Υ states are suppressed compared with those for J/ψ by more than two orders of magnitude at HERA — a consequence of the smaller b-quark electric charge and the phase-space reduction that follows from the larger b-quark mass.

5 QUARKONIUM PRODUCTION AT LEP

5.1 J/ψ production

The LEP collider was used to study e^+e^- collisions at the Z^0 resonance. Charmonium was produced at LEP through direct production in Z^0 decay, through the decays of b hadrons from Z^0 decay, and through $\gamma\gamma$ collisions. The contributions from the decays of b hadrons can be separated from those from direct production by using a vertex detector. Charmonium that is produced directly will be referred to as "prompt."

In Z^0 decay, the dominant mechanism for charmonium production is the decay of the Z^0 into $b\bar{b}$, followed by the fragmentation of the b or $\bar{b}$ into a heavy hadron and the subsequent decay of the heavy hadron into charmonium. The inclusive branching fraction of the Z^0 into a charmonium state H is to a good approximation the product of the branching fraction for $Z^0 \to b\bar{b}$, a weighted average of the inclusive branching fractions of b hadrons into H, and a factor of two to account for the b and the $\bar{b}$:

$$\mathrm{Br}[Z^0 \to HX] \approx 2\ \mathrm{Br}[Z^0 \to b\bar{b}] \sum_B D_{b\to B}\ \mathrm{Br}[B \to HX]. \tag{5.26}$$

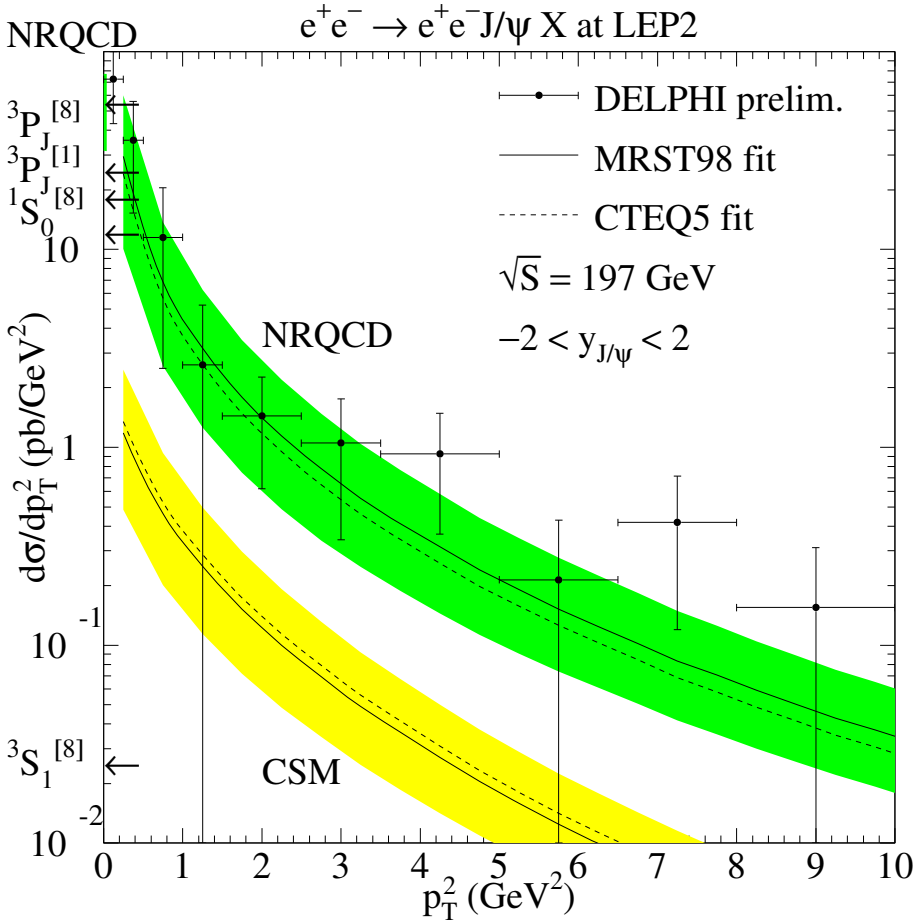

Fig. 5.26: Differential cross-section for the process $\gamma\gamma \to J/\psi + X$ as a function of p_T^2. The data points are from the DELPHI Collaboration [245, 246]. The upper set of curves is the NRQCD factorization predictions, and the lower set of curves is the colour-singlet model prediction. The solid and dashed curves correspond to the MRST98LO [79] and CTEQ5L [69] parton distributions, respectively. The arrows indicate the relative contributions at $p_T = 0$ from parton processes $ij \to c\bar{c}$, which were ignored in the analysis. Here $ij = \gamma\gamma$, gg, or $q\bar{q}$. From Ref. [251].

The branching fraction for the b hadron B to decay into a state that includes H is weighted by the probability $D_{b\to B}$ for a 45 GeV b quark to fragment into B. The inclusive branching fractions for Z^0 decay into several charmonium states have been measured. Since these measurements have more to do with b-hadron decay than Z^0 decay, they are presented in Section 7.

The ALEPH, DELPHI, L3, and OPAL collaborations at LEP have measured the inclusive branching fraction of Z^0 into prompt J/ψ [240–243]. In the NRQCD factorization approach, there are two mechanisms that dominate direct J/ψ production. The first is Z^0 decay into $c\bar{c}$, followed by the fragmentation of the c or $\bar{c}$ into J/ψ via the colour-singlet channel $c\bar{c}_1(^3S_1)$. The second is Z^0 decay into $q\bar{g}g$, followed by the fragmentation of the gluon into J/ψ via the colour-octet channel $c\bar{c}_8(^3S_1)$. Boyd, Leibovich, and Rothstein [244] have used the results from the four LEP collaborations to extract the colour-octet matrix element: $\langle \mathcal{O}_8^{J/\psi}(^3S_1)\rangle = (1.9 \pm 0.5_{stat} \pm 1.0_{theory}) \times 10^{-2}$ GeV^3. This is about a factor of two larger than the Tevatron value and has smaller theory errors, but feeddown from χ_c and $\psi(2S)$ states was not taken into account in the theoretical analysis. Boyd, Leibovich, and Rothstein [244] also carried out a resummation of the logarithms of M_Z^2/M_ψ^2 and z^2, where $z = 2E_{c\bar{c}}/m_Z$. Their result for the resummed z distribution for prompt J/ψ production is compared with data from the ALEPH

collaboration [240] in Fig. 5.25. Their analysis predicts an enhancement in the production rate near $z = 0.15$. The uncertainties in the data are too large to make a definitive statement about the presence or absence of this feature.

The inclusive cross-section for $\gamma\gamma \to J/\psi + X$ at LEP has been measured by the DELPHI Collaboration [245,246]. The cross-section at nonzero p_T has been computed at leading order in α_s. The computation includes the direct-photon process $\gamma\gamma{\to}(c\bar{c}) + g$, which is of order $\alpha^2\alpha_s$, the single-resolved-photon process $i\gamma{\to}(c\bar{c})+i$, which is of order $\alpha\alpha_s^2$, and the double-resolved-photon process $ij{\to}(c\bar{c})+k$, which is of order α_s^3 [247–251]. (Here, $ij = gg$, gq, $g\bar{q}$, or $q\bar{q}$.) Note that all processes contribute formally at the same order in perturbation theory since the leading behavior of the parton distributions in the photon is $\propto \alpha/\alpha_s$. The contribution to the $\gamma\gamma \to J/\psi + X$ cross-section at LEP that is by far dominant numerically is that from single-resolved processes, i.e., photon–gluon fusion.

The results of the LO computation [251] are shown in Fig. 5.26. The computation uses the NRQCD matrix elements of Ref. [78]. Theoretical uncertainties were estimated by varying the renormalization and factorization scales by a factor two and by incorporating the effects of uncertainties in the values of the colour-octet matrix elements. As can be seen from Fig. 5.26, the comparison with the DELPHI data [245, 246] clearly favors the NRQCD factorization approach over the colour-singlet model. However, the comparison of Fig. 5.26 is based on a leading-order calculation. It is known from the related process of J/ψ photoproduction at HERA, which is also dominated by photon–gluon fusion, that the LO colour-singlet cross-section fails to describe the J/ψ data at nonzero p_T. Inclusion of the NLO correction, however, brings the colour-singlet prediction in line with experiment. Similarly large NLO corrections can be expected for $\gamma\gamma \to J/\psi + X$ production at LEP, and a complete NLO analysis is needed before firm conclusions on the importance of colour-octet contributions can be drawn. A first step in this direction has been taken recently in Ref. [252], where the NLO corrections to the direct process $\gamma\gamma{\to}(c\bar{c}) + g$ have been calculated.

5.2 $\Upsilon(1S)$ production

The OPAL collaboration has measured the inclusive branching fraction for the decay of Z^0 into $\Upsilon(1S)$ [253]. The NRQCD factorization prediction for $\mathrm{Br}[Z^0 \to \Upsilon(1S) + X]$ is 5.9×10^{-5} [254]. The colour-singlet-model prediction is 1.7×10^{-5} [254–259]. The experimental result from OPAL [253] is $[1.0{\pm}0.4(\mathrm{stat.}){\pm}0.1(\mathrm{sys.}){\pm}0.2(\mathrm{prod.\ mech.})]{\times}10^{-4}$. This is compatible with the NRQCD factorization prediction, but not with the colour-singlet-model prediction.

6 CHARMONIUM PRODUCTION IN e^+e^- ANNIHILATIONS AT 10.6 GEV

The B factories have proved to be a rich source of data on charmonium production in e^+e^- annihilation. The B factories operate near the peak of the $\Upsilon(4S)$ in order to maximize the production rate for B mesons, but about 75% of the events are continuum e^+e^- annihilation events. The enormous data samples that have been accumulated compensate for the relatively small cross-sections for e^+e^- annihilation into states that include charmonium.

6.1 J/ψ production

The Belle and BaBar Collaborations have measured the inclusive cross-section $\sigma[e^+e^- \to J/\psi\, X]$. The Belle Collaboration obtains $2.52 \pm 0.21 \pm 0.21$ pb [260], while the BaBar Collaboration obtains $1.47 \pm 0.10 \pm 0.13$ pb [261]. The leading-order parton process in the colour-singlet model is $e^+e^-{\to}(c\bar{c}) + gg$, which is of order $\alpha^2\alpha_s^2$. The leading colour-octet contributions in the NRQCD factorization approach come from e^+e^- annihilation into $(c\bar{c}) + g$, which is order $\alpha^2\alpha_s$, and into $(c\bar{c}) + q\bar{q}$ and $(c\bar{c}) + gg$, which are order $\alpha^2\alpha_s^2$. The prediction for the cross-section $\sigma[e^+e^- \to J/\psi\, X]$ in the colour-singlet model is $0.45 - 0.81$ pb [262–265], while the NRQCD factorization prediction is $1.1 - 1.6$ pb [263–265]. There is a 3σ discrepancy between the experiments, but the NRQCD factorization prediction seems to be favored.

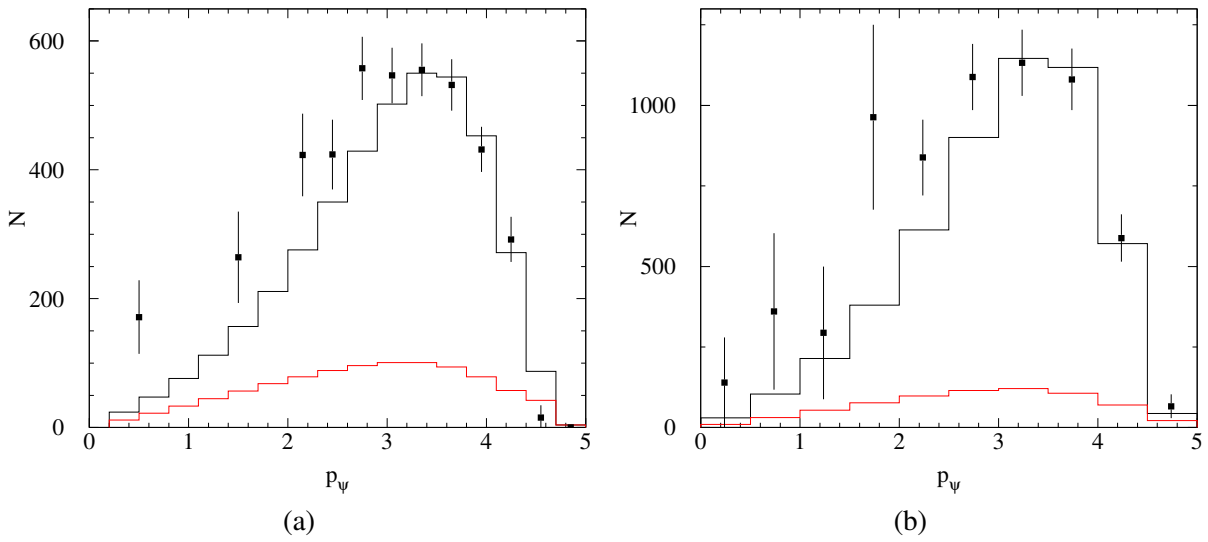

Fig. 5.27: J/ψ production rate in e^+e^- annihilation at 10.6 GeV as a function of $p^* = p_\psi$, the J/ψ momentum in the CM frame. The vertical axis is the number of J/ψ events per 0.5 GeV/c. The data points are from (a) the Belle Collaboration [260] and (b) the BaBar Collaboration [261]. The upper lines are the sum of the leading-order colour-singlet contribution and the colour-octet contribution, which includes a resummation of logarithms of $1-z$ and a phenomenological shape function. The lower lines are the leading-order colour-singlet contribution alone. From Ref. [11].

The discrepancies between the two experiments in this and other measurements may be due partly to differences in cuts that were used to suppress contributions from processes in which the charmonium is not produced by annihilation of e^+ and e^- with a centre-of-mass energy of 10.6 GeV. These include radiative-return processes, in which the e^+ or e^- loses a substantial fraction of its momentum by radiating a collinear photon before the collision, virtual photon radiation, in which the e^+ or e^- radiates a virtual photon that becomes a J/ψ or $\psi(2S)$, and two-photon collisions, which produce η_c, χ_{c0}, and χ_{c2}.

The momentum distribution of the J/ψ provides information about the production mechanism. The momentum of the J/ψ in the CM frame can be characterized in terms of its magnitude p^* and its angle θ^* with respect to the beam direction. The Belle [260] and BaBar [261] measurements for the differential cross-section for J/ψ production as a function of p^* are shown in Fig. 5.27. The colour-singlet prediction, which is shown in the lower curves in Fig. 5.27, is far too small to describe the data. The measurements from Belle and BaBar do not show any enhancement at the maximum value of p^*, as might be expected from the colour-octet process $e^+e^- \to (c\bar{c}) + g$ that is of leading order in α_s. However, there are two effects that are expected to modify the leading-order result. The first effect is that the v expansion of NRQCD breaks down near the kinematic maximum value of p^*. Resummation of the expansion is required [10, 12], and it leads to a nonperturbative shape function [10], which smears out the peak in the leading-order result. A second effect near the maximum value of p^* is that there are large logarithms of $1-z$, where $z = E_{c\bar{c}}/E_{c\bar{c}}^{\rm max}$, that must also be resummed. The effect of that resummation is again to smear out the peak in the leading-order result. A resummation of logarithms of $1-z$ has been combined with a phenomenological shape function in Ref. [11]. The results of this calculation are shown in the upper curves in Fig. 5.27. The shape function has been chosen to fit the Belle and BaBar data. The normalization of the shape function is fixed by the colour-octet NRQCD matrix elements, which were taken to be $\langle \mathcal{O}_8^{J/\psi}(^1S_0)\rangle = \langle \mathcal{O}_8^{J/\psi}(^3P_0)\rangle = 6.6 \times 10^{-2}$ GeV. These values of the colour-octet matrix elements are consistent with data from photoproduction and hadroproduction [129,169]. As can be seen, the resummations of the v expansion and the logarithms of $1-z$ produce reasonable fits to the data. The resummation prediction is not expected to be valid at small values of p^*. It should also be kept in

mind that hard-scattering factorization may not hold unless $p^* \gg \Lambda_{\rm QCD}$. While the comparison of the resummed theory with experiment indicates that it is plausible that the NRQCD factorization approach can describe the experimental data, the theoretical results rely heavily on the phenomenological shape function, whose shape is tuned to fit the data. The resummed theory will receive a much more stringent test when a phenomenological shape function that has been extracted from the e^+e^- data is used to predict the J/ψ production cross-section in some other process, for example, photoproduction at HERA.

Table 5.10: Angular asymmetry variable A and polarization variable α for various ranges of the CM momentum p^* of the J/ψ in $e^+e^- \to J/\psi X$ at $\sqrt{s} = 10.6$ GeV, as measured by the Belle [260] and BaBar [261] Collaborations.

Belle			BaBar		
Range of p^* (GeV)	A	α	Range of p^* (GeV)	A	α
$2.0 < p^* < 2.6$	$0.82^{+0.95}_{-0.63}$	$-0.62^{+0.30}_{-0.24}$	$p^* < 3.5$	0.05 ± 0.22	-0.46 ± 0.21
$2.6 < p^* < 3.4$	$1.44^{+0.42}_{-0.38}$	$-0.34^{+0.18}_{-0.16}$			
$3.4 < p^* < 5.0$	$1.08^{+0.44}_{-0.33}$	$-0.32^{+0.20}_{-0.18}$	$3.5 < p^*$	1.5 ± 0.6	-0.80 ± 0.09

The other variable that characterizes the momentum of the J/ψ is its angle θ^* with respect to the beam direction in the CM frame. The angular distribution $d\sigma/d(\cos\theta^*)$ is proportional to $1 + A\cos^2\theta^*$, which defines an angular asymmetry variable A. The Belle [260] and BaBar [261] Collaborations have measured A in several bins of p^*. Their results are shown in Table 5.10. The NRQCD factorization approach predicts that $A \approx 0$ at small p^* and $0.6 < A < 1.0$ at large p^* [266] . The colour-singlet model predicts that $A \approx 0$ at small p_T and $A \approx -0.8$ at large p^* [266]. The Belle and BaBar results favor the NRQCD factorization prediction, but the uncertainties are large.

The polarization of the J/ψ provides further information about the production mechanism. The polarization variable α for J/ψ production is defined by the angular distribution in Eq. (5.13). In e^+e^- annihilation, the most convenient choice for the polarization axis is the boost vector from the quarkonium rest frame to the e^+e^- centre-of-momentum frame. The Belle and BaBar Collaborations have measured the polarization variable α in several bins of p^*. Their results are shown in Table 5.10. The polarization of J/ψ's from e^+e^- annihilation at the B factories has not yet been calculated within the NRQCD factorization approach. In contrast to the production of J/ψ's with large p_T at the Tevatron, where the dominance of gluon fragmentation into colour-octet ${}^3S_1$ $c\bar{c}$ states implies a large transverse polarization, production of J/ψ's at the B factories occurs at values of p^* for which there are no simple qualitative expectations for the polarization. A comparison between theory and experiment must await an actual calculation of the J/ψ polarization, including the effects of feeddown from higher charmonium states. It may be necessary to include in such a calculation resummations of the v expansion and logarithms of $1 - z$ in order to make precise quantitative statements. However, the effects of these resummations is mainly to re-distribute the J/ψ's that are produced via the colour-octet mechanism over a range in p^* without affecting the total number of such J/ψ's.

A surprising result from the Belle Collaboration is that most of the J/ψ's that are produced in e^+e^- annihilation at 10.6 GeV are accompanied by charmed hadrons. The presence of a charmed hadron indicates the creation of a second $c\bar{c}$ pair in addition to the pair that forms the J/ψ. A convenient measure of the probability for creating the second $c\bar{c}$ pair is the ratio

$$R_{\rm double} = \frac{\sigma[e^+e^- \to J/\psi + X_{c\bar{c}}]}{\sigma[e^+e^- \to J/\psi + X]} \ . \tag{5.27}$$

The Belle Collaboration finds that $R_{\rm double} = 0.82 \pm 0.15 \pm 0.14$ with $R_{\rm double} > 0.48$ at the 90% confidence level [267]. The NRQCD factorization approach leads to the prediction $R_{\rm double} \approx 0.1$ [262, 263,268], which disagrees with the Belle result by almost an order of magnitude. The discrepancy seems

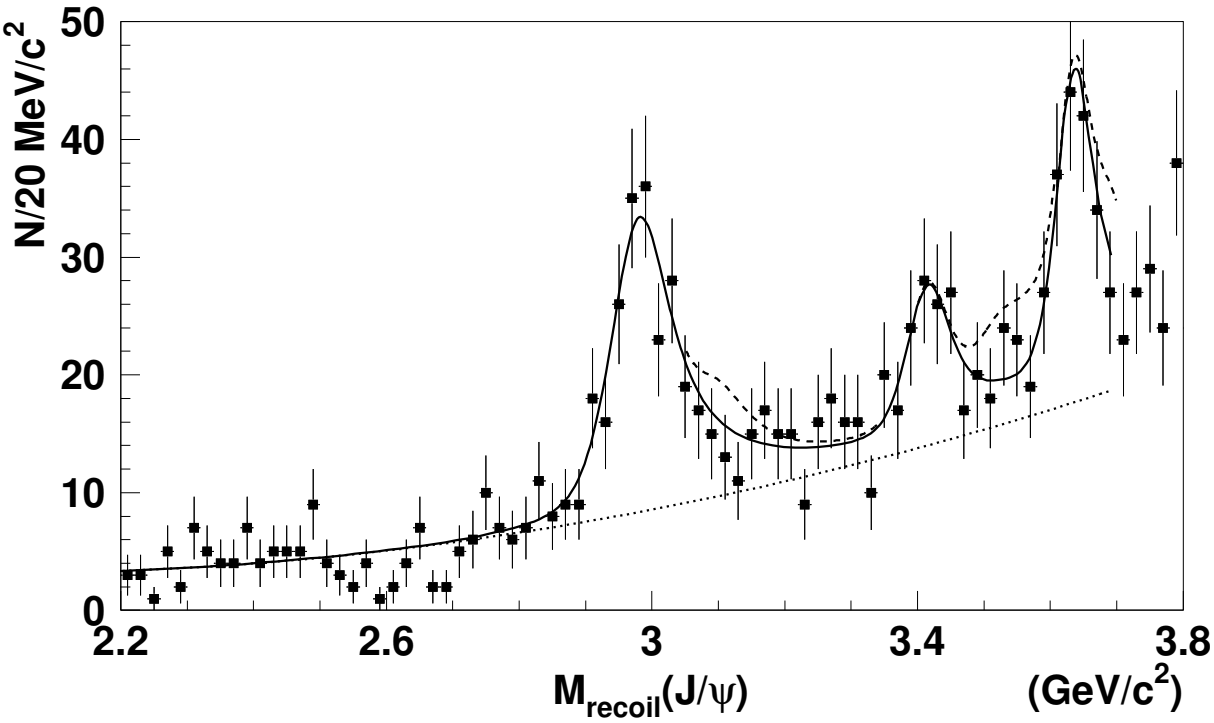

Fig. 5.28: Distribution of masses recoiling against the reconstructed J/ψ in inclusive $e^+e^- \to J/\psi X$ events at Belle [271]. The solid line is the best fit, including contributions from the η_c, $\chi_{c0}(1P)$, and $\eta_c(2S)$. The dotted line is a fit in which additional contributions from the J/ψ, $\chi_{c1}(1P)$, $\chi_{c2}(1P)$, and $\psi(2S)$ have been set at their largest possible values within the 90%-confidence-level limits.

to arise primarily from the cross-section in the numerator of (5.27). The Belle result for this cross-section is about 0.6–1.1 pb [269], while the prediction is about 0.10–0.15 pb [262, 263, 268, 270]. At leading order in α_s, which is α_s^2, the process of e^+e^- annihilation into $J/\psi + X_{c\bar{c}}$ proceeds through $(c\bar{c}) + c\bar{c}$. The contributions to this cross-section in which the J/ψ is formed from a colour-octet $c\bar{c}$ pair are suppressed by a factor $v^4 \approx 0.1$, and they have been found to yield only about 7% of the total cross-section [270]. Corrections of order α_s^3 and higher are also not expected to be particularly large. Thus, the source of the discrepancy between the Belle result for $R_{\rm double}$ and theory remains a mystery.

There is also a large discrepancy between theory and experiment in an exclusive double-$c\bar{c}$ cross-section. For the double-charmonium process $e^+e^- \to J/\psi + \eta_c$, the Belle Collaboration measures the product of the cross-section and the branching fraction for the η_c to decay into at least two charged tracks to be $25.6 \pm 2.8 \pm 3.4$ fb [271]. In contrast, leading-order calculations predict a cross-section of 2.31 ± 1.09 fb [272–274]. There are some uncertainties from uncalculated corrections of higher-order in α_s and v and from NRQCD matrix elements. However, because this is an exclusive process, only colour-singlet matrix elements enter, and these are fairly well determined from the decays $J/\psi \to e^+e^-$ and $\eta_c \to \gamma\gamma$.

Since the Belle mass resolution is 110 MeV but the J/ψ–η_c mass difference is only 120 MeV, it has been suggested that some of the $J/\psi + \eta_c$ data sample may consist of $J/\psi + J/\psi$ events [275, 276]. The state $J/\psi + J/\psi$ has charge-parity $C = +1$, and consequently, is produced in a two-photon process, whose rate is suppressed by a factor $(\alpha/\alpha_s)^2$ relative to the rate for $J/\psi + \eta_c$. However, as was pointed out in Refs. [275, 276], the two-photon process contains photon-fragmentation contributions that are enhanced by factors $(E_{\rm beam}/2m_c)^4$ from photon propagators and $\log[8(E_{\rm beam}/2m_c)^4]$ from a would-be collinear divergence. As a result, the predicted cross-section $\sigma[e^+e^- \to J/\psi + J/\psi] = 8.70 \pm 2.94$ fb is

larger than the predicted cross-section $\sigma[e^+e^- \to J/\psi + \eta_c] = 2.31 \pm 1.09$ fb [275, 276]. Corrections of higher order in α_s and v are likely to reduce the prediction for the $J/\psi + J/\psi$ cross-section by about a factor of three [276, 277]. These predictions spurred a re-analysis of the Belle data [278]. The invariant mass distribution of X in $e^+e^- \to J/\psi + X$ is shown in Fig. 5.28. No significant $J/\psi + J/\psi$ signal was observed. The upper limit on the cross-section times the branching fraction into at least two charged tracks [271] is $\sigma[e^+e^- \to J/\psi + J/\psi] < 9.1$ fb, which is consistent with the prediction of Refs. [275,276].

6.2 Prospects at BaBar and Belle

The BaBar and Belle detectors are accumulating ever larger data samples of charmonium that is produced directly in e^+e^- annihilation. The simplicity of the initial state makes the theoretical analysis of this process particularly clean. These two factors make charmonium production in continuum e^+e^- annihilation a particularly attractive process in which to compare theoretical predictions with experiment. The experimental results that have already emerged from these detectors provide further motivation for understanding this process. There are significant discrepancies between previous measurements by BaBar and Belle. There are also surprising results from Belle on double $c\bar{c}$ production that differ dramatically from theoretical expectations. The resolution of these problems will inevitably lead to progress in our understanding of charmonium production.

The surprising double-$c\bar{c}$ results from Belle include an inclusive measurement, the ratio $R_{\rm double}$ defined in Eq. (5.27), and exclusive double-charmonium cross-sections, such as $\sigma[e^+e^- \to J/\psi + \eta_c]$. The discrepancies between theory and experiment in these measurements are among the largest in the standard model. Theory and experiment differ by about an order of magnitude — a discrepancy which is larger than any known QCD K-factor. It is important to recognize that these discrepancies are problems not just for NRQCD factorization, but for perturbative QCD in general. It is difficult to imagine how any perturbative calculation of $R_{\rm double}$ could give a value as large as 80%. With regard to the cross-section for $e^+e^- \to J/\psi + \eta_c$, the perturbative QCD formalism for exclusive processes [274] gives a result that reduces to that of NRQCD factorization [272, 273] in the nonrelativistic limit and is well-approximated by it if one uses realistic light-cone wave functions for J/ψ and η_c.[5] Clearly, it is very important to have independent checks of the Belle inclusive and exclusive double-$c\bar{c}$ results. If the Belle results are confirmed, then we would be forced to entertain some unorthodox possibilities: the inapplicability of perturbative QCD to double-$c\bar{c}$ production, new charmonium production mechanisms within the standard model, or perhaps even physics beyond the standard model.

The larger data samples that are now available should allow much more accurate measurements of the inclusive process $e^+e^- \to J/\psi X$, including the momentum distribution of the J/ψ and its polarization. The measurements of the J/ψ momentum distribution may allow the determination of all the relevant NRQCD matrix elements. A comparison with the NRQCD matrix elements measured at the Tevatron would then provide a test of their universality. Once the NRQCD matrix elements are determined, they can be used to predict the polarization of the J/ψ as a function of its momentum, which would provide a stringent test of the NRQCD predictions for spin. Instead of imposing cuts to suppress contributions from radiative return, virtual photon radiation, and two-photon collisions, it might be better to choose cuts in order to maximize the precision of the measurements, without any regard to the production mechanism. The contributions from other mechanisms could instead be taken into account in the theoretical analyses.

The large data samples of BaBar and Belle should also allow measurements of the inclusive production of other charmonium states, such as the $\psi(2S)$ and the $\chi_c(1P)$. Such measurements could be used to determine the NRQCD matrix elements for these charmonium states. They are also important because they provide constraints on the contributions to inclusive J/ψ production from decays of higher charmonium states.

[5] The Belle result can be accommodated by using asymptotic light-cone wave functions that are appropriate for light hadrons [279], but there is no justification for using such wave functions for charmonium.

There are some straightforward improvements that could be made in the theoretical predictions for inclusive charmonium production in e^+e^- annihilation. For example, there are only a few components missing from a complete calculation of all contributions through second order in α_s. In the contribution from the colour-octet $^3S_1$ channel, the virtual corrections at order α_s^2 have not been calculated. There are also colour-octet contributions to $e^+e^- \to c\bar{c}c\bar{c}$ at order α_s^2 that have not been calculated. The theoretical predictions for inclusive charmonium production could also be improved by treating more systematically the contributions from the feeddown from decays of higher charmonium states and from other mechanisms, such as radiative return, virtual photon radiation, and two-photon collisions.

7 CHARMONIUM PRODUCTION IN B-MESON DECAYS

B-meson decays are an excellent laboratory for studying charmonium production because B mesons decay into charmonium with branching fractions greater than a percent. At a B factory operating near the peak of the $\Upsilon(4S)$ resonance, about 25% of the events consist of a B^+B^- pair or a $B^0\bar{B}^0$ pair. The large sample of B mesons accumulated by the CLEO experiment allowed the measurements of many exclusive and inclusive branching fractions into final states that include charmonium. The Belle and BaBar experiments are accumulating even larger samples of B mesons, providing a new source of precise data on charmonium production in B decays.

The inclusive branching fractions of B mesons into charmonium states can be measured most accurately for the mixture of B^+, B^0, and their antiparticles that are produced in the decay of the $\Upsilon(4S)$ resonance [280, 281]. Those that have been measured are listed in Table 5.11. The fraction of J/ψ's that come from decay of χ_c's, which is defined in Eq. (5.12), is $F_{\chi_c} = (11 \pm 2)\%$. This is significantly smaller than the value that is measured at the Tevatron, which is given in Table 5.3. The χ_{c1} to χ_{c2} ratio, which is defined in Eq. (5.10), is $R_{\chi_c} = 5.1 \pm 3.0$. Although the error bar is large, this ratio seems to be substantially larger than the value that is measured at the Tevatron, which is given in Eq. (5.18), and the values measured in fixed-target experiments, which are given in Table 5.6. Such differences in R_{χ_c} and F_{χ_c} are contrary to the predictions of the colour-evaporation model.

Inclusive branching fractions into charmonium states have also been measured at LEP for the mixtures of B^+, B^0, B_s^0, b baryons, and their antiparticles that are produced in Z^0 decay [241, 282, 283]. This mixture of b hadrons can be interpreted as the one that arises from the fragmentation of a b quark that is produced with a momentum of 45 GeV. The branching fractions that have been measured are listed in Table 5.11. The branching fraction into $\chi_{c1}(1P)$ seems to be significantly larger than for the mixture from $\Upsilon(4S)$ decay. The difference could be due to the contribution from b baryons. It is often assumed that the mixture of b hadrons that is produced at high-energy hadron colliders, such as the Tevatron, is similar to that produced in Z^0 decay. This assumption could be tested by measuring ratios of inclusive cross-sections for charmonium states that come from the decays of b hadrons at the Tevatron.

Table 5.11: Inclusive branching fractions (in units of 10^{-3}) for mixtures of b hadrons to decay into charmonium states.

mixture	J/ψ	$\psi(2S)$	$\chi_{c1}(1P)$	$\chi_{c2}(1P)$
from $\Upsilon(4S)$ decay	11.5 ± 0.6	3.5 ± 0.5	3.6 ± 0.5	0.7 ± 0.4
from Z^0 decay	11.6 ± 1.0	4.8 ± 2.4	11.5 ± 4.0	

The observed inclusive branching fractions of B mesons into J/ψ and $\psi(2S)$ are larger than the predictions of the colour-singlet model by about a factor of three. Ko, Lee, and Song applied the NRQCD factorization approach to the production of J/ψ and $\psi(2S)$ in B decays [284]. The colour-octet $^3S_1$ term in the production rate is suppressed by a factor of v^4 that comes from the NRQCD matrix element. However, the production rate also involves Wilson coefficients that arise from evolving the effective weak

Hamiltonian from the scale M_W to the scale m_b. The Wilson coefficient for the colour-octet ${}^3S_1$ term is significantly larger than that for the colour-singlet term, although the smallness of the colour-singlet term may be the result of an accidental cancellation that occurs in the leading-order treatment of the evolution of the coefficients. Moreover, the colour-singlet contribution is decreased by the relativistic correction of order v^2. The inclusion of the colour-octet ${}^3S_1$ term allows one to explain the factor of three discrepancy between the data and the colour-singlet-model prediction.

The observed branching fraction for decays of B directly into J/ψ, which excludes the feeddown from decays of $\psi(2S)$ and χ_c, is much larger than the prediction of the colour-evaporation model. The CEM prediction for the direct branching fraction is $0.24 - 0.66$ [285], where the range comes from the uncertainty in the CEM parameters. The CLEO collaboration has made a precise measurement of the direct branching fraction of B into J/ψ [286]: $\mathrm{Br}_{\mathrm{dir}}[B{\to}J/\psi + X] = (0.813 \pm 0.041)\%$. The CEM prediction is significantly smaller than the data. As we have already mentioned, the data can be accommodated within the NRQCD factorization approach by including colour-octet terms.

Beneke, Maltoni, and Rothstein [287] have calculated the inclusive decay rates of B mesons into J/ψ and $\psi(2S)$ to next-to-leading order in α_s. They used their results to extract NRQCD matrix elements from the data. Their results for the linear combinations of NRQCD matrix elements defined in Eq. (5.8) are $M_{3.1}^{J/\psi} = (1.5^{+0.8}_{-1.1}) \times 10^{-2}$ GeV^3 and $M_{3.1}^{\psi(2S)} = (0.5 \pm 0.5) \times 10^{-2}$ GeV^3. The uncertainties arise from experiment and from imprecise of knowledge of the matrix elements $\langle \mathcal{O}_8^H({}^3S_1)\rangle$ and $\langle \mathcal{O}_1^H({}^3S_1)\rangle$. Ma, taking into account initial-state hadronic corrections, has extracted slightly different linear combinations of matrix elements [288]: $M_{3.4}^{J/\psi} = 2.4 \times 10^{-2}$ GeV^3 and $M_{3.4}^{\psi(2S)} = 1.0 \times 10^{-2}$ GeV^3. In both extractions, the colour-octet matrix elements are considerably smaller than those from the Tevatron fits, but the uncertainties are large.

The effects of colour-octet terms on the polarization of J/ψ in B decays were considered by Fleming, Hernandez, Maksymyk, and Nadeau [289] and by Ko, Lee, and Song [285]. The polarization variable α for J/ψ production is defined by the angular distribution in Eq. (5.13). In B meson decays, the most convenient choice of the polarization axis is the direction of the boost vector from the J/ψ rest frame to the rest frame of the B meson. The colour-evaporation model predicts no polarization. The predictions of NRQCD factorization and of the colour-singlet model depend on the mass of the b quark. For $m_b = 4.7 \pm 0.3$ GeV, the prediction of NRQCD factorization is $\alpha = -0.33 \pm 0.08$ [289] and the prediction of the colour-singlet model is $\alpha = -0.40 \pm 0.07$ [289]. The uncertainties that arise from m_b have been added in quadrature with other uncertainties. We note that the uncertainty in m_b that was used in this calculation is considerably larger than the uncertainty of 2.4% that is given in Chapter 6. Measurements of the polarization by the CLEO Collaboration have given the results $\alpha = -0.30 \pm 0.08$ for J/ψ and $\alpha = -0.45 \pm 0.30$ for $\psi(2S)$ [286]. The result for J/ψ strongly disfavors the colour-evaporation model and is consistent with the predictions of the NRQCD factorization approach and the colour-singlet model.

Bodwin, Braaten, Yuan, and Lepage have applied the NRQCD factorization approach to the production of the P-wave charmonium states χ_{cJ} in B decays [290]. For P-wave quarkonium production, there is a colour-octet NRQCD matrix element that is of the same order in v as the leading colour-singlet matrix element. Therefore, the factorization formula must include both the colour-singlet P-wave and the colour-octet S-wave contributions. The short-distance coefficient in the colour-singlet ${}^3P_J$ term for χ_{cJ} production vanishes at leading order in α_s for $J = 0, 2$ [18, 291]. The colour-octet ${}^3S_1$ term for χ_{cJ} production is proportional to the number of spin states $2J + 1$. Thus, the relative importance of the colour-singlet and colour-octet terms can vary dramatically among the three χ_{cJ} states. The prediction of the colour-singlet model at leading order in α_s that the direct production rate of χ_{c2} should vanish can be tested. The feeddown from $\psi(2S)$ decay contributes $(0.24 \pm 0.04) \times 10^{-3}$ to the inclusive branching fraction into χ_{c2} given in Table 5.11. The remainder $(0.5 \pm 0.4) \times 10^{-3}$ is consistent with zero, and hence it is compatible with the prediction of the colour-singlet model, but it is also compatible with a small colour-octet contribution.

8 B_c PRODUCTION

The B_c and B_c^* are the ground state and the first excited state of the $\bar{b}c$ quarkonium system. Their total angular momentum and parity quantum numbers are $J^P = 0^-$ and 1^+, and their dominant Fock states have the angular momentum quantum numbers $^1S_0$ and $^3S_1$, respectively. In the following discussion, we will refer to general $\bar{b}c$ quarkonium states as B_c mesons and use the terms B_c and B_c^* specifically for the ground state and the first excited state.

In contrast to charmonium and bottomonium states, which have "hidden flavour," B_c mesons contain two explicit flavours. As a consequence, the B_c decays only through the weak interactions, and the B_c^* decays through an electromagnetic transition into the B_c with almost 100% probability. The higher-mass B_c mesons below the BD threshold decay through hadronic and electromagnetic transitions into lower-mass B_c mesons with almost 100% probability. They cascade down through the $\bar{b}c$ spectrum, eventually producing a B_c or a B_c^*. Another consequence of the explicit flavours is that the most important production mechanisms for B_c mesons are completely different from those for hidden-flavour quarkonia. In the production of B_c mesons by strong or electromagnetic interactions, two additional heavy quarks $\bar{c}$ and b are always produced. The production cross-sections for B_c mesons are suppressed compared with the production cross-sections for hidden-flavour quarkonia because the leading-order diagrams are of higher order in the coupling constants and also because the phase-space is suppressed, owing to the presence of the additional heavy quarks.

The small cross-sections for producing B_c mesons make the prospects for observing the B_c at e^+e^- and *ep* colliders rather bleak. A possible exception to this assessment exists for the case of production at an e^+e^- collider with energy at the Z^0 peak, for which the production rate of the B_c is predicted to be marginal for observation [292]. The B_c was not discovered at LEP, despite careful searches [293–295]. It was finally discovered at the Tevatron by the CDF collaboration in 1998 [296, 297]. We restrict our attention in the remainder of this subsection to the production of B_c mesons at hadron colliders.

The production of B_c mesons was studied before the discovery of the B_c [292,298–302,307–309]. If one assumes that all nonperturbative effects in the production of the B_c in hadron–hadron collisions can be absorbed into the hadrons' parton distribution functions (PDF's), then the inclusive production cross-section can be written in the factorized form

$$d\sigma[h_A h_B \to B_c + X] \;=\; \sum_{ij} \int dx_1 dx_2 \; f_i^{h_A}(x_1,\mu) f_j^{h_B}(x_2,\mu) \; d\hat{\sigma}[ij \to B_c + X] \; . \quad (5.28)$$

The NRQCD factorization formula for the parton–parton cross-section is

$$d\hat{\sigma}[ij \to B_c + X] = \sum_n d\hat{\sigma}[ij \to (\bar{b}c)_n + X] \; \langle \mathcal{O}_n^{B_c} \rangle \; , \quad (5.29)$$

where the sum is over 4-fermion operators that create and annihilate $\bar{b}c$. At the leading order in α_s, which is α_s^4, the parton–parton process is $ij \to (\bar{b}c) + b\bar{c}$, where $ij = gg$ (gluon fusion) or $q\bar{q}$ (quark–antiquark annihilation). Since $m_{B_c} > m_b > m_c \gg \Lambda_{QCD}$, the leading-order parton–parton process involves only hard propagators, even at small p_T. Nevertheless, because of soft-gluon interactions, for example between the B_c and the recoiling b and $\bar{c}$ quarks, it is not clear that hard-scattering factorization holds at small p_T.

According to the velocity-scaling rules of NRQCD, the matrix element for B_c production that is of leading order in v is $\langle \mathcal{O}_1^{B_c}(^1S_0) \rangle$. The vacuum-saturation approximation can be used to show that it is proportional to $F_{B_c}^2$, where F_{B_c} is the decay constant of the B_c, up to corrections of order v^4. The leading matrix element for B_c^* production is $\langle \mathcal{O}_1^{B_c^*}(^3S_1) \rangle$. The vacuum-saturation approximation and heavy-quark spin symmetry can be used to show that this matrix element is also proportional to $F_{B_c}^2$, up to corrections of order v^3. The leading colour-octet matrix elements are suppressed as v^3 or v^4. The colour-octet terms in (5.29) are probably not as important for B_c mesons as they are for hidden-flavour

quarkonia. In the case of J/ψ production, the short-distance coefficients of the colour-octet matrix elements are enhanced relative to those for the colour-singlet matrix element by an inverse power of the QCD-coupling α_s, by factors of p_T/m_c at large p_T, by factors of m_c/p_T at small p_T, and by colour factors. The only one of these enhancement factors that may apply to the B_c is the colour factor. Because there are many Feynman diagrams that contribute to the parton process $ij \to (\bar{b}c) + b\bar{c}$ at order α_s^4, the colour correlations implied by individual Feynman diagrams tend to average out. We therefore expect a $\bar{b}c$ pair to be created in a colour-octet state roughly eight times as often as in a colour-singlet state. We will assume that, in spite of the enhancement from this colour factor, the colour-octet contributions to the production cross-sections for B_c and B_c^* are small compared with the leading colour-singlet contributions. This assumption is equivalent to using the colour-singlet model to calculate the production rate.

Two approaches have been used to compute the cross-sections for B_c mesons: the complete order-α_s^4 approach [299–302, 307, 308] and the fragmentation approach [298, 310]. In the complete order-α_s^4 approach, the parton cross-section in Eq. (5.29) is computed at leading order in α_s, where the only subprocesses are $ij \to (\bar{b}c) + b\bar{c}$:

$$d\hat{\sigma}[ij \to B_c + X] = d\hat{\sigma}[ij \to \bar{b}c_1(^1S_0) + b\bar{c}] \, \langle \mathcal{O}_1^{B_c}(^1S_0) \rangle \; . \tag{5.30}$$

The fragmentation approach is based on the fact that, for asymptotically large $p_T \gg M_{B_c}$, the cross-section (5.29) can be further factored into a cross-section for producing $\bar{b}$ and a fragmentation function $D_{\bar{b} \to B_c}(z, \mu)$ that gives the probability for the $\bar{b}$ to fragment into a B_c carrying a fraction z of the $\bar{b}$ momentum:

$$d\hat{\sigma}[ij \to B_c + X] \approx \int dz \; d\hat{\sigma}[ij \to \bar{b} + b] \; D_{\bar{b} \to B_c}(z, \mu) \; . \tag{5.31}$$

If both factors are calculated only at leading order in α_s, this is just an approximation to the complete order-α_s^4 cross-section in Eq. (5.29). One advantage of the fragmentation approach is that the expressions for the $\bar{b}$ production cross-section $d\hat{\sigma}$ and the fragmentation function $D_{\bar{b} \to B_c}$ in Eq. (5.31) can be written down in a few lines. For $p_T \gg m_{B_c}$, the fragmentation approach has another advantage in that the Altarelli–Parisi evolution equations can be used to sum the leading logarithms of p_T/m_c to all orders. Unfortunately, as was pointed out in Ref. [300–302], the fragmentation cross-section does not become an accurate approximation to the complete order-α_s^4 cross-section until surprisingly large values of p_T. For example, if the parton centre-of-mass energy is $\sqrt{\hat{s}} = 200$ GeV, the fragmentation cross-section is a good approximation only for $p_T \geq 40$ GeV. We will therefore not consider the fragmentation approach further.

The authors of Ref. [311] recently developed a Monte Carlo event generator for hadronic B_c and B_c^* production, using the complete order-α_s^4 approach and taking advantage of helicity amplitude techniques [312]. The generator is a Fortran package, and it is implemented in PYTHIA [313], which allows one to generate complete events. The complete order-α_s^4 cross-section includes contributions from gluon–gluon fusion and quark–antiquark annihilation. At the Tevatron, the gluon–gluon fusion mechanism is dominant over quark–antiquark annihilation, except in certain kinematics regions [299, 314]. At the LHC, the gluon–gluon fusion mechanism is always dominant. All the results below are obtained from the gluon–gluon fusion mechanism only.

The inputs that are required to calculate the complete order-α_s^4 cross-sections are the masses m_b, m_c, and m_{B_c}, the decay constant F_{B_c}, the PDF's, the QCD coupling constant α_s, and the factorization scale Q. The masses m_b and m_c are known with uncertainties of about 2.4% and 8%, respectively. In the NRQCD factorization approach, one sets $m_{B_c} = m_c + m_b$ and $m_{B_c^*} = m_c + m_b$ in the short-distance coefficients. Contributions from operators of higher order in v then account for the binding energy in m_{B_c} and $m_{B_c^*}$. This procedure is also required in order to preserve gauge invariance if one makes use of on-shell spin-projection operators for the B_c and B_c^* states [20, 315]. Since an experimental measurement of the decay constant F_{B_c} is not available, one has to use a value that is obtained from potential

Table 5.12: The cross-sections (in nb) for direct production of B_c and B_c^* at the Tevatron and at the LHC for various values of the charm-quark mass m_c. The gluon distribution function is CTEQ5L, the running of α_s is leading order, the scale is $\mu^2 = \hat{s}/4$, and the other parameters are $F_{B_c} = 480$ MeV, and $m_b = 4.9$ GeV.

	Tevatron ($\sqrt{s} = 2$ TeV)					LHC ($\sqrt{s} = 14$ TeV)				
m_c (GeV)	1.4	1.5	1.6	1.7	1.8	1.4	1.5	1.6	1.7	1.8
$\sigma[B_c]$ (nb)	3.87	3.12	2.56	2.12	1.76	61.0	49.8	41.4	34.7	28.9
$\sigma[B_c^*]$ (nb)	9.53	7.39	5.92	4.77	3.87	153.	121.	97.5	80.0	66.2

models [316–319] or from lattice gauge theory [320]. The uncertainty in the factor $F_{B_c}^2$ is about 6%. Since the order-α_s^4 cross-section is at leading order in perturbation theory, the running of α_s can be taken at leading order, and LO versions of the PDF's can be used.

The running coupling constant and the PDF's depend on the renormalization/factorization scale μ, and, so, a prescription for the scale μ is also required. There is no general rule for choosing the scale in an LO calculation, especially in the case of a $2 \to 3$ subprocess, such as $ij \to B_c + b\bar{c}$. The factorization formula (5.31) for asymptotically large p_T suggests that an appropriate choice for the scales in the fragmentation contribution to the cross-section might be to set $\mu = m_{bT} \equiv (m_b^2 + p_T^2)^{1/2}$ in the PDF's and $\alpha_s^4 = \alpha_s^2(m_{bT})\alpha_s^2(m_c)$ in the parton cross-section. However, the fragmentation term does not dominate until very large p_T, and there are important contributions to the cross-section that have nothing to do with fragmentation [300–302]. For example, there are contributions that involve the splitting of one of the colliding gluons into a $c\bar{c}$ pair, followed by the creation of a $b\bar{b}$ pair in the hard scattering of the c from the other gluon and then by the recombination of the $\bar{b}$ and c into a B_c. The sensitivity to the choice of μ could be decreased by carrying out a complete calculation of the production cross-section for the B_c at next-to-leading order in α_s, but this is, at present, prohibitively difficult. In the absence of such a calculation, we can use the variation in the complete order-α_s^4 cross-section for several reasonable choices for the scale as an estimate of the uncertainty that arises from the choice of scale.

The hadronic production cross-section for B_c mesons depends strongly on the collision energy. In Table 5.12, we give the direct cross-sections for B_c and B_c^* production at the Tevatron and the LHC for several values of the charm quark mass m_c and for typical values for the other parameters. The cross-section for B_c production at the LHC is larger than at the Tevatron by a factor of about 16. The cross-sections for B_c^* production are larger than those for B_c production by a factor of about 2.4. The cross-sections are fairly sensitive to the charm-quark mass, varying by more than a factor of two as m_c is varied from 1.4 to 1.8 GeV. In Fig. 5.29, we show the differential cross-sections for B_c production as a function of the B_c transverse momentum p_T and B_c rapidity y at the Tevatron and the LHC, using four different prescriptions for the scale μ. At central rapidity, the variations among the four choices of scale is about a factor of three at the Tevatron and a factor of two at the LHC. The differential cross-sections decrease more slowly with p_T and $|y|$ at the LHC than at the Tevatron. The total uncertainty from combining all of the uncertainties in the direct cross-section for B_c production is less than an order of magnitude. The uncertainty in the ratio of the direct-production cross-sections for the B_c^* and the B_c is much smaller because many of the uncertainties cancel in the ratio.

The results presented above are for the direct production of the B_c and the B_c^*. Experiments at the Tevatron and the LHC will measure the inclusive cross-sections, including the feeddown from all of the higher states of the $\bar{b}c$ system. The $\bar{b}c$ system has a rich spectrum of excited states below the BD threshold. They include an additional S-wave multiplet, one or two P-wave multiplets, and a D-wave multiplet. After being produced, these excited B_c mesons all cascade eventually down to the ground state B_c. Since the B_c^* decays into the B_c with a probability of almost 100%, the feeddown from directly-produced B_c^*'s increases the cross-section for the B_c by about a factor of 3.4. The complete

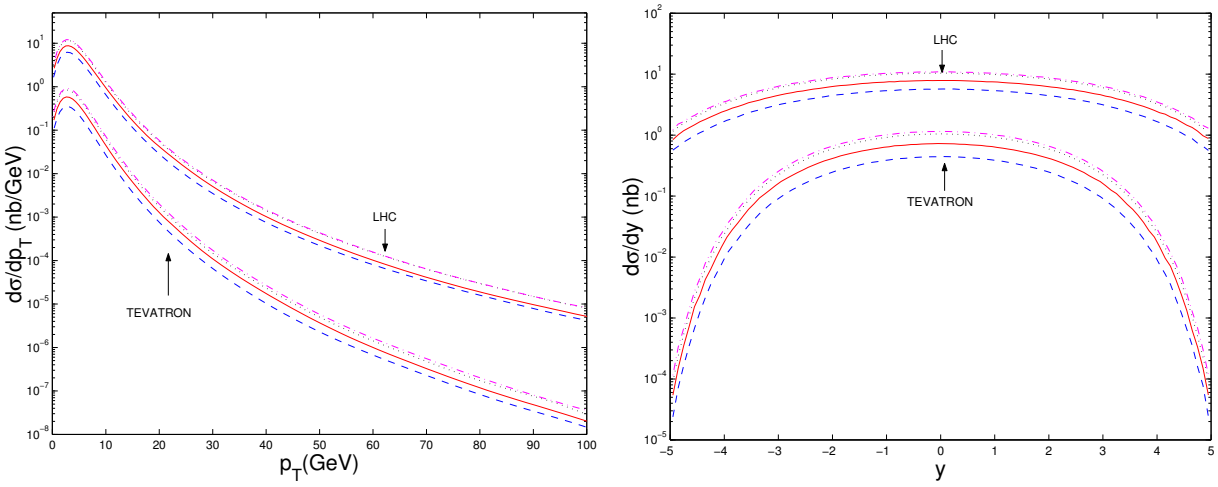

Fig. 5.29: The differential cross-sections for the direct production of the B_c as a function of its transverse momentum p_T and its rapidity y at the Tevatron ($\sqrt{s} = 2$ TeV) and at the LHC ($\sqrt{s} = 14$ TeV) for four choices of the scale: $\mu^2 = \hat{s}/4$ (solid line), $\mu^2 = p_T^2 + m_{B_c}^2$ (dotted line), $\mu^2 = \hat{s}$ (dashed line), and $\mu^2 = p_{Tb}^2 + m_b^2$ (dash–dot line). The gluon distribution is CTEQ5L, the running of α_s is leading order, and the other parameters are $F_{B_c} = 480$ MeV, $m_c = 1.5$ GeV, and $m_b = 4.9$ GeV.

order-α_s^4 cross-sections for B_c and B_c^* production can be applied equally well to the $2S$ multiplet. The direct-production cross-sections for these states are smaller than those for the $1S$ states by the ratio of the squares of the wave functions at the origin, which is about 0.6. Thus, the inclusive cross-section for B_c production, including the effect of feeddown from the direct production of all of the S-wave B_c states, is larger than the cross-section for direct B_c production, which is given in Table 5.12 and shown in Fig. 5.29, by a factor of about 5.4.

The production of B_c in $p\bar{p}$ collisons at $\sqrt{s} = 1.8$ TeV has been measured at the Tevatron by the CDF collaboration [296, 297]. CDF has measured the ratio

$$R[J/\psi l\nu] = \frac{\sigma[B_c]\mathrm{Br}[B_c^+ \to J/\psi l^+\nu]}{\sigma[B^+]\mathrm{Br}[B^+ \to J/\psi K^+]} \tag{5.32}$$

for B_c^+ and B^+ with transverse momenta $p_T > 6.0$ GeV and with rapidities $|y| < 1.0$. Their result is $R[J/\psi l\nu] = 0.132^{+0.041}_{-0.037}(\mathrm{stat.}) \pm 0.031(\mathrm{syst.})^{+0.032}_{-0.020}(\mathrm{lifetime})$. This result is consistent with results from previous searches [293–295]. Figure 5.30 compares the CDF measurements of $R[J/\psi l\nu]$ and the B_c lifetime with theoretical predictions from Refs. [303,304] for two different values of the semileptonic width $\Gamma_{s.l.} = \Gamma[B_c \to J/\psi l\nu]$. The theoretical predictions use the values $|V_{cb}| = 0.041 \pm 0.005$ [305], $\sigma[B_c^+]/\sigma[\bar{b}] = 1.3 \times 10^{-3}$ [306], $\sigma[B^+]/\sigma[\bar{b}] = 0.378 \pm 0.022$ [305], and $\mathrm{Br}[B^+ \to J/\psi K^+] = (1.01 \pm 0.14) \times 10^{-3}$ [305]. The predictions and the measurement are consistent within experimental and theoretical uncertainties.

Quantitative predictions for the contribution to the inclusive B_c production cross-section from the feeddown from P-wave states would require complete knowledge of the order-α_s^4 cross-sections for the production of P-wave states. It is theoretically inconsistent to use the colour-singlet model to calculate these cross-sections for the P-wave states. There are colour-octet terms in the P-wave production cross-sections that are of the same order in both v and α_s as the colour-singlet terms, and they must be included. The colour-singlet production matrix elements for the P-wave states can be estimated from potential models or determined from lattice gauge theory. The colour-octet production matrix elements for the P-wave states can perhaps be estimated by interpolating between the corresponding matrix elements for charmonium and bottomonium states.

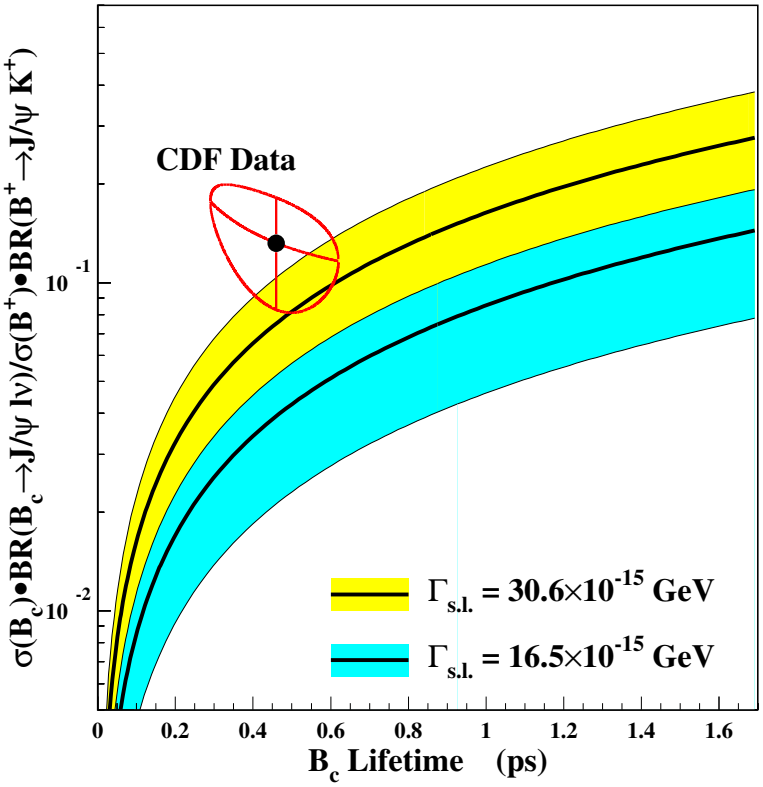

Fig. 5.30: The ratio $R[J/\psi l\nu]$, which is defined in Eq. (5.32), versus the B_c lifetime. The point, surrounded by a one-standard-deviation contour, shows the values of $R[J/\psi l\nu]$ and the B_c lifetime that were measured by CDF [296, 297]. The shaded region represents the theoretical predictions and their uncertainty bands from Refs. [303, 304] for two different values of the semileptonic width $\Gamma_{s.l.} = \Gamma[B_c \to J/\psi l\nu]$.

In summary, the order-α_s^4 colour-singlet production cross-section for S-wave $\bar{b}c$ mesons can be used to predict the B_c production cross-section, including feeddown from excited S-wave states. The uncertainty in the normalization of that prediction is less than an order of magnitude. If the inclusive cross-section for B_c production that is measured at the Tevatron or the LHC is much larger than that prediction, it could indicate that there is a large contribution from the feeddown from P-wave or higher-orbital-angular-momentum states. It could also indicate that the colour-octet contributions to the direct production of the B_c and the B_c^* are important.

9 SUMMARY AND OUTLOOK

NRQCD factorization, together with hard-scattering factorization, provides a systematic formalism for computing inclusive quarkonium production rates in QCD. Nonperturbative effects associated with the binding of a $Q\bar{Q}$ pair into a quarkonium are factored into NRQCD matrix elements that scale in a definite manner with the typical relative velocity v of the heavy quark in the quarkonium. The NRQCD matrix elements are predicted to be universal, i.e., independent of the process that creates the $Q\bar{Q}$ pair. The NRQCD factorization formula for inclusive cross-sections is believed to hold when $p_T \gg \Lambda_{\rm QCD}$, where p_T is the transverse momentum of the quarkonium with respect to the colliding particles. It is well-motivated by the effective field theory NRQCD and by factorization theorems that have been proven for simpler hard-scattering processes. Explicit proofs of factorization for quarkonium production would be welcome, because they would help quantify the sizes of corrections to the factorization formula. It

is important to bear in mind that conventional proofs of hard-scattering factorization fail at small p_T. Consequently, NRQCD factorization formulas, even those that include soft-gluon resummation, may be unreliable in this region. It also follows that the NRQCD factorization approach may not be applicable to total cross-sections if they are dominated by contributions at small p_T.

The NRQCD factorization approach incorporates elements of both the colour-singlet model and the colour-evaporation model. It includes the colour-singlet model terms, for which the NRQCD matrix elements can be determined from annihilation decays. It also includes colour-octet production mechanisms, as in the colour-evaporation model. The NRQCD factorization approach extends these models into a systematically improvable framework. The colour-singlet model is emphatically ruled out by the observation of prompt J/ψ and $\psi(2S)$ production at the Tevatron at rates that are more than an order of magnitude larger than the colour-singlet-model predictions. The colour-evaporation model is ruled out by the observations of nonzero polarization of J/ψ's in B meson decays and in e^+e^- annihilation at 10.6 GeV and by the observation of nonzero polarization of $\Upsilon(2S)$'s and $\Upsilon(3S)$'s in fixed-target experiments. It is also ruled out by the fact that different values of the fraction of J/ψ's that come from χ_c decays are measured at the Tevatron and in B-meson decays. Despite having been ruled out, the colour-singlet model and the colour-evaporation model can still play useful roles as "straw men" with which to compare the predictions of NRQCD factorization. The colour-evaporation model has not yet been ruled out, for example, as a description of differential cross-sections at the Tevatron and in fixed-target experiments.

The NRQCD factorization approach provides a general phenomenological framework that cannot be ruled out easily. The factorization formula involves infinitely many NRQCD matrix elements, most of which are adjustable parameters. It is only the truncation in v that reduces those parameters to a finite set. The standard truncation has four independent NRQCD matrix elements for each S-wave multiplet and two independent NRQCD matrix elements for each P-wave multiplet. NRQCD factorization with the standard truncation in v remains a phenomenologically viable description of inclusive quarkonium production. As one tests NRQCD factorization at higher levels of precision, the standard truncation must ultimately fail. The NRQCD factorization approach itself may remain viable if one truncates at a higher order in v, but only at the cost of introducing many new adjustable parameters.

In the effort to make the predictions of the NRQCD factorization approach more quantitative, the most urgent need is to extend all calculations to next-to-leading order (NLO) in α_s. For hadron collisions at small p_T ($p_T \ll m$), the leading-order parton process is $ij \to Q\bar{Q}$. NLO calculations of that process are already available, but a resummation of multiple gluon emissions is required in order to tame large logarithms of m^2/p_T^2 and to turn the singular p_T distribution into a smooth distribution. For very large p_T ($p_T \gg m$), the production of quarkonium is dominated by gluon fragmentation. The leading-order fragmentation process is $g \to Q\bar{Q}_8(^3S_1)$, and the NLO calculation of the gluon fragmentation function into $Q\bar{Q}$ is available. What is still lacking is the NLO calculation at intermediate p_T, for which the leading-order parton process is $ij \to Q\bar{Q} + k$. By taking into account the NLO corrections in α_s, one should significantly decrease some of the uncertainties in the NRQCD factorization predictions.

One problematic source of uncertainties in the NRQCD factorization predictions is relativistic corrections. The first relativistic corrections of order v^2 in the channel that corresponds to the colour-singlet model have been calculated for many processes. In many cases, they have large coefficients that cast doubt on the validity of the expansion in powers of v for charmonium, and even for bottomonium. The success of lattice NRQCD in describing bottomonium spectroscopy ensures the applicability of the velocity expansion for this system in some form. It is possible that some reorganization or resummation of the velocity expansion might be necessary in order to make precise quantitative calculations of charmonium production.

The best individual experiments for determining the NRQCD production matrix elements for both charmonium and bottomonium are probably those at the Tevatron, because of the large range of p_T that is accessible. It will be important to take advantage of the measurements down to small p_T that were

achieved at the CDF detector for bottomonium in Run I and for charmonium in Run II. This will require taking into account the effects of multiple gluon emission in the theoretical analysis. Measurements of charmonium production in other experiments are also important because they provide tests of the universality of the production matrix elements. These experiments include those that measure charmonium production in ep collisions at HERA, in e^+e^- annihilation at the B factories, and in B meson decays at the B factories. One can use these experiments to extract values of the NRQCD matrix elements or, as has typically been the practice to date, one can use the matrix elements that have been extracted from the Tevatron data to make predictions for charmonium production in other experiments.

The ratios of the production cross-sections for different quarkonium states may also provide important tests of NRQCD factorization. (Here, particularly, one must keep in mind the *caveats* about the applicability of the NRQCD factorization approach to total cross-sections.) The uncertainties in the predictions for ratios of cross-sections are much smaller than those in the individual cross-sections because many of the uncertainties cancel in the ratio. The variations of the ratios from process to process and as functions of kinematic variables provide important information about the production mechanisms. The ratios of production rates of spin-triplet S-wave states, such as the $\psi(2S)$ to J/ψ ratio, do not seem to vary much. However, a significant variation has been observed in a ratio of the production rates of P-wave and S-wave states, namely the fraction of J/ψ's that come from decays of χ_c's. A substantial variation has also been observed in a ratio of production rates of P-wave states, namely the χ_{c1} to χ_{c2} ratio. More precise measurements of these and other ratios would be valuable. Of particular importance would be measurements of ratios of production rates of spin-singlet and spin-triplet quarkonium states, such as the η_c to J/ψ ratio. The absence of clean signatures for spin-singlet quarkonium states makes such measurements difficult.

The polarization of quarkonium is another important test of NRQCD factorization. The standard truncation in v leads to unambiguous predictions for the ratios of production rates of different spin states, without introducing any new parameters. The predictions are most easily tested for the quarkonium states with $J^{PC} = 1^{--}$, but they can also be tested for other states. It is extremely important to test the simple qualitative predictions that in hadron collisions the 1^{--} states should become transversely polarized at sufficiently large p_T. More careful quantitative estimates of the polarization of the J/ψ, the $\psi(2S)$, and the $\Upsilon(nS)$ as functions of p_T at the Tevatron and the LHC would be useful. More precise measurements of the polarization of the J/ψ and the $\psi(2S)$ in other production processes, such as ep collisions, e^+e^- annihilations, and B decay, would also be valuable.

The most puzzling experimental results in quarkonium production in recent years have been the double-$c\bar{c}$ results from e^+e^- annihilation at the B factories. The measurements by the Belle collaboration of the fraction of J/ψ's that are accompanied by charmed hadrons and of the exclusive cross-section for $J/\psi + \eta_c$ production are both much larger than expected. No satisfactory theoretical explanation of these results has emerged. It would be worthwhile to measure the fraction of J/ψ's accompanied by charm hadrons in other processes, such as $p\bar{p}$ annihilation at the Tevatron and ep collisions at HERA, to see if there are any surprises.

The outlook for progress in understanding quarkonium production is very bright. The NRQCD factorization approach provides a general framework for describing inclusive quarkonium production. Current experiments will provide severe tests of NRQCD factorization with the standard truncation of the velocity expansion. These tests will either provide a firm foundation for predictions of quarkonium production in future experiments or lead us to new insights into the physics of quarkonium production.

REFERENCES

[1] W. E. Caswell and G. P. Lepage, Phys. Lett. B **167** (1986) 437.

[2] B. A. Thacker and G. P. Lepage, Phys. Rev. D **43** (1991) 196.

[3] G. T. Bodwin, E. Braaten and G. P. Lepage, Phys. Rev. D **51** (1995) 1125 [Erratum-ibid. D **55** (1997) 5853] [hep-ph/9407339].
[4] G. T. Bodwin, S. Kim, and D. K. Sinclair, Nucl. Phys. B (Proc. Suppl.) **34** (1994) 434.
[5] G. T. Bodwin, S. Kim, and D. K. Sinclair, Nucl. Phys. Proc. Suppl. **42** (1995) 306 [hep-lat/9412011].
[6] G. T. Bodwin, D. K. Sinclair, and S. Kim, Phys. Rev. Lett. **77** (1996) 2376 [hep-lat/9605023].
[7] G. T. Bodwin, D. K. Sinclair, and S. Kim, Int. J. Mod. Phys. A **12** (1997) 4019 [hep-ph/9609371].
[8] G. T. Bodwin, D. K. Sinclair, and S. Kim, Phys. Rev. D **65** (2002) 054504 [hep-lat/0107011].
[9] J.-w. Qiu and G. Sterman (private communication).
[10] M. Beneke, I. Z. Rothstein, and M. B. Wise, Phys. Lett. B **408** (1997) 373 [hep-ph/9705286].
[11] S. Fleming, A. K. Leibovich and T. Mehen, Phys. Rev. D **68** (2003) 094011 [hep-ph/0306139].
[12] M. Beneke, G. A. Schuler, and S. Wolf, Phys. Rev. D **62** (2000) 034004 [hep-ph/0001062].
[13] M. B. Einhorn and S. D. Ellis, Phys. Rev. D **12** (1975) 2007.
[14] S. D. Ellis, M. B. Einhorn, and C. Quigg, Phys. Rev. Lett. **36** (1976) 1263.
[15] C. E. Carlson and R. Suaya, Phys. Rev. D **14** (1976) 3115.
[16] J. H. Kühn, Phys. Lett. B **89** (1980) 385.
[17] T. A. DeGrand and D. Toussaint, Phys. Lett. B **89** (1980) 256.
[18] J. H. Kühn, S. Nussinov, and R. Rückl, Z. Phys. C **5** (1980) 117.
[19] M. B. Wise, Phys. Lett. B **89** (1980) 229.
[20] C. H. Chang, Nucl. Phys. B **172** (1980) 425.
[21] R. Baier and R. Rückl, Nucl. Phys. B **201** (1982) 1.
[22] R. Baier and R. Rückl, Phys. Lett. B **102** (1981) 364.
[23] E. L. Berger and D. L. Jones, Phys. Rev. D **23** (1981) 1521.
[24] R. Baier and R. Rückl, Z. Phys. C **19** (1983) 251.
[25] W. Y. Keung, Print-81-0161 (BNL) *Presented at Z0 Physics Workshop, Ithaca, N.Y., Feb 6-8, 1981*.
[26] G. A. Schuler, hep-ph/9403387.
[27] H. Fritzsch, Phys. Lett. B **67** (1977) 217.
[28] F. Halzen, Phys. Lett. B **69** (1977) 105.
[29] M. Glück, J. F. Owens and E. Reya, Phys. Rev. D **17** (1978) 2324.
[30] V. D. Barger, W. Y. Keung and R. J. Phillips, Phys. Lett. B **91** (1980) 253.
[31] R. Gavai, D. Kharzeev, H. Satz, G. A. Schuler, K. Sridhar and R. Vogt, Int. J. Mod. Phys. A **10** (1995) 3043 [hep-ph/9502270].
[32] G. A. Schuler and R. Vogt, Phys. Lett. B **387** (1996) 181 [hep-ph/9606410].
[33] M. L. Mangano, P. Nason and G. Ridolfi, Nucl. Phys. B **405** (1993) 507.
[34] J. F. Amundson, O. J. P. Eboli, E. M. Gregores and F. Halzen, Phys. Lett. B **390** (1997) 323 [hep-ph/9605295].
[35] A. Edin, G. Ingelman and J. Rathsman, Phys. Rev. D **56** (1997) 7317 [hep-ph/9705311].
[36] O. J. P. Eboli, E. M. Gregores and F. Halzen, Phys. Lett. B **451** (1999) 241 [hep-ph/9802421].
[37] O. J. P. Eboli, E. M. Gregores and F. Halzen, Phys. Rev. D **67** (2003) 054002.
[38] O. J. P. Eboli, E. M. Gregores and J. K. Mizukoshi, Phys. Rev. D **68** (2003) 094009 [hep-ph/0308121].
[39] O. J. P. Eboli, E. M. Gregores and F. Halzen, Phys. Rev. D **64** (2001) 093015 [hep-ph/0107026].
[40] E. M. Gregores, F. Halzen and O. J. P. Eboli, Phys. Lett. B **395** (1997) 113 [hep-ph/9607324].

[41] E. L. Berger, J. w. Qiu, and Y. l. Wang, hep-ph/0404158.
[42] J. C. Collins, D. E. Soper and G. Sterman, Nucl. Phys. B **250** (1985) 199.
[43] H. Contopanagos, E. Laenen and G. Sterman, Nucl. Phys. B **484** (1997) 303 [hep-ph/9604313].
[44] see e.g., M. Cacciari, M. Greco, and P. Nason, JHEP **9805** (1998) 007 [hep-ph/9803400].
[45] F. E. Paige and S. D. Protopopescu, BNL-29777.
[46] F. E. Paige, S. D. Protopescu, H. Baer, and X. Tata, hep-ph/0312045.
[47] T. Sjöstrand, Comput. Phys. Commun. **39** (1986) 347.
[48] T. Sjöstrand and M. Bengtsson, Comput. Phys. Commun. **43** (1987) 367.
[49] G. Marchesini and B. R. Webber, Nucl. Phys. B **310** (1988) 461.
[50] G. Marchesini, B. R. Webber, G. Abbiendi, I. G. Knowles, M. H. Seymour, and L. Stanco, Comput. Phys. Commun. **67** (1992) 465.
[51] S. Frixione and B. R. Webber, JHEP **0206** (2002) 029 [hep-ph/0204244].
[52] S. Frixione and B. R. Webber, hep-ph/0207182.
[53] S. Frixione, P. Nason and B. R. Webber, JHEP **0308** (2003) 007 [hep-ph/0305252].
[54] S. Frixione and B. R. Webber, hep-ph/0402116.
[55] D. E. Soper, Phys. Rev. D **69** (2004) 054020 [hep-ph/0306268].
[56] M. Krämer and D. E. Soper, Phys. Rev. D **69** (2004) 054019 [hep-ph/0306222].
[57] G. T. Bodwin, S. J. Brodsky, and G. P. Lepage, Phys. Rev. D **39** (1989) 3287.
[58] J. w. Qiu and G. Sterman, Int. J. Mod. Phys. E **12** (2003) 149 [hep-ph/0111002].
[59] G. T. Bodwin, S. J. Brodsky, and G. P. Lepage, Phys. Rev. Lett. **47** (1981) 1799.
[60] G. T. Bodwin, Phys. Rev. D **31** (1985) 2616 [Erratum-ibid. D **34** (1986) 3932].
[61] F. Abe *et al.* [CDF Collaboration], Phys. Rev. Lett. **79** (1997) 572.
[62] F. Abe *et al.* [CDF Collaboration], Phys. Rev. Lett. **79** (1997) 578.
[63] S. R. Klein and J. Nystrand, Phys. Rev. Lett. **92** (2004) 142003 [hep-ph/0311164].
[64] M. Krämer, Prog. Part. Nucl. Phys. **47** (2001) 141 [hep-ph/0106120].
[65] E. Braaten and S. Fleming, Phys. Rev. Lett. **74** (1995) 3327 [hep-ph/9411365].
[66] M. Beneke and M. Krämer, Phys. Rev. D **55** (1997) 5269 [hep-ph/9611218].
[67] W. Buchmüller and S. H. Tye, Phys. Rev. D **24** (1981) 132.
[68] E. J. Eichten and C. Quigg, Phys. Rev. D **52** (1995) 1726 [hep-ph/9503356].
[69] H. L. Lai *et al.* [CTEQ Collaboration], Eur. Phys. J. C **12** (2000) 375 [hep-ph/9903282].
[70] A. Petrelli, M. Cacciari, M. Greco, F. Maltoni, and M. L. Mangano, Nucl. Phys. **B514** (1998) 245 [hep-ph/9707223].
[71] F. Maltoni, hep-ph/0007003.
[72] P. L. Cho and A. K. Leibovich, Phys. Rev. D **53** (1996) 150 [hep-ph/9505329].
[73] P. L. Cho and A. K. Leibovich, Phys. Rev. D **53** (1996) 6203 [hep-ph/9511315].
[74] A. D. Martin, W. J. Stirling, and R. G. Roberts, Phys. Lett. B **306** (1993) 145; **309** (1993) 492 (erratum).
[75] H. L. Lai *et al.*, Phys. Rev. D **55** (1997) 1280 [hep-ph/9606399].
[76] M. Glück, E. Reya and A. Vogt, Z. Phys. C **67** (1995) 433.
[77] A. D. Martin, R. G. Roberts and W. J. Stirling, Phys. Lett. B **387** (1996) 419 [hep-ph/9606345].
[78] E. Braaten, B. A. Kniehl and J. Lee, Phys. Rev. D **62** (2000) 094005 [hep-ph/9911436].
[79] A. D. Martin, R. G. Roberts, W. J. Stirling, and R. S. Thorne, Eur. Phys. J. C **4** (1998) 463 [hep-ph/9803445].
[80] M. A. Sanchis-Lozano, Nucl. Phys. Proc. Suppl. **86** (2000) 543 [hep-ph/9907497].

[81] W. K. Tung, *Prepared for International Workshop on Deep Inelastic Scattering and Related Subjects, Eilat, Israel, 6-11 Feb 1994*.

[82] B. A. Kniehl and G. Kramer, Eur. Phys. J. C **6** (1999) 493 [hep-ph/9803256].

[83] A. Petrelli, Nucl. Phys. Proc. Suppl. **86** (2000) 533 [hep-ph/9910274].

[84] K. Sridhar, A. D. Martin and W. J. Stirling, Phys. Lett. B **438** (1998) 211 [hep-ph/9806253].

[85] P. Hägler, R. Kirschner, A. Schäfer, L. Szymanowski and O. V. Teryaev, Phys. Rev. D **63** (2001) 077501 [hep-ph/0008316].

[86] J. Kwiecinski, A. D. Martin and A. M. Stasto, Phys. Rev. D **56** (1997) 3991 [hep-ph/9703445].

[87] F. Yuan and K. T. Chao, Phys. Rev. D **63** (2001) 034006 [hep-ph/0008302].

[88] F. Yuan and K. T. Chao, Phys. Rev. Lett. **87** (2001) 022002 [hep-ph/0009224].

[89] M. Beneke and I. Z. Rothstein, Phys. Lett. B **372** (1996) 157 [Erratum-ibid. B **389** (1996) 769] [hep-ph/9509375].

[90] J. P. Ma, Nucl. Phys. **B447** (1995) 405 [hep-ph/9503346].

[91] E. Braaten and J. Lee, Nucl. Phys. B **586** (2000) 427 [hep-ph/0004228].

[92] M. Cacciari and M. Greco, Phys. Rev. Lett. **73** (1994) 1586 [hep-ph/9405241].

[93] E. Braaten, M. A. Doncheski, S. Fleming, and M. L. Mangano, Phys. Lett. B **333** (1994) 548 [hep-ph/9405407].

[94] D. P. Roy and K. Sridhar, Phys. Lett. **B339** (1994) 141 [hep-ph/9406386].

[95] T. Affolder *et al.* [CDF Collaboration], Phys. Rev. Lett. **86** (2001) 3963.

[96] F. Maltoni (unpublished).

[97] http://www-cdf.fnal.gov/physics/new/bottom/030904.blessed-bxsec-jpsi/.

[98] http://www-d0.fnal.gov/Run2Physics/ckm/approved_results/approved_results.html; http://www-d0.fnal.gov/Run2Physics/ckm/Moriond_2003/index2.html.

[99] D. Acosta *et al.* [CDF Collaboration], Phys. Rev. D **66** (2002) 092001.

[100] B. Abbott *et al.* [D0 Collaboration], Phys. Rev. Lett. **82** (1999) 35.

[101] M. Cacciari, S. Frixione, M. L. Mangano, P. Nason and G. Ridolfi, JHEP **0407** (2004) 033 [hep-ph/0312132].

[102] D. Acosta *et al.* [CDF Collaboration], Phys. Rev. Lett. **88** (2002) 161802.

[103] T. Affolder *et al.* [CDF Collaboration], Phys. Rev. Lett. **85** (2000) 2886 [hep-ex/0004027].

[104] M. Krämer and F. Maltoni, in 'Bottom Production', P. Nason, G. Ridolfi, O. Schneider, G.F. Tartarelli, P. Vikas et al., [hep-ph/0003142], published in CERN-YR-2000/01, G. Altarelli and M.L. Mangano editors.

[105] E. Braaten, S. Fleming, and A. K. Leibovich, Phys. Rev. D **63** (2001) 094006 [hep-ph/0008091].

[106] J. L. Domenech and M. A. Sanchis-Lozano, Nucl. Phys. B **601** (2001) 395 [hep-ph/0012296].

[107] F. Abe *et al.* [CDF Collaboration], Phys. Rev. Lett. **75** (1995) 4358.

[108] P. L. Cho and M. B. Wise, Phys. Lett. B **346** (1995) 129 [hep-ph/9411303].

[109] A. K. Leibovich, Phys. Rev. D **56** (1997) 4412 [hep-ph/9610381].

[110] G. T. Bodwin and J. Lee, Phys. Rev. D **69** (2004) 054003 [hep-ph/0308016].

[111] M. Beneke, hep-ph/9703429.

[112] N. Brambilla, A. Pineda, J. Soto and A. Vairo, Nucl. Phys. B **566** (2000) 275 [hep-ph/9907240].

[113] S. Fleming, I. Z. Rothstein and A. K. Leibovich, Phys. Rev. D **64** (2001) 036002 [hep-ph/0012062].

[114] M. A. Sanchis-Lozano, Int. J. Mod. Phys. A **16** (2001) 4189 [hep-ph/0103140].

[115] N. Brambilla, D. Eiras, A. Pineda, J. Soto and A. Vairo, Phys. Rev. D **67** (2003) 034018 [hep-ph/0208019].

[116] N. Marchal, S. Peigne and P. Hoyer, Phys. Rev. D **62** (2000) 114001 [hep-ph/0004234].
[117] M. Maul, Nucl. Phys. B **594** (2001) 89 [hep-ph/0009279].
[118] E. Braaten and J. Lee, Phys. Rev. D **63** (2001) 071501 [hep-ph/0012244].
[119] R. Cropp [CDF collaboration], hep-ex/9910003.
[120] V. Papadimitriou [CDF Collaboration], Int. J. Mod. Phys. A **16S1A** (2001) 160.
[121] P. Mathews, P. Poulose and K. Sridhar, Phys. Lett. **B438** (1998) 336 [hep-ph/9803424].
[122] K. Sridhar, Phys. Rev. Lett. **77** (1996) 4880 [hep-ph/9609285].
[123] C. Qiao, F. Yuan and K. Chao, Phys. Rev. D **55** (1997) 5437 [hep-ph/9701249].
[124] C. S. Kim, J. Lee and H. S. Song, Phys. Rev. **D55** (1997) 5429 [hep-ph/9610294].
[125] P. Mathews, K. Sridhar and R. Basu, Phys. Rev. **D60** (1999) 014009 [hep-ph/9901276].
[126] V. Barger, S. Fleming and R. J. Phillips, Phys. Lett. B **371** (1996) 111 [hep-ph/9510457].
[127] F. Maltoni and A. D. Polosa, hep-ph/0405082.
[128] E. Braaten, J. Lee and S. Fleming, Phys. Rev. **D60** (1999) 091501 [hep-ph/9812505].
[129] M. Beneke and I. Z. Rothstein, Phys. Rev. D **54** (1996) 2005 [Erratum-ibid. D **54** (1996) 7082] [hep-ph/9603400].
[130] W. K. Tang and M. Vanttinen, Phys. Rev. D **54** (1996) 4349 [hep-ph/9603266].
[131] S. Gupta and K. Sridhar, Phys. Rev. D **54** (1996) 5545 [hep-ph/9601349].
[132] C. Akerlof *et al.*, Phys. Rev. D **48** (1993) 5067.
[133] M. H. Schub *et al.* [E789 Collaboration], Phys. Rev. D **52** (1995) 1307 [Erratum-ibid. D **53** (1996) 570].
[134] T. Alexopoulos *et al.* [E771 Collaboration], Phys. Lett. B **374** (1996) 271.
[135] S. Eidelman *et al.* [Particle Data Group Collaboration], Phys. Lett. B **592** (2004) 1.
[136] S. Gupta and P. Mathews, Phys. Rev. D **56** (1997) 3019 [hep-ph/9703370].
[137] D. A. Bauer *et al.*, Phys. Rev. Lett. **54** (1985) 753.
[138] L. Antoniazzi *et al.* [E705 Collaboration], Phys. Rev. D **49** (1994) 543.
[139] T. Alexopoulos *et al.* [E771 Collaboration], Phys. Rev. D **62** (2000) 032006 [hep-ex/9908010].
[140] H. L. Lai *et al.*, Phys. Rev. D **51** (1995) 4763 [hep-ph/9410404].
[141] M. Arenton [E705 Collaboration], Int. J. Mod. Phys. A **12** (1997) 3837.
[142] J. Spengler [HERA-B Collaboration], J. Phys. G **30**, S871 (2004) [arXiv:hep-ex/0403043].
[143] Y. Lemoigne *et al.*, Phys. Lett. B **113** (1982) 509 [Erratum-ibid. B **116** (1982) 470].
[144] S. R. Hahn *et al.*, Phys. Rev. D **30** (1984) 671.
[145] V. Koreshev *et al.* [E672-E706 Collaborations], Phys. Rev. Lett. **77** (1996) 4294.
[146] A. Gribushin *et al.* [E672 and E706 Collaborations], Phys. Rev. D **53** (1996) 4723.
[147] J. F. Amundson, O. J. Eboli, E. M. Gregores, and F. Halzen, Phys. Lett. B **372** (1996) 127 [hep-ph/9512248].
[148] A. Gribushin *et al.* [E672 Collaborations], Phys. Rev. D **62** (2000) 012001 [hep-ex/9910005].
[149] G. Introzzi [E771 Collaboration], Nucl. Phys. Proc. Suppl. **55A** (1997) 188.
[150] T. H. Chang *et al.* [FNAL E866/NuSea collaboration], Phys. Rev. Lett. **91** (2003) 211801 [hep-ex/0308001].
[151] M. Vanttinen, P. Hoyer, S. J. Brodsky and W. K. Tang, Phys. Rev. D **51** (1995) 3332 [hep-ph/9410237].
[152] Jungil Lee, presentation at the HERA-B Collaboration Meeting, December 7, 2000.
[153] J. G. Heinrich *et al.*, Phys. Rev. D **44** (1991) 1909.
[154] C. N. Brown *et al.* [FNAL E866 Collaboration], Phys. Rev. Lett. **86** (2001) 2529 [hep-

ex/0011030].

[155] A. Kharchilava, T. Lohse, A. Somov, and A. Tkabladze, Phys. Rev. D **59** (1999) 094023 [hep-ph/9811361].

[156] A. Tkabladze, Phys. Lett. B **462** (1999) 319.

[157] J. L. Cortes and B. Pire, Phys. Rev. D **38**, 3586 (1988).

[158] M. Bedjidian *et al.*, hep-ph/0311048.

[159] S. Digal, P. Petreczky and H. Satz, Phys. Rev. D **64** (2001) 094015 [hep-ph/0106017].

[160] M. Glück, E. Reya and A. Vogt, Eur. Phys. J. C **5** (1998) 461 [hep-ph/9806404].

[161] R. Vogt, in proceedings of the $18^{\rm th}$ Winter Workshop on Nuclear Dynamics, edited by R. Bellweid *et al.*, Debrecen, Hungary (2002) p. 253 [hep-ph/0203151].

[162] R. Vogt, Heavy Ion Phys. **18** (2003) 11 [hep-ph/0205330].

[163] T. Affolder *et al.* [CDF Collaboration], Phys. Rev. Lett. **84** (2000) 2094 [hep-ex/9910025].

[164] J. F. Gunion and R. Vogt, Nucl. Phys. B **492** (1997) 301 [hep-ph/9610420].

[165] M. Krämer, J. Zunft, J. Steegborn, and P. M. Zerwas, Phys. Lett. B **348** (1995) 657 [hep-ph/9411372].

[166] M. Krämer, Nucl. Phys. B **459** (1996) 3 [hep-ph/9508409].

[167] M. Cacciari and M. Krämer, Phys. Rev. Lett. **76** (1996) 4128 [hep-ph/9601276].

[168] M. Beneke, M. Krämer, and M. Vanttinen, Phys. Rev. D **57** (1998) 4258 [hep-ph/9709376].

[169] J. Amundson, S. Fleming and I. Maksymyk, Phys. Rev. D **56** (1997) 5844 [hep-ph/9601298].

[170] P. Ko, J. Lee and H. S. Song, Phys. Rev. D **54** (1996) 4312 [Erratum-ibid. D **60** (1999) 119902] [hep-ph/9602223].

[171] R. M. Godbole, D. P. Roy, and K. Sridhar, Phys. Lett. B **373** (1996) 328 [hep-ph/9511433].

[172] B. A. Kniehl and G. Kramer, Phys. Lett. B **413** (1997) 416 [hep-ph/9703280].

[173] B. A. Kniehl and G. Kramer, Phys. Rev. D **56** (1997) 5820 [hep-ph/9706369].

[174] C. Adloff *et al.* [H1 Collaboration], Eur. Phys. J. C **25** (2002) 25 [hep-ex/0205064].

[175] S. Chekanov *et al.* [ZEUS Collaboration], Eur. Phys. J. C **27** (2003) 173 [hep-ex/0211011].

[176] H. Jung and G. P. Salam, Eur. Phys. J. C **19** (2001) 351 [hep-ph/0012143].

[177] H. Jung, Comput. Phys. Commun. **143** (2002) 100 [hep-ph/0109102].

[178] V. A. Saleev and N. P. Zotov, Mod. Phys. Lett. A **9** (1994) 151 [Erratum-ibid. A **9** (1994) 1517].

[179] S. P. Baranov, Phys. Lett. B **428** (1998) 377.

[180] C. Adloff *et al.* [H1 Collaboration], Eur. Phys. J. C **10** (1999) 373 [hep-ex/9903008].

[181] S. Fleming and T. Mehen, Phys. Rev. D **57** (1998) 1846 [hep-ph/9707365].

[182] B. A. Kniehl and L. Zwirner, Nucl. Phys. **B621** (2002) 337 [hep-ph/0112199].

[183] C. Adloff *et al.* [H1 Collaboration], Eur. Phys. J. C **25** (2002) 41 [hep-ex/0205065].

[184] S. Chekanov *et al.* [ZEUS Collaboration], contributed paper 565, International Europhysics Conference on High Energy Physics (EPS 2003), Aachen, Germany, 2003.

[185] A. V. Lipatov and N. P. Zotov, Eur. Phys. J. C **27** (2003) 87 [hep-ph/0210310].

[186] J. G. Körner, J. Cleymans, M. Kuroda, and G. J. Gounaris, Phys. Lett. B **114** (1982) 195.

[187] J. P. Guillet, Z. Phys. C **39** (1988) 75.

[188] H. Merabet, J. F. Mathiot, and R. Mendez-Galain, Z. Phys. C **62** (1994) 639.

[189] D. Krücker, Ph.D. Thesis, RWTH Aachen, 1995.

[190] F. Yuan and K. T. Chao, Phys. Rev. D **63** (2001) 034017 [hep-ph/0008301].

[191] M. G. Ryskin, Z. Phys. C **57** (1993) 89.

[192] S. J. Brodsky, L. Frankfurt, J. F. Gunion, A. H. Mueller and M. Strikman, Phys. Rev. D **50** (1994)

3134 [hep-ph/9402283].
[193] J. C. Collins, L. Frankfurt and M. Strikman, Phys. Rev. D **56** (1997) 2982 [hep-ph/9611433].
[194] J. C. Collins, Phys. Rev. D **57** (1998) 3051 [Erratum-ibid. D **61** (2000) 019902] [hep-ph/9709499].
[195] T. Teubner, hep-ph/9910329.
[196] J. Bartels and H. Kowalski, Eur. Phys. J. C **19** (2001) 693 [hep-ph/0010345].
[197] A. Hayashigaki and K. Tanaka, hep-ph/0401053.
[198] S. Aid *et al.* [H1 Collaboration], Nucl. Phys. B **463** (1996) 3 [hep-ex/9601004].
[199] C. Adloff *et al.* [H1 Collaboration], Eur. Phys. J. C **13** (2000) 371 [hep-ex/9902019].
[200] C. Adloff *et al.* [H1 Collaboration], Phys. Lett. B **483** (2000) 23 [hep-ex/0003020].
[201] C. Adloff *et al.* [H1 Collaboration], Phys. Lett. B **483** (2000) 360 [hep-ex/0005010].
[202] C. Adloff *et al.* [H1 Collaboration], Phys. Lett. B **539** (2002) 25 [hep-ex/0203022].
[203] C. Adloff *et al.* [H1 Collaboration], Phys. Lett. B **541** (2002) 251 [hep-ex/0205107].
[204] A. Aktas *et al.* [H1 Collaboration], Phys. Lett. B **568** (2003) 205 [hep-ex/0306013].
[205] A. Aktas *et al.* [H1 Collaboration], contributed paper 6-0180, International Conference on High Energy Physics (ICHEP04), Beijing, China, 2004.
[206] J. Breitweg *et al.* [ZEUS Collaboration], Eur. Phys. J. C **6** (1999) 603 [hep-ex/9808020].
[207] J. Breitweg *et al.* [ZEUS Collaboration], Phys. Lett. B **437** (1998) 432 [hep-ex/9807020].
[208] J. Breitweg *et al.* [ZEUS Collaboration], Eur. Phys. J. C **14** (2000) 213 [hep-ex/9910038].
[209] J. Breitweg *et al.* [ZEUS Collaborations], Eur. Phys. J. C **12** (2000) 393 [hep-ex/9908026].
[210] J. Breitweg *et al.* [ZEUS Collaboration], Phys. Lett. B **487** (2000) 273 [hep-ex/0006013].
[211] S. Chekanov *et al.* [ZEUS Collaboration], Eur. Phys. J. C **26** (2003) 389 [hep-ex/0205081].
[212] S. Chekanov *et al.* [ZEUS Collaboration], contributed paper 549, International Europhysics Conference on High Energy Physics (EPS 2003), Aachen, Germany, 2003.
[213] S. Chekanov *et al.* [ZEUS Collaboration], Eur. Phys. J. C **24** (2002) 345 [hep-ex/0201043].
[214] S. Chekanov *et al.* [ZEUS Collaboration], Nucl. Phys. B **695** (2004) 3 [hep-ex/0404008].
[215] L. Frankfurt, W. Koepf and M. Strikman, Phys. Rev. D **57** (1998) 512 [hep-ph/9702216].
[216] M. McDermott, L. Frankfurt, V. Guzey and M. Strikman, Eur. Phys. J. C **16** (2000) 641 [hep-ph/9912547].
[217] L. Frankfurt, M. McDermott and M. Strikman, JHEP **0103** (2001) 045 [hep-ph/0009086].
[218] M. G. Ryskin, R. G. Roberts, A. D. Martin and E. M. Levin, Z. Phys. C **76** (1997) 231 [hep-ph/9511228].
[219] A. D. Martin and M. G. Ryskin, Phys. Rev. D **57** (1998) 6692 [hep-ph/9711371].
[220] A. D. Martin, M. G. Ryskin and T. Teubner, Phys. Rev. D **62** (2000) 014022 [hep-ph/9912551].
[221] D. Y. Ivanov, A. Schäfer, L. Szymanowski and G. Krasnikov, Eur. Phys. J. C **34** (2004) 297 [hep-ph/0401131].
[222] T. Regge, Nuovo Cim. **14** (1959) 951.
[223] T. Regge, Nuovo Cim. **18** (1960) 947.
[224] J. J. Sakurai, Phys. Rev. Lett. **22** (1969) 981.
[225] A. Donnachie and P. V. Landshoff, Phys. Lett. B **296** (1992) 227 [hep-ph/9209205].
[226] A. Donnachie and P. V. Landshoff, Phys. Lett. B **437** (1998) 408 [hep-ph/9806344].
[227] E. A. Kuraev, L. N. Lipatov and V. S. Fadin, Sov. Phys. JETP **44** (1976) 443 [Zh. Eksp. Teor. Fiz. **71** (1976) 840].
[228] E. A. Kuraev, L. N. Lipatov and V. S. Fadin, Sov. Phys. JETP **45** (1977) 199 [Zh. Eksp. Teor. Fiz. **72** (1977) 377].

[229] I. I. Balitsky and L. N. Lipatov, Sov. J. Nucl. Phys. **28** (1978) 822 [Yad. Fiz. **28** (1978) 1597].

[230] A. H. Mueller and B. Patel, Nucl. Phys. B **425** (1994) 471 [hep-ph/9403256].

[231] N. N. Nikolaev and B. G. Zakharov, Z. Phys. C **64** (1994) 631 [hep-ph/9306230].

[232] V. N. Gribov and L. N. Lipatov, Yad. Fiz. **15** (1972) 781 and 1218 [Sov. J. Nucl. Phys. **15** (1972) 438 and 675].

[233] M. Cacciari and M. Krämer, Talk given at the Workshop on Future Physics at HERA, Hamburg, Germany, 30-31 May 1996 [hep-ph/9609500].

[234] S. Fleming and T. Mehen, Phys. Rev. D **58** (1998) 037503 [hep-ph/9801328].

[235] L. Hao, F. Yuan and K. Chao, Phys. Rev. Lett. **83** (1999) 4490 [hep-ph/9902338].

[236] L. Hao, F. Yuan and K. Chao, Phys. Rev. D **62** (2000) 074023 [hep-ph/0004203].

[237] C. S. Kim and E. Reya, Phys. Lett. B **300** (1993) 298.

[238] T. Mehen, Phys. Rev. D **55** (1997) 4338 [hep-ph/9611321].

[239] M. Cacciari, M. Greco and M. Krämer, Phys. Rev. D **55** (1997) 7126 [hep-ph/9611324].

[240] [ALEPH Collaboration], CERN-OPEN-99-343 *Prepared for International Europhysics Conference on High-Energy Physics (HEP 97), Jerusalem, Israel, 19-26 Aug 1997.*

[241] P. Abreu *et al.* [DELPHI Collaboration], Phys. Lett. B **341** (1994) 109.

[242] M. Wadhwa [L3 Collaboration], Nucl. Phys. Proc. Suppl. **64** (1998) 441.

[243] G. Alexander *et al.* [OPAL Collaboration], Phys. Lett. B **384** (1996) 343.

[244] C. G. Boyd, A. K. Leibovich, and I. Z. Rothstein, Phys. Rev. D **59** (1999) 054016 [hep-ph/9810364].

[245] S. Todorova-Nova, hep-ph/0112050.

[246] J. Abdallah *et al.* [DELPHI Collaboration], Phys. Lett. B **565** (2003) 76 [hep-ex/0307049].

[247] J. P. Ma, B. H. J. McKellar and C. B. Paranavitane, Phys. Rev. D **57** (1998) 606 [hep-ph/9707480].

[248] G. Japaridze and A. Tkabladze, Phys. Lett. B **433** (1998) 139 [hep-ph/9803447].

[249] R. M. Godbole, D. Indumathi and M. Krämer, Phys. Rev. D **65** (2002) 074003 [hep-ph/0101333].

[250] M. Klasen, B. A. Kniehl, L. Mihaila and M. Steinhauser, Nucl. Phys. B **609** (2001) 518 [hep-ph/0104044].

[251] M. Klasen, B. A. Kniehl, L. N. Mihaila, and M. Steinhauser, Phys. Rev. Lett. **89** (2002) 032001 [hep-ph/0112259].

[252] M. Klasen, B. A. Kniehl, L. N. Mihaila and M. Steinhauser, [hep-ph/0407014].

[253] G. Alexander *et al.* [OPAL Collaboration], Phys. Lett. B **370** (1996) 185.

[254] P. L. Cho, Phys. Lett. B **368** (1996) 171 [hep-ph/9509355].

[255] W. Y. Keung, Phys. Rev. D **23** (1981) 2072.

[256] J. H. Kühn and H. Schneider, Z. Phys. C **11** (1981) 263.

[257] K. J. Abraham, Z. Phys. C **44** (1989) 467.

[258] K. Hagiwara, A. D. Martin and W. J. Stirling, Phys. Lett. B **267** (1991) 527 [Erratum-ibid. B **316** (1993) 631].

[259] E. Braaten, K. m. Cheung, and T. C. Yuan, Phys. Rev. D **48** (1993) 4230 [hep-ph/9302307].

[260] K. Abe *et al.* [BELLE Collaboration], Phys. Rev. Lett. **88** (2002) 052001 [hep-ex/0110012].

[261] B. Aubert *et al.* [BABAR Collaboration], Phys. Rev. Lett. **87** (2001) 162002 [hep-ex/0106044].

[262] P. L. Cho and A. K. Leibovich, Phys. Rev. D **54** (1996) 6690 [hep-ph/9606229].

[263] F. Yuan, C. F. Qiao, and K. T. Chao, Phys. Rev. D **56** (1997) 321 [hep-ph/9703438].

[264] F. Yuan, C. F. Qiao, and K. T. Chao, Phys. Rev. D **56** (1997) 1663 [hep-ph/9701361].

[265] G. A. Schuler, Eur. Phys. J. C **8** (1999) 273 [hep-ph/9804349].

[266] E. Braaten and Y. Q. Chen, Phys. Rev. Lett. **76** (1996) 730 [hep-ph/9508373].

[267] K. Abe *et al.* [Belle Collaboration], BELLE-CONF-0331, contributed paper, International Europhysics Conference on High Energy Physics (EPS 2003), Aachen, Germany, 2003.

[268] S. Baek, P. Ko, J. Lee, and H. S. Song, Phys. Lett. B **389** (1996) 609 [hep-ph/9607236].

[269] K. Abe *et al.* [Belle Collaboration], Phys. Rev. Lett. **89** (2002) 142001 [hep-ex/0205104].

[270] K. Y. Liu, Z. G. He and K. T. Chao, Phys. Rev. D **69** (2004) 094027.

[271] K. Abe *et al.* [Belle Collaboration], hep-ex/0407009.

[272] E. Braaten and J. Lee, Phys. Rev. D **67** (2003) 054007 [hep-ph/0211085].

[273] K. Y. Liu, Z. G. He, and K. T. Chao, Phys. Lett. B **557** (2003) 45 [hep-ph/0211181].

[274] S. J. Brodsky, C.-R. Ji, and J. Lee, private communication.

[275] G. T. Bodwin, J. Lee, and E. Braaten, Phys. Rev. Lett. **90** (2003) 162001 [hep-ph/0212181].

[276] G. T. Bodwin, J. Lee, and E. Braaten, Phys. Rev. D **67** (2003) 054023 [hep-ph/0212352].

[277] A. V. Luchinsky, hep-ph/0301190.

[278] K. Abe *et al.* [Belle Collaboration], hep-ex/0306015.

[279] J. P. Ma and Z. G. Si, hep-ph/0405111.

[280] R. Balest *et al.* [CLEO Collaboration], Phys. Rev. D **52** (1995) 2661.

[281] S. Chen *et al.* [CLEO Collaboration], Phys. Rev. D **63** (2001) 031102 [hep-ex/0009044].

[282] D. Buskulic *et al.* [ALEPH Collaboration], Phys. Lett. B **295** (1992) 396.

[283] O. Adriani *et al.* [L3 Collaboration], Phys. Lett. B **317** (1993) 467.

[284] P. Ko, J. Lee and H. S. Song, Phys. Rev. D **53** (1996) 1409 [hep-ph/9510202].

[285] P. Ko, J. Lee and H. S. Song, J. Korean Phys. Soc. **34** (1999) 301.

[286] S. Anderson *et al.* [CLEO Collaboration], Phys. Rev. Lett. **89** (2002) 282001.

[287] M. Beneke, F. Maltoni and I. Z. Rothstein, Phys. Rev. D **59** (1999) 054003 [hep-ph/9808360].

[288] J. P. Ma, Phys. Lett. B **488** (2000) 55 [hep-ph/0006060].

[289] S. Fleming, O. F. Hernandez, I. Maksymyk and H. Nadeau, Phys. Rev. D **55** (1997) 4098 [hep-ph/9608413].

[290] G. T. Bodwin, E. Braaten, T. C. Yuan and G. P. Lepage, Phys. Rev. D **46** (1992) 3703 [hep-ph/9208254].

[291] J. H. Kühn and R. Rückl, Phys. Lett. **135B** (1984) 477 [Erratum-ibid. B **258** (1991) 499].

[292] C. H. Chang and Y. Q. Chen, Phys. Rev. D **46** (1992) 3845 [Erratum-ibid. D **50** (1994) 6013].

[293] P. Abreu *et al.* [DELPHI Collaboration], Phys. Lett. B **398** (1997) 207.

[294] R. Barate *et al.* [ALEPH Collaboration], Phys. Lett. B **402** (1997) 213.

[295] K. Ackerstaff *et al.* [OPAL Collaboration], Phys. Lett. B **420** (1998) 157 [hep-ex/9801026].

[296] F. Abe *et al.* [CDF Collaboration], Phys. Rev. Lett. **81** (1998) 2432 [hep-ex/9805034].

[297] F. Abe *et al.* [CDF Collaboration], Phys. Rev. D **58** (1998) 112004 [hep-ex/9804014].

[298] E. Braaten, K. m. Cheung and T. C. Yuan, Phys. Rev. D **48** (1993) 5049 [hep-ph/9305206].

[299] C. H. Chang and Y. Q. Chen, Phys. Rev. D **48** (1993) 4086.

[300] C. H. Chang, Y. Q. Chen, G. P. Han and H. T. Jiang, Phys. Lett. B **364** (1995) 78 [hep-ph/9408242].

[301] C. H. Chang, Y. Q. Chen and R. J. Oakes, Phys. Rev. D **54** (1996) 4344 [hep-ph/9602411].

[302] K. Kolodziej, A. Leike and R. Rückl, Phys. Lett. B **355** (1995) 337 [hep-ph/9505298].

[303] M. Lusignoli and M. Masetti, Z. Phys. C **51** (1991) 546.

[304] D. Scora and N. Isgur, Phys. Rev. D **52** (1995) 2783.

[305] R. M. Barnett *et al.*, "Review of Particle Physics", Phys. Rev. D **54** (1996) 1.

[306] M. Lusignoli, M. Masetti and S. Petrarca, Phys. Lett. B **266** (1991) 142.

[307] A. V. Berezhnoy, V. V. Kiselev and A. K. Likhoded, Z. Phys. A **356** (1996) 89.

[308] S. P. Baranov, Phys. Rev. D **55** (1997) 2756.

[309] A. V. Berezhnoi, V. V. Kiselev, A. K. Likhoded and A. I. Onishchenko, Phys. Atom. Nucl. **60** (1997) 1729 [hep-ph/9703341].

[310] K. m. Cheung, Phys. Lett. B **472** (2000) 408 [hep-ph/9908405].

[311] C. H. Chang, C. Driouichi, P. Eerola and X. G. Wu, Comput. Phys. Commun. **159** (2004) 192 [hep-ph/0309120].

[312] M. L. Mangano and S. J. Parke, Phys. Rept. **200** (1991) 301, and references therein.

[313] T. Sjöstrand, Comput. Phys. Commun. **82** (1994) 74.

[314] C. H. Chang and X. G. Wu, hep-ph/0309121.

[315] B. Guberina, R. Meckbach, R. D. Peccei and R. Rückl, Nucl. Phys. B **184** (1981) 476.

[316] Y. Q. Chen and Y. P. Kuang, Phys. Rev. D **46** (1992) 1165 [Erratum-ibid. D **47** (1993) 350].

[317] E. J. Eichten and C. Quigg, Phys. Rev. D **49** (1994) 5845 [hep-ph/9402210].

[318] V. V. Kiselev, A. K. Likhoded and A. V. Tkabladze, Phys. Rev. D **51** (1995) 3613 [hep-ph/9406339].

[319] A. Abd El-Hady, J. H. Munoz and J. P. Vary, Phys. Rev. D **62** (2000) 014019 [hep-ph/9909406].

[320] C. T. H. Davies, K. Hornbostel, G. P. Lepage, A. J. Lidsey, J. Shigemitsu and J. H. Sloan, Phys. Lett. B **382** (1996) 131 [hep-lat/9602020].